LEVEL

(14)

DISCLAIMER NOTICE

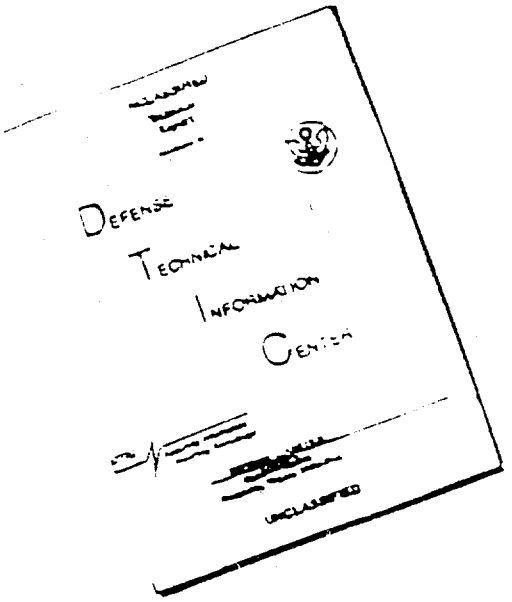

THIS DOCUMENT IS BEST QUALITY AVAILABLE. THE COPY FURNISHED TO DTIC CONTAINED A SIGNIFICANT NUMBER OF PAGES WHICH DO NOT REPRODUCE LEGIBLY.

PWA Report No. FR-11545

Contract No. F44620-76-C-0123

LEVEL I

(14)

HOT CORROSION DEGRADATION OF METALS AND ALLOYS

- A UNIFIED THEORY -

C. S. Giggins and F. S. Pettit

June 1979

Final Scientific Report: 1 June 1976 - 30 September 1978

Approved for public release; distribution unlimited

Prepared for

Air Force Office of Scientific Research
Electronic and Solid State Sciences
Bolling AFB, D.C. 20332

PRATT & WHITNEY AIRCRAFT GROUP
Government Products Division
P. O. Box 2691
West Palm Beach, Florida 33402

UNITED TECHNOLOGIES ®

Printed in the United States of America

Unclassified

SECURITY CLASSIFICATION OF THIS PAGE (When Data Entered)

REPORT DOCUMENTATION PAGE

READ INSTRUCTIONS BEFORE COMPLETING FORM

1. REPORT NUMBER: AFOSR-TR-79-0905	2. GOVT ACCESSION NO.
3. RECIPIENT'S CATALOG NUMBER	
4. TITLE (and Subtitle): Hot Corrosion Degradation of Metals and Alloys - A Unified Theory	5. TYPE OF REPORT & PERIOD COVERED: Final Scientific Report. 1 June 1976-30 Sept 1978
	6. PERFORMING ORG. REPORT NUMBER: PWA-FR-11545
7. AUTHOR(s): C. S. Giggins and F. S. Pettit	8. CONTRACT OR GRANT NUMBER(s): F44620-76-C-0123
9. PERFORMING ORGANIZATION NAME AND ADDRESS: Pratt & Whitney Aircraft Group, Commercial Products Division, United Technologies Corporation, Middletown, Connecticut 06457	10. PROGRAM ELEMENT, PROJECT, TASK AREA & WORK UNIT NUMBERS: 2306/A2, 61102F
11. CONTROLLING OFFICE NAME AND ADDRESS: Air Force Office of Scientific Research, Electronic and Solid State Sciences, Bldg. 410, Bolling AFB, D.C. 20332	12. REPORT DATE: June 1979; 13. NUMBER OF PAGES: 142
14. MONITORING AGENCY NAME & ADDRESS (if different from Controlling Office)	15. SECURITY CLASS. (of this report): Unclassified
	15a. DECLASSIFICATION/DOWNGRADING SCHEDULE

16. DISTRIBUTION STATEMENT (of this Report)

Approved for public release; distribution unlimited.

17. DISTRIBUTION STATEMENT (of the abstract entered in Block 20, if different from Report)

18. SUPPLEMENTARY NOTES

407624

19. KEY WORDS (Continue on reverse side if necessary and identify by block number)

Hot Corrosion Theory and Mechanisms
Sodium Sulfate-Induced Hot Corrosion
Hot Corrosion Initiation
Hot Corrosion Propagation
Nickel-Base Alloys
Cobalt-Base Alloys

20. ABSTRACT (Continue on reverse side if necessary and identify by block number)

The hot corrosion attack of metals and alloys has been examined over an extensive range of experimental conditions in order to develop a hot corrosion theory that is generally applicable to all such processes. Experiments have been performed at temperatures from 700° to 1000°C in air and in gases containing oxygen and SO_3. Sodium sulfate was the principal deposit used to induce attack and the effects of NaCl and carbon in the Na_2SO_4 was also studied. Nickel- and cobalt-base alloys containing →

DD FORM 1473 EDITION OF 1 NOV 65 IS OBSOLETE

Unclassified

20. Abstract (Cont'd)

various amounts of chromium, aluminum, molybdenum and tungsten constituted the principal materials studied.

The hot corrosion attack of alloys has been found to consist of an initiation stage and a propagation stage. During the initiation stage the attack is similar to that occurring between the gas and the alloy in the absence of the deposit, but the alloys are being preconditioned in a way that determines the particular propagation mode that will cause the degradation. The factors which determine the length of the initiation stage and the type of propagation mode are identified by using illustrations and are shown to be; alloy composition, fabrication condition, gas composition and velocity, salt composition, salt deposition rate, condition of salt, temperature, temperature cycles, erosion and specimen geometry.

The hot corrosion propagation modes are described and shown to consist of fluxing processes and processes involving the oxidation of phases formed in alloys as a result of reaction with components in the deposit (e.g. sulfides, chlorides). The fluxing processes are shown to consist of basic (oxide ion excess) or acidic (oxide ion deficient) reactions where the acidic conditions can be developed by components of the gas (e.g. SO_3) or by oxides of elements in the alloys.

The effects produced by a number of different elements (e.g. Cr, Al, Mo, W) on the hot corrosion of alloys is examined. It is shown that by using the unified theory for hot corrosion, previous inconsistencies are resolved.

PREFACE

This final report covers the work performed under Contract F44620-76-C-0123 during the period 1 June 1976 through 30 September 1978.

The research program discussed in this report was administered through the Pratt & Whitney Aircraft Group, Government Products Division, West Palm Beach, Florida, with the experimental work being performed by the Materials Engineering and Research Laboratory of the Pratt & Whitney Aircraft Group, Commercial Products Division, Middletown, Connecticut.

The contract was accomplished under the technical direction of Major W. C. Simmons of the Air Force Office of Scientific Research, Electronic and Solid State Sciences, United States Air Force, Bolling Air Force Base, D.C.

Dr. F. S. Pettit, Program Manager and Principal Investigator, Materials Engineering and Research Laboratory, Pratt & Whitney Aircraft Group, Commercial Products Division, directed this program. Mr. C. S. Giggins, of the P&WA Materials Engineering and Research Laboratory was the co-principal investigator. The authors wish to acknowledge helpful discussions concerning the results provided by G. W. Goward, J. A. Goebel and R. H. Barkalow as well as technical assistance from V. Nevins, R. B. Burdon, J. C. Whittles and C. V. Prue.

INTRODUCTION

When materials are exposed to combustion environments, deposition of ash or salts upon their surfaces is a common occurrence. The compositions of such deposits can vary over a wide range depending upon the characteristics of the combustion process (i.e. air composition, fuel composition). In many instances the formation of deposits causes the nature of the reactions that take place between the combustion gases and materials to be substantially different than those occurring in the absence of the deposit. It is therefore not uncommon for materials, especially metals and alloys, to be attacked by environments much more severely when deposits are present on their surfaces. The degradation of materials under such conditions is called hot corrosion. The hot corrosion of metals and alloys has been observed in a variety of processes, the essential ingredients being; elements in an alloy for oxidation, components in a gas for reduction, and a deposit on the surface of the alloy capable of influencing the oxidation-reduction process.

Alloys used in gas turbines are susceptible to hot corrosion attack. Turbine blades and vanes can become covered with deposits of sulfates which are composed primarily of Na_2SO_4 containing different amounts of Ca, Mg, Pb, V, Zn and chloride ion. The severity of the hot corrosion attack of alloys in gas turbines depends on the operating conditions with marine and industrial service being more conducive to causing attack than aircraft service. Hot corrosion of alloys in aircraft gas turbines is however, not negligible. Hot corrosion attack of alloys is also a problem in the exhaust systems of automobiles, incinerators and the fireside of tubes for steam boilers. The

nature of the deposits may be different than those in gas turbines but the phenomenon is the same, namely, the deposit causes more attack of alloys by gases to occur.

Since the hot corrosion of alloys has resulted in shorter lives for alloys, a substantial effort has been directed towards determining the mechanism(s) by which the hot corrosion of alloys takes place [1-14]. As mentioned in an earlier paper,[6] at first sight it appears that the mechanisms developed by various investigators are inconsistent with each other. However, closer examination of the problem indicates that hot corrosion can occur via different mechanisms depending upon the conditions. There is a need, therefore, to put hot corrosion theory into a perspective such that the various mechanisms of degradation and the effects produced by different elements are not inconsistent with one another. The purpose of this paper is to present a unified theory for hot corrosion. An important feature of this theory is that it proposes that hot corrosion can take place via different mechanisms. To establish this point conclusively, experimental data are presented to identify each of the mechanisms in some detail and to describe their interdependence.

EXPERIMENTAL

One of the difficulties in studying the hot corrosion of alloys is the selection of appropriate tests. The hot corrosion behavior of alloys can be markedly dependent upon test conditions. It is therefore possible to obtain widely differing results depending upon the conditions established by the test. For example, as shown in Figure 1, the amount of hot corrosion attack of a Ni-8Cr-6Al* alloy after 6 hrs. at 1000°C is essentially negligible

*Alloy compositions are expressed in weight-percent.

when 0.5 mg/cm^2 Na_2SO_4 is present on the surface of the alloy but very severe attack is observed if this alloy is immersed into 1 gm of Na_2SO_4. In attempting to develop a hot corrosion theory that applies to all metals and alloys, it is therefore necessary to utilize tests that encompass as many as possible of the combinations of conditions which can give rise to hot corrosion attack. Hence, it is necessary to use a variety of different hot corrosion tests.

The tests available to examine the hot corrosion of metals and alloys can be put into two general categories. One category involves tests in which the primary reason for developing the test is simulation of the conditions established by a specific process or operation. For example, burner rigs[15,16] have been developed to attempt to simulate the conditions that exist in the hotter sections of gas turbines. The problem with such tests is that the definition and control of the test conditions often become less precise as the degree of simulation is increased. The other category of tests are those in which the primary reason for developing the test is to precisely control and observe the effects produced by changing certain specific parameters known to be important to the hot corrosion process. The problem with these tests is that conditions are usually rather far removed from those that actually exist in the process under consideration. In order to understand the hot corrosion process, tests from both categories must be utilized.

This paper will emphasize the hot corrosion attack of alloys that occurs in gas turbines but the results will be generally applicable since it is desired to formulate a unified hot corrosion theory. Burner rig tests were used to help define the experimental parameters that were critical to the

hot corrosion process, and laboratory tube furnace tests were performed to study the effects these parameters had on the hot corrosion process. The burner rig tests were performed in a dynamic combustor designed by Dils,[16] Figure 2. This rig was operated on distillate jet fuel and compressed air. Six specimens could be exposed in this apparatus simultaneously. The entire array of specimens was oscillated about the combustor axis in order to provide uniform specimen exposure conditions. Gas velocities over the specimens were about 200 m/s. The laboratory tube furnace experiments were performed at temperatures between about 700° and 1000°C. Deposits of salt, usually 0.5 - 5 mg/cm^2 Na_2SO_4, were formed by spraying warm (~ 150°C) test coupons (~ 2 cm x 2 cm x 0.2 cm) with an aqueous solution of the salt. Tests using large amounts of salt (~ 1 gm) were performed by using an α-Al_2O_3 crucible to contain the salt into which the test coupons were immersed. Most of the experiments were performed in static air or flowing oxygen at 1 atm, but some tests were performed in flowing oxygen having an SO_3 pressure of about 10^{-4} atm. The SO_3 pressure was developed by adding SO_2 to oxygen using capillary flowmeters and passing these gases over a platinum catalyst.

Both isothermal and cyclic temperature tests were utilized. In the isothermal tests the furnace hot zone temperatures were controlled to better than ± 2°C. In the cyclic tests, specimens were subjected to hot zone temperatures for 50 minutes and cold zone temperatures (~ 25° - 40°C) for ten minutes during each hour of exposure. The metals and alloys used in this investigation are presented in Table I. Prior to testing, all specimens were polished through 600 grit silicon carbide abrasive paper, ultrasonically agitated in ethylene trichloride, rinsed in ethyl alcohol and dried.

The attack of exposed specimens was evaluated by using weight change versus time data, and detailed analyses of microstructural and surface morphological features. These analyses were accomplished by using standard techniques involving the light microscope, scanning electron microscope, electron beam microprobe and X-ray diffraction.

RESULTS AND DISCUSSION

Hot Corrosion Degradation Sequence

In attempting to develop a unified theory for hot corrosion of alloys, one of the first problems encountered is caused by the fact that the degradation mechanisms can change with time. An initial question involves, therefore, the time at which the hot corrosion process should be analyzed. Examination of hot corrosion data obtained as a function of time, Figures 3 and 4, shows that there appears to be two distinct stages of the attack, in particular, an initial stage during which the attack is not too severe and a later stage for which the attack has substantially increased. Examination of exposed specimens as a function of time, Figure 5, shows that microstructural features developed during the attack undergo a marked change as the severity of the attack increases. Initially the microstructural features are not too much different than those that would have developed in the absence of the salt deposit, but after the rate of attack increases, the microstructural features are much different than those that could be developed by reaction of the alloy with the gas in the absence of the salt.

The observed tendency for the hot corrosion process to consist of two stages is really not an uncommon phenomenon. The usual practice in developing alloys with resistance to high temperature corrosion is to utilize the concept of selective oxidation[17]. During the initial stages of de-

gradation the reaction product formed because of selective oxidation predominates, whereas other, less protective phases are formed as reaction products later in the degradation sequence. Typical weight change versus time curves for such alloys are presented in Figure 6. In view of this behavior, it is reasonable to describe the gas-induced degradation of alloys as composed of essentially two stages, namely, an initial stage where the reaction product formed at the surface of the alloy is composed predominantly of the most protective phase, and a subsequent stage involving more rapid propagation of the degradation where the reaction product consists of substantial amounts of less protective phases. It is important to note that the time at which the transition from the more protective reaction product (initiation stage) to the less protective product (propagation stage) takes place is dependent upon test conditions. For example, as indicated schematically in Figure 7, the transition would take place much sooner in a cyclic oxidation test compared to an isothermal test. Since the gas-induced degradation of virtually all corrosion resistant alloys can be considered as composed of initiation and propagation stages, it is reasonable to suppose that similar stages are operative during hot corrosion attack but occur after shorter times as shown in Figure 7. Moreover, the hot corrosion process can be conveniently analyzed in terms of how the salt deposits alter the processes that would have taken place during these two stages in the absence of such a deposit.

It is necessary to emphasize in discussing results obtained from studies on the hot corrosion of alloys, that it is very important to define whether the degradation process is in the initiation or propagation stage. In the case of a particularly mild test the degradation of a given alloy may be in the

initiation stage and with continued exposure a substantial increase in the degradation rate would be expected. However, in the case of very severe tests, the propagation stage can be reached after short exposures and no subsequent increase in the degradation rate is to be expected.

Initiation Stage of Hot Corrosion Attack

During the initiation stage, elements in the alloy are oxidized and electrons can be considered to be transferred from metallic atoms to reducible substances in the deposit. When the reduced substances are the same as those that would have reacted with the alloy in the absence of the deposit, the reaction product barrier forms beneath the salt on the alloy surface, Figure 8, and exhibits mostly features resulting from the gas - alloy reaction. As the hot corrosion process is continued however, features begin to become apparent which indicate that the salt is affecting the corrosion process and eventually the selective oxidation process is rendered ineffective. The increasing amount of sulfide particles in the photographs presented in Figure 5 is an example of this condition. The time for which the most effective reaction product barrier is stable beneath the salt layer is influenced by a number of factors identified in Figure 8. It is important to note that these factors also have significance in that they precondition the alloy, thus determining the type of propagation mode to be followed. In the following, the most important factors affecting the initiation of hot corrosion attack are discussed in some detail and examples are presented to illustrate their effects.

Alloy Composition

Numerous examples can be cited to illustrate the influence of alloy composition on the length of the initiation stage. The data presented in Figure 3 show that the length of the initiation stage for hot corrosion induced by Na_2SO_4 in air is increased as the aluminum content of nickel-chromium or cobalt-chromium alloys is increased from 6 to about 11%. It also shows that the initiation stage for Co-Cr-Al alloys is longer than that for nickel-base alloys. As will be shown subsequently, the degradation associated with the propagation mode for the alloys in this test (Na_2SO_4 deposit and air) consists of combined basic fluxing-sulfidation. In this propagation mode, degradation is believed to occur because oxide ions are produced as a result of the removal of sulfur from the Na_2SO_4 by the alloy. The oxide ions degrade the protective scales by reacting with them and oxidation of the sulfide particles within the alloys also results in increased rates of attack. By increasing the aluminum content from 6 to about 11% an α-Al_2O_3 scale is stable for a longer period of time which prevents sulfur removal from the Na_2SO_4 by the alloy and, hence, the production of oxide ions. As the Al_2O_3 scales become unstable, the Co-Cr-Al type alloys incorporate sulfur from the Na_2SO_4 much more slowly than the Ni-Cr-Al alloys.

In discussing the influence of alloy composition it is necessary to emphasize that some elements can produce beneficial effects over certain concentration ranges but deleterious effects over others. The data presented in Figure 9 show that the degradation of a Ni-30Cr-6Al alloy is less than that for a Ni-30Cr alloy after about 80 hours, but substantially

more after 100 hours. This occurs because, in nickel-base alloys which are not Al_2O_3 formers, aluminum causes the sulfidation propagation mode to be especially pronounced. In such alloys sulfur is very rapidly removed from the Na_2SO_4 due to the formation of numerous sulfide particles in the alloys. The Ni-30Cr-6Al alloy is not attacked severely as long as it can maintain a continuous, external scale of Al_2O_3 on its surface. As other oxides become stable, however, very severe degradation ensues. Hence, aluminum in alloys can produce both beneficial and deleterious effects on their hot corrosion resistance.

The data presented in Figure 10 show that by increasing the chromium content of a Ni-8Cr-6Al to 15% the initiation stage for hot corrosion induced by a large amount of Na_2SO_4 in air is substantially increased. The propagation mode for these two alloys under such conditions is via basic fluxing. In order for this propagation mode to occur, it is necessary to establish a substantial oxygen gradient across the Na_2SO_4. By increasing the chromium content, continuous external scales of Al_2O_3 or Cr_2O_3 remain stable longer and these types of scales consume less oxygen than when these oxides are discontinuous. The same type of results are obtained when the aluminum concentration of this alloy is increased.

Fabrication Condition

The hot corrosion attack of alloys can be significantly influenced by fabrication condition. As shown by the weight change versus time data presented in Figure 11, an as-cast NiCrAlY alloy was more severely attacked than a vapor deposited alloy.* One effect of fabrication condition on

*Vapor deposited alloys are of interest because overlay coatings are often fabricated by using vapor deposition techniques.

the initiation of hot corrosion attack is through compositional inhomogeneities. As-cast alloys are less homogeneous than vapor deposited alloys and hot corrosion attack is initiated in localized areas of cast alloys at which the composition is more susceptible to attack. Once initiated, the hot corrosion attack spreads laterally to locations with compositions more resistant to attack.

Gas Composition and Velocity

The composition of the gas phase can produce very substantial effects on the initiation and degradation rate of hot corrosion attack. In Figure 12 weight change versus time data are compared for the oxidation of a Na_2SO_4 - coated CoCrAlY coating in oxygen and in oxygen containing SO_3 at 10^{-4} atm. The hot corrosion attack is initiated virtually from the beginning of weight-increase measurements in the gas with SO_3 but no attack was observed after 20 hrs. in pure oxygen. The influence of the SO_3 in this example is two-fold. Sodium sulfate is not liquid at 700°C. When oxidation of CoCrAlY occurs at this temperature in SO_3, a liquid solution of Na_2SO_4 - $CoSO_4$ is formed. Hot corrosion attack is more easily induced when a liquid phase is present. Sulfur trioxide, however, also influences the rate at which the hot corrosion attack is propagated. For example, the attack in oxygen is not as severe as in oxygen with SO_3 even when a deposit of Na_2SO_4 - $MgSO_4$ is used which is liquid at 700°C in oxygen, Figure 12. The mechanism by which SO_3 influences the hot corrosion attack will be considered subsequently. The point to be stressed here is that the initiation and type of hot corrosion attack are dependent on the composition of the gas.

The velocity of the gas is a parameter of significance in the hot corrosion of alloys. Gas velocity effects are especially evident in situations where volatile components play a role in the hot corrosion process. For example, as will be shown subsequently, the accumulation of MoO_3 in Na_2SO_4 on Ni-8Cr-6Al-6Mo causes very severe hot corrosion attack. As can be seen in Figure 13, the attack of this alloy is initiated in static air much sooner than in flowing oxygen because less MoO_3 is lost from the Na_2SO_4 to the gas in the static environment. Velocity induced effects can be especially prevalent in burner rig experiments where gas velocities in excess of 300 m/s can be achieved.

Salt Composition

The composition of the salt can effect the hot corrosion of alloys. In Figure 14 photographs are presented to compare the degradation microstructures developed in coatings exposed to Na_2SO_4 containing different amounts of NaCl. The degradation becomes more severe as the NaCl concentration in the deposit is increased. As will be shown subsequently, the NaCl in the deposit causes the hot corrosion degradation to be different than that induced by pure Na_2SO_4. Numerous other examples are available to illustrate the importance of salt composition on hot corrosion attack. It is sufficient at this point to indicate that there are two types of salt composition effects. One type occurs because the deposit transforms from solid to liquid with the compositional change, Figure 12. The other type involves changes in the mechanism of the hot corrosion attack, Figure 14.

Salt Deposition Rate

The amount of salt that is present at the surface of alloys exerts very significant effects on the rates and, in some instances, the mechanisms of hot corrosion attack. The amount of salt which is present on the surfaces of alloys affects hot corrosion attack by two means. Some degradation mechanisms are not self-sustaining. Salt is consumed in the corrosion process, and therefore, the more salt present the more attack, Figure 1. Other mechanisms require the salt to have a certain composition for initiation. These specific compositions are formed at the salt-alloy interface by modification of the as-deposited salt as a result of reaction with the alloy. The thickness of the deposit influences the time required to obtain the composition necessary to initiate attack. When attack occurs because of the development of a gradient across the salt from the gas phase, thicker deposits cause attack to be initiated sooner than thinner deposits. On the other hand, when attack occurs as a result of the accumulation of elements from the alloy in the deposit, then attack can be observed sooner with thinner deposits, Figure 15.

Condition of Salt

Hot corrosion attack takes place because the deposit modifies the type of reaction which occurs between alloys and the gas environments. The condition of the deposit plays an important role in how the deposit modifies the reaction. Normally, a liquid deposit is most effective in causing hot corrosion attack, Figure 12, but it cannot be said that a liquid deposit is required for hot corrosion attack. Very dense, solid deposits can cause the chemical potentials

of reactants in the gas to be much different at the alloy-deposit interface compared to bulk gas values[18]. Dense solid deposits on alloys can therefore, in principle, cause hot corrosion attack.

When liquid salts are present on the surfaces of alloys, they are more effective in causing hot corrosion when they wet these surfaces. In many instances hot corrosion attack has been observed to stop after very thick, porous scales have been developed. It has been proposed[8] that the liquid is retained in the porous scale rather than wetting the alloy surface and thus the attack stops. In hot corrosion-erosion[19] studies, it has been found that deposition of small α-Al_2O_3 particles inhibited attack, Figure 16. This condition may result from the Na_2SO_4 being retained in the porous Al_2O_3 deposit, however, it is also possible that the Al_2O_3 deposit reacts chemically with the Na_2SO_4.

Temperature

Hot corrosion processes are dependent upon temperature. In many cases the time to initiate hot corrosion attack decreases as temperature is increased. This effect is evident in Figure 17 where the time to initiate attack of Ni-30Cr-6Al using Na_2SO_4 deposits and air is greater at 900°C than 1000°C.

Hot corrosion conditions do exist, however, where the attack becomes less severe as the temperature is increased. In burner rig hot corrosion tests it is more or less common procedure to ingest a controlled amount of salt which is then deposited on specimens during test. For the same ingestion rate of salt, less is deposited on the specimens as the temperature is increased. It is therefore possible to observe less hot corrosion attack at the higher temperatures because of the smaller amounts of salt on the specimens. Even

when the salt deposition rate is the same, there are conditions for which the rate of attack is greater at lower temperatures. One example is the case where the deposit is liquid at low temperatures but solid at higher temperatures. Such a case may be expected when Na_2SO_4 is in contact with oxides of nickel or cobalt and SO_3 is present in the gas. At low temperatures ($\sim$ 650°C) the SO_3 pressure can be sufficient to form a liquid Na_2SO_4 - $CoSO_4$ solution. At higher temperatures ($\sim$ 850°C), the SO_3 may not be sufficient to form a significant amount of $CoSO_4$ in the Na_2SO_4 and the deposit will be solid. Another example involves the hot corrosion mechanism where SO_3 in the gas phase plays a significant role in the corrosion process. This mechanism will be discussed subsequently. As shown in Figure 18, the hot corrosion of CoCrAlY with a Na_2SO_4 deposit and an SO_3 pressure of $7 \cdot 10^{-4}$ atm occurs at a faster rate at 700°C than 1000°C. For a fixed amount of sulfur in the gas, the SO_3 pressure becomes less as the temperature is increased. As shown in Figure 18, the decreased SO_3 pressure also results in a slower hot corrosion rate at the higher temperature.

Temperature Cycles

During the initiation stage of hot corrosion attack the reaction product barrier that forms due to reaction of the alloy with the gas is developing beneath the salt deposit, Figure 8. Thermal cycling of specimens causes this product to crack and spall. The transition from the initiation stage to the propagation stage therefore occurs after shorter times as the number of thermal cycles is increased, Figure 19.

Erosion

The time at which the transition from the initiation stage to the propagation stage takes place is reduced when erosive conditions are present in addition to the conditions causing hot corrosion attack, Figure 16. Particulate impact damages the oxide that is formed during the initiation stage and the result is the same as for effects produced by thermal cycling. It has been found, however, that erosion-hot corrosion (propagation stage) conditions interact such that the combined effect is substantially greater than the sum of these two processes acting independently[19]. It appears that erosion accelerates hot corrosion attack (propagation stage) by removing portions of the porous scale which, when present, absorbs the salt and inhibits it from wetting the alloy surface, Figure 20. Hot corrosion causes erosion to be more effective by causing portions of the alloy to be undercut by corrosion product which are then more easily dislodged from the alloy by the impacting particles, Figure 21.

Specimen Geometry

It has been observed that hot corrosion attack frequently is initiated at the edges of specimens, Figure 22. Such results indicate that there are certain configurations of the oxide scale that form beneath the Na_2SO_4 layer, Figure 8, which are more susceptible to damage and penetration by the Na_2SO_4 than others. It is rather common to observe the spalling of oxide scales initiating at the sharp angles of specimens or service hardware. Hence, the observed influence of specimen geometry on the transition from the initiation stage to the propagation stage of hot corrosion attack is to be expected.

Propagation Stage of Hot Corrosion Attack

The preceeding discussion shows that there are a great many factors which influence hot corrosion attack. Such a situation is partly responsible for what appears to be divergent results obtained by investigators studying hot corrosion, since the experimental conditions usually are not identical.

While there are numerous factors which affect the initiation of hot corrosion attack and precondition alloys for the onset of the propagation stage, the mechanisms which are operative in the propagation stage are not unmanageable. As indicated in Figure 23, results obtained from hot corrosion tests indicate the propagation stages for degradation of alloys with salt deposits fall into three general categories. In one of these categories the salt is innocous and degradation in the propagation stage proceeds by the mechanism determined by the alloy and the gas. Such a situation is likely to occur with porous, solid deposits through which the gas can easily penetrate. (In principle it is possible that the salt could produce beneficial effects, e.g. decrease growth rate of scale via doping, and cause the onset of the propagation stage to be delayed. No clear cut example of such an effect has been observed). The other two categories involve degradation mechanisms which are different from those that occur in the absence of salt deposits. One category requires the salt, or a product of the salt-alloy-gas reaction, to be liquid. Reaction between elements in the alloy and components from the gas in the presence of the liquid results in the formation of nonprotective reaction products. The nature of the reactions that take place under such conditions are similar to those where surfaces are cleaned by using salt baths for descaling

or fluxes [20,21]. Hence, this category of the propagation stages has been labeled salt fluxing reactions. The final category involves propagation stages where a component from the salt is added to the alloy, or reacts with the alloy or its corrosion products, such that nonprotective reaction product barriers are developed. This category of the propagation stages can be called salt component-induced hot corrosion, or degradation resulting from salt component-alloy reactions.

In the following, propagation stages included in the general categories of salt fluxing reactions and salt component-induced degradation will be discussed in some detail. These degradation processes can be explained most effectively by considering effects produced by a given salt, namely, Na_2SO_4. This salt is very often a major component of deposits that have been observed to initiate hot corrosion attack. Hence the experiments performed in this study used primarily Na_2SO_4 deposits. The hot corrosion theory that is presented in the present paper is applicable therefore to deposits having Na_2SO_4 as a major component, however, the fundamental concepts are believed to be generally valid.

Salt Fluxing Reactions

Some of the first proposals that protective oxide scales could be removed from the surfaces of alloys by molten deposits were generated in studies concerned with fireside corrosion in boilers [22]. In these investigations the corrosion observed in certain metal temperature regimes was associated with certain types of deposits, in particular, alkali metal pyrosulfates (e.g. $Na_2S_2O_7$) at temperatures between about 250°-430°C, alkali metal-iron

trisulfates (e.g. $Na_3Fe(SO_4)_3$) between 480° - 730°C, and alkali sulfates at temperatures above 750°C. A point of concern in the studies of the mechanisms for fireside corrosion was that the measured SO_3 pressures in the gas streams were usually much lower than those required to form pyrosulfates and trisulfates. It was proposed that localized SO_3 pressures over deposits were much higher than the measured values due to catalytic activity of the deposits. Recent studies[23] have shown that SO_3 production is indeed a function of boiler fouling, increasing as the amount of deposits increases.

At elevated temperatures comparatively high SO_3 pressures are required to form sulfates of elements such as nickel, cobalt and aluminum. Furthermore, SO_3 pressures are lower for the same amount of sulfur in the gas stream. Sulfur trioxide can therefore be expected to play a progressively less dominant role as the temperature is increased and investigators began to develop mechanisms not involving SO_3 to account for hot corrosion attack at temperatures above about 750°C.

Bornstein and DeCrescente[3] were among the first to propose that hot corrosion of alloys involved a basic fluxing process, as opposed to the lower temperature acidic fluxing process involving SO_3. It was proposed that protective oxide scales were destroyed as a result of reactions with oxide ions in the salt where the oxide ions were produced by removal of sulfur from the Na_2SO_4. Goebel et al[7] extended the high temperature fluxing reactions to acidic processes, where the component to make the salt acidic was proposed to be certain oxides of elements in the alloys (e.g. MoO_3, WO_3), and suggested that porous, oxide scales may be formed during either basic or acidic fluxing by precipitation from the molten salts into which these oxide scales had initially dissolved.

Goebel et al[7] proposed that the dissolution and reprecipitation processes were controlled by the oxide ion activity of the melts which, in turn, was regulated by the removal of sulfur from the salt (Na_2SO_4) or by the addition of oxides of certain metals to the salt (e.g. MoO_3, WO_3). Rapp and Goto[24] proposed that the dissolution-precipitation process may occur whenever a negative gradient exists in the solubility of the oxide across the salt film and that such gradients may be developed by the electrochemical reduction reaction that accompanies oxidation of the metallic elements. The Rapp-Goto proposal is therefore a more general, and a more powerful, criterion for oxide scale dissolution and reprecipitation.

In the present paper the most important objective is to present as complete and as self-consistent a picture of the hot corrosion process as possible. It therefore will be attempted to show that, as with all hot corrosion processes, the type of fluxing mechanism depends upon experimental conditions. Hence, experimental results will be presented to identify the types of fluxing processes that are relevant to the hot corrosion of metals and alloys. As these processes are introduced and discussed, possible mechanisms will be described to provide credibility, however, the point to be emphasized is the types of fluxing reactions and how the different fluxing reactions are interrelated as opposed to the details of specific mechanisms.

Thermodynamic Stability Diagrams

Before discussing the types of fluxing processes that are relevant to hot corrosion, it is helpful to examine thermodynamic stability diagrams as a means of predicting the fluxing reactions that are feasible. In

Figure 24a a schematic diagram is presented defining the regions of stability of some of the phases in the Na - O - S system as a function of oxygen and SO_3 pressures. The construction of such diagrams has been discussed in previous papers[6,7]. The Na_2SO_4 region of this diagram describes the compositions of Na_2SO_4 that can be deposited on materials where a specific composition has been indicated by a dot. When the Na_2SO_4 covers the alloy as a layer, Figure 21b, as is often the case, components from the gas must diffuse through the Na_2SO_4 to react with the alloy. Hence the composition of the Na_2SO_4 adjacent to the alloy can become significantly different from that in equilibrium with the gas as indicated schematically with arrows in Figures 24a and b. Three compositional changes of importance can take place, in particular, the salt can become more basic, or more acidic, and it almost always becomes more sulfidizing as a result of the lower oxygen activity.

The process by which the salt becomes more sulfidizing is straightforward. The oxygen, sulfur and SO_3 pressures are interrelated by the following expression:

$$P_{O_2}^{3/2} \quad P_{S_2}^{1/2} / P_{SO_3} = K \qquad (1)$$

and, providing the SO_3 is not decreased substantially, the sulfur pressure is increased as the oxygen pressure is decreased, Figure 24a. There are at least two processes by which the Na_2SO_4 becomes more basic (i.e. production of oxide ions). One involves the removal of sulfur from the Na_2SO_4 by the alloy whereby

$$SO_4^{2-} \longrightarrow S(\text{alloy}) + \frac{3}{2} O_2 + O^{2-} \qquad (2)$$

and oxide ions are produced. The other process arises because the oxide product formed on the surface of the alloy may donate oxide ions to the salt as proposed by Rapp and Goto[24]. While the oxide that is attempting to be formed at the alloy surface may donate oxide ions to the salt, it could also react with existing oxide ions by reactions such as

$$MO + O^{2-} \longrightarrow MO_2^{2-} \qquad (3)$$

This latter reaction is a means by which the salt can become more acidic.

The question of whether the oxides beginning to be formed upon the surfaces of alloys will make the salt basic or acidic is determined by the oxide ion concentration of the as-deposited salt (defined by that at the salt-gas interface) and the affinity of the oxides and their metal ions for oxide ions. The affinities of various relevant metals for oxide ions can be described by using stability diagrams superimposed on the Na_2SO_4 region of Figure 24a. In Figure 25 some diagrams for nickel, aluminum and chromium are presented. These diagrams indicate the phases which are stable in Na_2SO_4. It can be seen that there are acid melts (Ⓧ) for which NiO is more effective in developing basic conditions than Al_2O_3. On the other hand, there are basic melts, (•), for which Al_2O_3 is more effective in making acidic conditions than Cr_2O_3.

Examples of basic and acidic fluxing will be presented in the following sections and some superimposed diagrams will be used to help account for results. It is important to emphasize that care must be exercised when using superimposed diagrams. For convenience, a number of diagrams have been superimposed on the same Figure, Figure 25. These diagrams have been con-

structed with no consideration of the interaction that can occur between the individual metals[25] and therefore in the case of alloys they can only be used to indicate the phases of the metals that may be stable in Na_2SO_4 at specific SO_3 and oxygen pressures.

Basic Fluxing

A feature that is common to basic fluxing is that the total amount of attack becomes greater as the amount of the salt is increased, Figure 1. The microstructural features that are developed during basic fluxing are dependent upon the alloy composition. Photographs illustrating what is believed to be degradation due to pure basic fluxing are presented in Figure 26. The microstructures shown in Figure 26 were developed by using a large amount of Na_2SO_4 and a Ni-8Cr-6Al alloy. Similar structures can be developed in this alloy using smaller amounts of Na_2SO_4 but it is necessary to examine the specimens during the early stages of attack, Figure 27a because the microstructural features change with time as the Na_2SO_4 becomes depleted of oxide ions, Figure 27b.

The sequence of events that take place during pure basic fluxing can be reconstructed from the photomicrographs presented in Figures 26 and 27 and analyses of the salt after test. The balls of nickel sulfide on the surface of the alloy, Figure 26a, show that the oxygen pressure must be low while the sulfur pressure is high enough to form nickel sulfide. At the corrosion front, aluminum and chromium are being removed from the alloy by the Na_2SO_4 and virtually pure nickel is being left behind, Figure 26c and X-ray images. In addition, analyses of the solutions obtained by washing test specimens during the very early stages of attack show that the solution is basic and contains

soluble aluminum and chromium, Table II. It therefore appears that at the beginning of attack an oxygen gradient is developed across the Na_2SO_4. It should be noted that in such tests the Ni-15Cr-6Al alloy is not attacked, Figure 10. Hence the oxygen gradient must be established because a continuous layer of Cr_2O_3 and Al_2O_3 is not developed on the Ni-8Cr-6Al alloy as indicated schematically in Figure 28a. As a result of this gradient in the oxygen pressure, the sulfur activity, Figure 24a, is increased and nickel sulfide is formed at the surface of the alloy, Figure 28b. The oxide ion concentration in the Na_2SO_4, which has been increased due to the nickel sulfide formation, reaches values at which the Al_2O_3 and Cr_2O_3 dissolve into the Na_2SO_4, Figure 28b. A process is therefore developed where sulfate ions diffuse toward the alloy and as regions of lower oxygen pressure are approached these ions sulfidize nickel whereby oxide ions are produced which in turn react with Al_2O_3 and Cr_2O_3 to form products that are soluble in the oxide ion enriched Na_2SO_4, Figure 28c. The aluminate and chromate ions diffuse away from the alloy and are precipitated at higher oxygen pressures as Al_2O_3 and Cr_2O_3 along with oxide ions that diffuse out into the bulk Na_2SO_4 in exchange for sulfate ions The important feature of the process is the compositional differences that are developed across the Na_2SO_4, Figures 28c and d. Schematic phase stability diagrams, Figure 28d, can be constructed to account for the various phases observed in the corrosion product, Figure 28c. As long as there is a supply of sulfate ions from the Na_2SO_4 the hot corrosion process proceeds at approximately a linear rate, Figure 1, but as the source of sulfate ions is depleted the attack diminishes and oxygen becomes more plentiful in the corrosion product. The nickel sulfide particles in the scale become oxidized

and some of the sulfur from this process moves deeper into the alloy where, in the case of a Ni-8Cr-6Al specimen, chromium sulfide is formed, Figure 27b.

The example of basic fluxing that has been presented was for Na_2SO_4 - induced hot corrosion in air or oxygen. In a gas containing SO_3 the corrosion process could be significantly different but the degradation will still be affected by the composition of the alloy. For some alloys the melt may become so basic at the Na_2SO_4-alloy interface that the SO_3 pressure in the gas may exert no significant effect but in others, as will be shown subsequently, it may play a very important role.

The particular example of basic fluxing which has been presented was given to document as conclusively as possible that degradation via a basic fluxing process can occur. It must be emphasized that the generation of oxide ions necessary for the attack need not arise from the formation of nickel sulfide as was the case in this example. Formation of other sulfides (e.g. chromium sulfide) in alloys can lead to oxide ion production in Na_2SO_4. More importantly, as suggested by Rapp and Goto,[24] oxide ion production need not occur as a result of sulfur removal from the Na_2SO_4. In the Rapp and Goto model increased basicity is proposed to occur because of the reduction process that accompanies oxidation of the elements in the alloy. In this model the hot corrosion process involves dissolution and reprecipitation of oxide where the criterion for such a condition to exist is a negative gradient of the oxide solubility in the salt at the oxide-salt interface.

Data are available which suggest that reprecipitation of oxide does occur during hot corrosion of some metals. For example, during the Na_2SO_4 - induced hot corrosion of cobalt in oxygen an oxide slag floating on the salt has been

observed, Figure 29a. Beneath the salt the CoO is composed of a network of pores, Figure 29b, and it appears that once the Na_2SO_4 penetrates the oxide scale conditions are developed whereby the scale is stripped from the metal, Figures 29c and d. A model for the hot corrosion of cobalt induced by a thin ($\sim$ 1 mg/cm^2) layer of Na_2SO_4 is presented in Figure 30. Upon heating a Na_2SO_4 - coated specimen to a test temperature near about 1000°C, a layer of CoO is formed before the Na_2SO_4 melts, Figure 30a. After the Na_2SO_4 melts an oxygen gradient is developed across the liquid which, in turn, causes the sulfur activity over the CoO to be increased. Sulfur may then diffuse through the CoO and form sulfide at the Co-CoO interface which indeed has been observed. Oxide ions should therefore be produced in the Na_2SO_4 which can react with the oxide scale to form CoO_2^{2-} ions that then diffuse to the Na_2SO_4-gas interface and decompose due to the lower oxide ion activity, Figure 30b. This hot corrosion mechanism is similar to that described for Ni-8Cr-6Al except the sulfide phase would be formed beneath the oxide scale rather than within the corrosion product. By using the Rapp and Goto model it is not necessary to have the sulfur go into the metal in order to produce oxide ions. It can be proposed that the Na_2SO_4 composition is such that it becomes more basic at the CoO-Na_2SO_4 interface due to the reduction of oxygen (i.e. $1/2\ O_2 + 2e = O^{2-}$). In addition, it can be proposed that the oxide solubility in the Na_2SO_4 decreases as the salt becomes less basic. The oxide will therefore reprecipitate in the Na_2SO_4 near the gas interface, Figure 30b.

Regardless of the mechanism by which the oxide is dissolved and reprecipitated, hot stage microscope observations made during the hot corrosion

of cobalt show that the oxide scale is eventually penetrated in localized areas and a gas is evolved from the Na_2SO_4. It appears that penetration of the scale by Na_2SO_4 causes the oxygen pressure to be reduced and the sulfur pressure to be increased whereby the pressure of SO_2 approaches unity. Beneath the scale, oxide ions are produced not only because of sulfide formation but also due to SO_2 evolution and consequently the scale is stripped from the metal surface, Figure 30c. Meier[26] has proposed that sulfide formation at the oxide-metal interface may be sufficient to result in stripping of oxide scales. The scales formed during the hot corrosion of cobalt, as well as nickel,[6] are composed of discrete layers of oxide, Figures 29c and d. It therefore appears as though the penetration and stripping process is a cyclic process, Figure 30d. Fluxing of the scale, as a result of sulfur removal from Na_2SO_4, would be cyclic since large amounts of oxide ions would be formed as the oxide scale is initially penetrated. Meier's proposal on sulfide formation giving rise to stripping would also be cyclic in nature.

The basic fluxing models involving dissolution and reprecipitation, and oxide stripping permit large amounts of attack to be produced by comparatively small amounts of Na_2SO_4. For example, if it is assumed that a localized penetration of 5 μm in diameter causes detachment of an oxide layer, with a thickness of 3 μm, over an area of 10^4 square microns, then the molar ratio of nonprotective oxide to available Na_2SO_4 is about 3 to 1 for a specimen with 1 mg/cm^2 of Na_2SO_4. Moreover, the number of moles of oxide ions required to form the hole is at least 2 orders of magnitude less than the number of moles of oxide ions available in the Na_2SO_4 over 10^4 square microns. While both oxide stripping and reprecipitation can be used to account for the observation that the molar ratio of nonprotective oxide to Na_2SO_4 deposited on

specimen surfaces is commonly between 10 and 100, it is important to emphasize that basic fluxing usually does not proceed indefinitely. One reason for this, first proposed by Reising,[8] is that as the thicknesses of nonprotective scales are increased, the Na_2SO_4 is absorbed into the porous scale rather than remaining on the metal surface and accelerated attack therefore stops. (The reduced hot corrosion observed in the burner rig tests where α-Al_2O_3 was deposited along with Na_2SO_4 may be an example of such an effect, Figure 16). Another reason which applies only for hot corrosion in air is that the reprecipitation of oxide causes the oxide ion concentration at the Na_2SO_4-gas interface to be increased and saturation must eventually occur.

Binary alloys containing chromium are not attacked very substantially via the basic fluxing degradation process. (These types of alloys are susceptible to hot corrosion via sulfur-induced attack which will be discussed subsequently). This is surprising because Cr_2O_3 reacts with Na_2SO_4 in air at temperatures of approximately 1000°C to form $NaCr_2O_4$. In discussing these alloys it is useful to consider alloys with low chromium concentrations on which continuous layers of Cr_2O_3 are not formed, and then alloys with higher chromium contents where continuous Cr_2O_3 layers are developed. In nickel or cobalt alloys with low chromium concentrations the external scales are NiO or CoO and these oxides are susceptible to basic fluxing. During the initial phases of attack, however, these oxides are competing with Cr_2O_3 for oxide ions. Since the Cr_2O_3 has a greater affinity for oxide ions, as was first noted by Bornstein and DeCrescente,[3] the NiO or CoO forms on the specimen surface as a continuous and protective layer. The condition that the Cr_2O_3 reacts with oxide ions is not sufficient by itself to stop or

inhibit attack. Hot corrosion attack is occurring via dissolution of Cr_2O_3 and if there is not enough Cr_2O_3 then the NiO or CoO will eventually react. It is therefore necessary for the initial reaction of the melt with Cr_2O_3, in preference to NiO or CoO, to result in a situation where, after the Cr_2O_3 is consumed, the Na_2SO_4 cannot return to a composition at which reaction with NiO or CoO can occur. One possibility is that the thicknesses of NiO or CoO become sufficiently large such that sulfur is not removed from the Na_2SO_4 by the metal and therefore oxide ions are not produced. Indeed, preoxidation of nickel or cobalt can be used to stop hot corrosion attack providing the preformed oxides are not cracked during application of the Na_2SO_4.

The lack of hot corrosion attack of alloys with higher chromium concentrations for which continuous layers of Cr_2O_3 are formed can be explained by using the model of Rapp and Goto if it is supposed that the solubility of Cr_2O_3 is less at the Cr_2O_3-Na_2SO_4 interface than at the Na_2SO_4-gas interface. Chromia will react with the Na_2SO_4 but it will become saturated and a continuous layer of Cr_2O_3 will then form on the alloy surface. Stroud and Rapp[27] have measured the solubility of Cr_2O_3 in Na_2SO_4 at two oxygen pressures. These data have values for which the solubilities across the Na_2SO_4 indeed can be such that a dissolution and reprecipitation fluxing process is not possible.

Other elements in binary nickel and cobalt base alloys can produce effects similar to chromium at low concentrations. Aluminum, molybdenum or tungsten can be used to prevent the attack of nickel or cobalt via basic fluxing. At concentrations of aluminum for which continuous α-Al_2O_3 scales are formed, however, this oxide is susceptible to basic fluxing, Figure 4. As will be shown subsequently, the oxides of molybdenum or tungsten can make the Na_2SO_4 too acid and degradation via acidic fluxing becomes possible.

Acidic Fluxing

A feature of acidic fluxing that differs from basic fluxing is that acidic-induced attack is usually self-sustaining. Hence small amounts of deposits produce much more attack for acidic fluxing compared to basic fluxing. Ash or salt deposits can be made acidic by two different processes. One process (alloy-induced acidity) has already been described under basic fluxing. It involves the formation of oxides on the surface of alloys which have a great affinity for oxide ions (e.g. MoO_3, WO_3, Cr_2O_3). The other process (gas-induced acidity) occurs because of a species in the gas that makes the salt acidic. The most common gas components that make the deposit acidic are SO_3 and V_2O_5 which are often introduced to the gas via combustion of fuels containing sulfur and vanadium. At this point it is worth noting that a situation analogous to gas-induced acidity was not considered for basic fluxing. In principle, hot corrosion produced by gas-induced basicity is also possible. The impurities which are usually present in fuels, however, normally are not capable of producing highly basic salts.

Alloy-Induced Acidic Fluxing

The weight change versus time data presented in Figure 31 compares the hot corrosion attack of Co-25Al and Co-25Al-12W alloys. The hot corrosion propagation mode for the Co-25Al alloy proceeds by combined effects of basic fluxing and sulfidation. The sulfidation propagation mode as well as interaction between basic fluxing and sulfidation will be discussed subsequently. At this point it is sufficient to note that the Na_2SO_4 - induced hot corrosion of Co-25Al involves localized penetration of the Al_2O_3 scales formed on these

alloys via a basic fluxing process. Subsequent degradation after penetration of the Al_2O_3 by the Na_2SO_4 appears to involve oxidation of aluminum sulfides. The addition of tungsten to the Co-25Al alloy causes the time required to initiate hot corrosion attack to be extended, Figure 31, (the weight losses observed during the first 50 hrs. of attack are believed to result from vaporization of Na_2SO_4 and evolution of SO_3 as WO_3 is dissolved into the Na_2SO_4). Once the attack is initiated, however, it is self-sustaining in the alloy with tungsten and hence more attack takes place compared to Co-25Al, Figure 31. The tungsten in the Co-25Al-12W alloy is producing effects similar to those of chromium in nickel or cobalt alloys with low chromium concentrations, in particular, WO_3 is preventing the basic fluxing of Al_2O_3 by preferentially reacting with oxide ions. The eventual self-sustaining attack that occurs is an example of alloy-induced acidic fluxing due to tungsten. The time required to initiate alloy-induced acidic hot corrosion of Co-25Al-12W is greatly reduced when Na_2SO_4-coated specimens are annealed in argon prior to exposure in oxygen, Figure 31. This result shows that a reduction of the oxygen pressure in the Na_2SO_4 favors the introduction of tungsten into the Na_2SO_4. Washing of specimens after the alloy-induced attack has been initiated causes the attack to stop, Figure 31. It is apparent that the salt deposit is required for the attack to continue even though tungsten from the alloy plays a significant role in the corrosion process. Microstructural features, typical of the alloy-induced acidic propagation mode, are presented in Figure 32 for the Co-25Al-12W alloy and thick corrosion products are quite evident. An important feature is that there is a zone in the oxide scale immediately adjacent to the alloy which is enriched in tungsten, Figure

32 b, c and d. Other elements were also present in this zone, in particular, cobalt, aluminum, and sodium. Sulfur was detected throughout the scale along with sodium, and sulfide particles were present in the alloy just beneath the scale, Figure 32b. The scale away from the tungsten enriched zone contained relatively uniform distributions of cobalt and aluminum with discrete layers of tungsten enrichment.

The features observed for Co-25Al-12W alloy have been observed for numerous other alloys (nickel-, cobalt or iron base) containing tungsten, molybdenum or vanadium. However, the mere presence of these elements does not mean that such features will be developed during hot corrosion attack. Usually, certain minimum concentrations of these elements are required, but the exact amount necessary for the attack is also dependent upon other elements in the alloy. For example, during isothermal oxidation with Na_2SO_4, 12% tungsten causes alloy-induced acidic fluxing of Co-20Cr-12W but not Co-25Cr-12W, Figure 33. During cyclic testing, however, the Co-25Cr-12W, as well as a nickel-base alloy containing the same amount of chromium and tungsten, undergo alloy-induced acidic hot corrosion, Figure 34.

The Na_2SO_4-induced hot corrosion of a Ni-8Cr-6Al-8Mo alloy has been studied in some detail because these are the concentrations of chromium, aluminum and molybdenum in the nickel-base superalloy B-1900, an alloy that is very susceptible to hot corrosion attack. Weight change versus time data obtained for the oxidation of Na_2SO_4 - coated specimens of Ni-8Cr-6Al-6Mo and Ni-8Cr-6Al are compared in Figure 35. A comparison of the behaviors of these two alloys will be made in a subsequent section where the interaction

between basic and acidic fluxing processes will be considered. At this point, it is sufficient to state that the Ni-8Cr-6Al-6Mo alloy eventually exhibits alloy-induced acidic hot corrosion attack and the microstructures obtained during this attack are good examples to illustrate the features of alloy-induced hot corrosion. The scales that are formed on this alloy are thick and exhibit a layered texture, Figure 36. At the scale-alloy interface, a thin zone of sulfide particles is evident in the alloy and the scale immediately adjacent to the alloy, Figure 36b, contains Na, S, O, Mo, Ni, Cr and Al, Figure 36c. It appears as though this zone may be a solution of Na_2SO_4 and Na_2MoO_4 into which Al_2O_3, Cr_2O_3 and NiO are dissolved. The molybdenum enriched areas of the scale are restricted to a narrow zone about a few tenths of a millimeter thick immediately adjacent to the alloy. Beyond this zone the scale contains more or less uniform distributions of all the elements in the alloy with the molybdenum concentration substantially below that of the enriched zone. The layered texture of the scale, Figure 36a, apparently did not arise from gross compositional differences but rather from different amounts of porosity of the scales.

The microstructures of degraded Ni-25Al-12W and Ni-8Cr-6Al-6Mo are very similar. Both have undergone alloy-induced acidic hot corrosion which consists of the following important steps. Oxides of the metals tungsten, molybdenum and vanadium dissolve into the Na_2SO_4 forming tungstates, molybdates and vanadates and some SO_3 is displaced from the Na_2SO_4. The addition of the refractory element oxides to the Na_2SO_4 depends on the oxidation characteristics of the alloy. For some alloys, the refractory elements are oxidized at the very beginning of the oxidation process, whereas for others selective oxidation of other elements results in longer exposure times before the refractory element oxides are available to react with the Na_2SO_4. The Na_2SO_4 solutions

gradually become enriched in the oxides of these metals since such solutions probably have a high solubility for the oxides, as evidenced by the large amount of WO_3 that can dissolve into Na_2WO_4 (greater than 50 mole percent at 750°C)[28]. It appears as though Al_2O_3, Cr_2O_3 and CoO can dissolve into these refractory metal oxide enriched melts by donating oxide ions to the melts. The reactions that may take place are

$$2Al + 3W + 6O_2 \rightarrow Al_2O_3 + 3WO_3 = 2Al^{3+} + 3WO_4^{2-}$$

$$2Cr + 3W + 6O_2 \rightarrow Cr_2O_3 + 3WO_3 = 2Cr^{3+} + 3WO_4^{2-}$$

$$Co + W + 2O_2 \rightarrow CoO + WO_3 = Co^{2+} + WO_4^{2-}$$

These ions diffuse through the solution (i.e. the zone enriched in refractory metal, Figures 32 and 36) to the outer zone of the melt where the reactions listed above proceed in reverse direction due to the lower activity of the refractory metal oxides in this region as a result of the loss of the refractory metal oxides to the gas phase. Hence, oxides of Al_2O_3, Cr_2O_3 and CoO are dissolved at one side of the melt, Figure 36b, (alloy-melt interface) and reprecipitated as a nonprotective scale at the other side (melt-porous oxide). In addition, the melt is continually enriched in the refractory metal oxide, however, the precipitation process does result in some of the melt being incorporated into the outer, porous part of the scale, Figures 32c and d.

The most important features of alloy-induced acidic fluxing is that a zone of liquid is formed immediately above the alloy due to the accumulation of certain refractory metal oxides (e.g. MoO_3, WO_3, V_2O_5) in the Na_2SO_4, and the oxides normally relied upon for protection against attack (e.g. Al_2O_3,

Cr_2O_3, NiO, CoO) become nonprotective due to a solution-reprecipitation process. This attack is self-sustaining because a small amount of salt appears adequate to cause the development of the refractory metal oxide zone. It is important to emphasize, however, that while very small amounts of salt cause very large amounts of attack, the presence of the salt is necessary for the attack to continue. For example, the alloy-induced acidic hot corrosion stops after water washing, Figure 31. When data is presented to show the processes which take place during the initiation of alloy-induced acidic hot corrosion, it will be shown that the sulfate ion is removed from the melt rather quickly but sodium remains during the attack. It is believed that the sodium permits a liquid phase to be established at activities of the refractory metal oxides less than unity.

The effects produced by the refractory metal oxides in Na_2SO_4 and the resulting solution and reprecipitation of oxides can be rationalized to some extent by using stability diagrams. Stability diagrams identifying the regions of Na_2SO_4 where basic or acidic fluxing reactions involving aluminum may occur are presented in Figure 37 for two temperatures. The SO_3 pressures at which acidic reactions may occur are greater than one atmosphere at the higher temperature. Since alloy-induced acidic fluxing is observed at these temperatures, it does not seem reasonable to suppose that the refractory metal oxides cause such attack by producing high SO_3 pressures. It has been determined that when Al_2O_3 is exposed to Na_2SO_4 in air at 1000°C no reaction can be detected after 3 hrs. of exposure. If, however, MoO_3 vapor at an activity of about 0.1 is added to the gas stream, a significant amount of reaction occurs between the melt and the Al_2O_3[29]. It therefore appears that the refractory metal oxides cause acidic fluxing reactions for oxides such as Al_2O_3 and Cr_2O_3 to become favorable at lower SO_3 pressures. Such a condition is indicated schematically in Figure 37b.

Gas Phase-Induced Acidic Fluxing

The experimental data presented in Figure 12 show the importance of the gas composition to the hot corrosion attack of a CoCrAlY coating alloy. Substantial attack of this alloy is observed at rather low temperatures (e.g. ~ 700°C) but the rate of attack is decreased abruptly when SO_3 is removed from the gas. After thousands of hours, this alloy is not noticeably attacked using Na_2SO_4 in air, Figure 38a, but substantial attack is observed within hours when SO_3 is added to the gas, Figure 38b. The attack of this alloy requires a Na_2SO_4 deposit since exposure to gases containing SO_3 and O_2 without Na_2SO_4 does not produce significant degradation, Figure 38c.

Microstructural features observed via optical metallography and scanning electron microscopy can be used, along with thermodynamic considerations, to develop a model by which SO_3 and Na_2SO_4 cause the hot corrosion attack of a CoCrAlY alloy. A zone enriched in cobalt is usually evident at the corrosion product-gas interface, Figure 39a. X-ray diffraction analysis of this zone of the corrosion product indicates that the cobalt is present as an oxide, but it is not unusual to also detect sodium-cobalt sulfates (e.g. $Na_2Co(SO_4)_2$). Within the corrosion product, two types of ghost images are often observed, Figure 40a and b. These images are most clear at the corrosion product-alloy interface. Platinum marker experiments indicate that the corrosion product is formed predominantly via inward diffusion, of an oxidant, and outward diffusion of cobalt. The ghost images, which are apparent due to compositional differences in the corrosion product, become more diffuse as diffusional processes lessen these compositional gradients.

One type of ghost image is parallel to the corrosion front and appears to define the position of the corrosion front at earlier times in the corrosion process, Figure 40a. Such ghost images, which can be called corrosion front ghosts, appear as sequential dark and light zones in electron backscatter images, Figure 40a. Microprobe analyses show that the dark zone is enriched in aluminum and light zone in chromium, Figure 40d. Oxygen is present in both zones, as well as detectable amounts of cobalt, sodium and sulfur, Figure 39. A larger concentration of sulfur was always detected in the corrosion product just adjacent to the corrosion front. The sodium could always be removed from the corrosion product by using water in the metallographic preparation of specimens. This procedure did not remove the sulfur in the corrosion product adjacent to the corrosion front, but often caused the sulfur to be removed from the outer part of the corrosion product.

The other type of ghost image is coincidental with the position of the α-chromium phase of the CoCrAlY alloy prior to the formation of corrosior product, Figure 40b. This image also is composed of dark and light zones, but the proportion of the light zone is greater than the dark due to the larger amount of chromium in the α-chromium phase which it replicated, Figure 40c.

At temperatures between about 600° to 700°C, diffusion zones in the alloy, in advance of the corrosion front, signifying the preferential removal of certain elements from the alloy, usually are not evident, Figure 40a and b. At the corrosion front, the dark zone of the corrosion product is adjacent to the alloy, Figure 41, and it undercuts pieces of alloy which subsequently appear to be converted to the light zone material in the corrosion product, Figure 41 (arrows).

As the temperature is increased, zones in the alloy depleted of aluminum and chromium are more readily observed, Figure 42. Chromium sulfide particles are also evident within these zones and the rate of attack is decreased, Figure 18.

The results obtained from the microstructural examination of CoCrAlY specimens that were degraded via gas-induced hot corrosion at temperatures between 600°-700°C permit the following remarks to be made about this degradation mechanism:

- Na_2SO_4 is distributed throughout the corrosion product.
- Cobalt diffuses through the corrosion product to the gas interface where oxides and sulfates of this element are formed.
- Chromium is converted to oxide close to the corrosion front and little diffusion of this element is evident.
- Aluminum is preferentially removed from the alloy by the hot corrosion process and it appears not only to be associated with sulfur and oxygen immediately adjacent to the corrosion front but also seems to be present as oxide throughout the remainder of the corrosion product.
- Yttrium is difficult to detect in the corrosion product but can be found in the water used to wash tested specimens.

The distribution of Na_2SO_4 uniformly throughout the corrosion product indicates that the Na_2SO_4 was liquid at the temperature where the hot corrosion took place. Studies of Na_2SO_4 deposits in gases containing SO_3 and oxygen show that the melting point of Na_2SO_4 is depressed as the SO_3 pressure is increased[30]. More importantly, however, the melting point of liquid solutions of Na_2SO_4 and $CoSO_4$ or $NiSO_4$ can be substantially below the melting point of Na_2SO_4 (e.g. the melting point of a Na_2SO_4 - $CoSO_4$ solution containing 50 mole % $CoSO_4$ is about 600°C)[28]. During the hot corrosion of CoCrAlY, covered with Na_2SO_4, in a gas containing SO_3 and oxygen it appears that liquid solutions of Na_2SO_4 - $CoSO_4$ having melting points as low as about 600°C may be formed. Even though Al_2O_3 scales are formed on CoCrAlY alloys during oxidation, some cobalt oxide will be formed as the Al_2O_3 is becoming continuous. Visual examination of CoCrAlY specimens as a function of time shows that hot corrosion attack often is initiated after the specimens have been subjected to a number of test cycles. Cracking of the Al_2O_3 scale may be necessary before sufficient amounts of cobalt oxide are formed to permit the deposit to become liquid. As a result of such a condition, gas-induced acidic fluxing can often result in very localized pit-type attack, Figure 39a. Such degradation microstructures are very similar to pits developed during aqueous corrosion as a result of local cell activity. In the case of gas-induced acidic attack of CoCrAlY however, the localized attack can be made much more uniform by vapor honing the specimen surface prior to exposure in the corrosion test to remove the preformed oxide scale, Figure 39c. When the preformed oxide is removed, cobalt oxide is formed, more or less uniformly, over the surface during the initial stages of oxidation and a liquid Na_2SO_4-$CoSO_4$ solution covers most of the specimen surface.

A schematic model to describe the gas-induced acidic fluxing of a CoCrAlY alloy is presented in Figure 43. At low temperatures the salt becomes molten as $CoSO_4$ dissolves into it, Figure 43a. Beneath this liquid layer the alloy begins to react with components in the liquid. The principal reaction is one of oxygen removal from the melt since the most favorable reactions for elements in the alloy are those involving oxide formation. It has been determined that SO_3 is much more mobile in Na_2SO_4 than oxygen[31]. Consequently, it is reasonable to propose that gradients in both oxygen and SO_3 are developed across the liquid layer with SO_3 also supplying oxygen to react with the elements in the alloy, Figure 43b. The processes by which the SO_3 and oxygen diffuse through the liquid layer is not known, but it would seem reasonable that the SO_3 combines with sulfate ions and diffuses as pyrosulfate ions ($S_2O_7^{2-}$) whereas oxygen may be dissolved in the liquid as atoms.

The sequence of corrosion front ghosts, Figure 40a, composed of alternating zones enriched in aluminum and chromium are formed by the selective removal of aluminum from the alloy, Figure 43b, and then conversion of the chromium to oxide in situ, Figure 43c. Cobalt is not present as a discrete phase at the surface of the alloy since the oxygen pressure is too low. It dissolves in the liquid and diffuses to the outer zone of the liquid where oxides are formed and some of this oxide is converted to sulfate which is soluble in the Na_2SO_4, Figure 43c. Aluminum removal from the alloy occurs by dissolution in the liquid followed by reprecipitation at higher oxygen pressures as it diffuses away from the alloy surface, Figure 43c. The precipitated Al_2O_3 forms the aluminum rich zone of the corrosion product, and conversion of chromium, remaining in the aluminum depleted alloy, to oxide gives rise to the chromium rich zone, Figure 43d. This latter zone can be formed, not only parallel to the corrosion front

due to preferential removal of aluminum from the alloy, but also as extensions of the α-cobalt phase in the alloy, Figure 43d.

The preferential removal of aluminum from the alloy and its subsequent precipitation as Al_2O_3 is believed to occur because of sulfite formation at the liquid-alloy interface where the oxygen pressure is low and then conversion of the sulfite to oxide in the liquid where the oxygen pressure is higher, Figure 43d. At low oxygen pressures the oxidation of aluminum is proposed to be accompanied by reduction of SO_3 rather than by reduction of oxygen. The existence of SO_3^{2-} ions seems plausible since, at low oxygen pressures, with a supply of SO_3 from the gas, the SO_2 pressure should be relatively high, Figure 37a, which indicates that such conditions are conducive for sulfur to be present as S^{4+}. Indeed, sulfite ions were formed in the cathode compartment when melts of Li_2SO_4 - K_2SO_4 were electrolyzed at 625°C (32). The solubility of the aluminum sulfite in the liquid and its eventual conversion to oxide has been assumed in order to account for the observed morphology of the corrosion product, but the schematic stability diagram, Figure 43e, does show that conversion of sulfite to oxide is to be expected as the oxygen pressure is increased.

As temperature is increased the likelihood of acidic fluxing reactions involving sulfite becomes less since, as indicated schematically in Figure 43e, higher SO_3 pressures are required to form sulfates and sulfites as the temperature is increased and lower SO_3 pressures exist in the gas due to a larger proportion of SO_2. Hence, as temperature is increased the gas phase-induced acidic component of the degradation becomes less, and sulfide phases are formed with increased frequency in the alloy, Figure 42a. Eventually, oxidation of these sulfides are the primary means of hot corrosion degradation.

The Rapp-Goto model[24] could be used to account for gas-induced acidic fluxing and there would be no need to postulate the supposed formation of a sulfite region. For this model to be operative the solubility of Al_2O_3 should be less in the more acidic melts. The available data[27] for the solubility of Al_2O_3 in Na_2SO_4 are not consistent with such a proposal but the data are not available for Na_2SO_4 melts exposed to extremely low oxygen pressures (e.g. $\sim 10^{-10}$ atms).

In concluding the discussion of fluxing reactions it is to be emphasized that the solution - precipitation feature of the salt fluxing processes results in substantial amounts of attack being produced by a small amount of salt. The conditions that lead to solution of the oxidized elements followed by precipitation of nonprotective reaction products are not unusual nor unique. They can be established by: the production of oxide ions resulting from the removal of sulfur from Na_2SO_4; the consumption of oxide ions due to the addition of a component with an affinity for oxide ions (e.g. MoO_3, SO_3) to the melt; or the development, in the melt, of negative gradients for the solubilities of the oxides that are normally formed on the surfaces of alloys in the absence of salt deposits[24]. A similar phenomenon has been observed for the oxidation of zinc [33]. As a result of the high vapor pressure of zinc, its oxidation proceeds rapidly when the oxide is formed as a smoke or fume above the surface of the zinc, Figure 44. As the oxygen pressure is increased, the fume is formed closer and closer to the surface of the metal and the oxidation rate increases since the zinc vapor has a shorter distance to diffuse. As the reaction site for oxide reaches the metal surface, there is a very substantial decrease in the oxidation rate because protective oxide is formed on the metal surface rather than a fume of nonprotective oxide particles above it. The solution and precipitation process

in salts is very similar to the formation of ZnO fume. The salt will be successful in causing increased attack providing it can cause the metallic elements in the alloy to react with oxygen above the alloy surface rather than on it. There are a variety of processes by which this can occur and a few have been described above. In Figure 44 a general model is presented whereby an ion in the melt allows the metallic elements to be oxidized by accepting electrons and oxide is precipitated away from the alloy surface where the oxygen pressure is higher.

Interaction Between Basic and Acidic Fluxing Processes

The previous discussion has considered basic and acidic fluxing as independent of each other. Actually these processes can affect one another. To illustrate this interaction the hot corrosion attack of two nickel-base superalloys will be considered, namely, B-1900 (Ni-8Cr-6Al-6Mo-10Co-1Ti-4.3Ta-0.11C-0.15B-0.07Zr) an alloy extremely susceptible to hot corrosion attack, and IN 738 (Ni-16Cr-3.4Al-1.75Mo-2.6W-8.5Co-3.4Ti-1.75Ta-0.012C-0.012B-0.12Zr-0.85Cb) an alloy with substantially better hot corrosion resistance. The hot corrosion attack of these two alloys in air under isothermal conditions is compared in Figure 45. Both alloys can be seen to undergo severe attack but it takes much longer to initiate this attack for IN 738. Analysis of IN 738 specimens after exposure times for which severe attack was observed indicated the hot corrosion propagation mode was similar to that of B-1900. In particular, a zone enriched in molybdenum and tungsten oxides was detected between the alloy and the nonprotective scale which caused alloy-induced acidic attack to occur.

To describe the hot corrosion attack of B-1900, results already presented for Ni-8Cr-6Al and Ni-8Cr-6Al-6Mo alloys can be used, Figure 35. The Ni-8Cr-6Al is attacked due to a basic fluxing process, Figure 27a, which eventually stops when the Na_2SO_4 is not replenished, Figure 27b. The propagation mode of attack of the Ni-8Cr-6Al-6Mo alloy has been shown to proceed due to alloy-induced acidic fluxing, Figure 36. The processes which take place prior to the establishment of the alloy-induced acidic degradation of the Ni-8Cr-6Al-6Mo will now be examined. To do this it is helpful to divide the degradation process into the eight steps identified in the weight change versus time data presented in Figure 35. For each of these steps specimens were examined metallographically and the water obtained by heating exposed specimens in boiling water was analyzed. The results obtained from these chemical analyses are presented in Table III.

During steps 1 and 2 virtually all of the Na_2SO_4 was recovered and a small amount of chromium and molybdenum had dissolved into the sulfate. The weight change data, Figure 35, and metallographic results showed no hot corrosion attack had occurred. Such results were in contrast to the results obtained with the Ni-8Cr-6Al alloy, Figure 27a, and it appears that the molybdenum has inhibited the onset of attack via the basic fluxing mechanism.

At step 3 a significant amount of the sulfate component of the salt has been consumed and chromium, aluminum and molybdenum are present in the wash water which now has a substantially higher pH, Table III, and metallographic examination shows that considerable hot corrosion attack has occurred, Figure 46a. A degradation microstructure very similar to that obtained with the Ni-8Cr-6Al alloy, Figure 27a, was obtained and microprobe analysis showed that the corrosion

product was composed of partially sulfided nickel particles surrounded by a Na_2SO_4 melt containing aluminum, chromium and molybdenum, Figure 46b. Such results show that the Ni-8Cr-6Al-6Mo is being degraded by the same mechanism as the Ni-8Cr-6Al alloy, namely, basic fluxing.

At step 4 the weight change versus time data exhibit a substantial decrease in rate, Figure 35. The most significant results obtained from the wash water analyses were that the amount of soluble aluminum decreased and the pH became significantly more acidic, Table III. Typical microstructures for this step contained chromium sulfide particles in the alloy and an oxide scale which was permeated with Na_2SO_4 and contained oxides of all the elements in the alloy, Figure 46c. Microprobe analyses of such sections showed that in the scale immediately adjacent to the alloy localized areas of molybdenum enrichment were present. These results show that during step 4 the oxides formed during step 3 are reacting with Na_2SO_4 and making it acidic. Since MoO_3 has a greater affinity for oxide ions than Al_2O_3, it converts the AlO_2^- - ions to Al_2O_3, hence the amount of water soluble aluminum is decreased.

In steps 5, 6, 7 and 8 the rate of attack gradually increases. The pH of the wash water gradually becomes more acidic and the amount of soluble molybdenum and nickel increases whereas the chromium and sulfate concentration gradually decrease and the aluminum remains at very low values, Table III. Metallographic examination reveals structures similar to Figure 46c but the localized molybdenum enrichment becomes increasingly larger and more prevalent, Figure 46d. During steps 5, 6, 7, 8 there is a gradual enrichment of MoO_3 in the Na_2SO_4 and the attack rate increases as more of the surface is covered with the MoO_3 - Na_2MoO_4 - Na_2SO_4 solution which causes degradation via the acidic fluxing process described previously.

The results obtained with the Ni-8Cr-6Al-6Mo are essentially the same as those obtained by Fryburg et al[12]. These authors, as well as Goebel et al[7], proposed that the attack of the B-1900 alloy took place by acidic fluxing whereas Bornstein and DeCrescente favored basic fluxing [3]. The results obtained in the present study indicate that the initial stages of degradation of B-1900 take place because of basic fluxing but the propagation mode changes to acidic fluxing as the activity of MoO_3 in the salt (i.e. Na_2MoO_4 - Na_2SO_4) is increased to appropriate levels. It is apparent that substantial attack occurs at activities of MoO_3 in the Na_2SO_4 significantly lower than unity (e.g. 0.1)[29].

The results obtained with IN 738 show that hot corrosion degradation of this alloy can occur because of alloy-induced acidic fluxing. It is apparent however, that much longer times are required to induce this attack in IN 738 than in B-1900, Figure 45. In the case of B-1900, it was found that the Ni-8Cr-6Al composition was very susceptible to basic fluxing, Figures 1 and 26. On the other hand, the Ni-16Cr-3.4Al composition is much more resistant to basic fluxing, Figure 47. Hence, IN 738 is more resistant to the onset of alloy-induced acidic fluxing than B-1900 because the chromium and aluminum concentrations of the IN 738 are resistant to basic fluxing degradation, which is a precursor to acidic fluxing in both B-1900 and IN 738. Another factor favoring the longer times for hot corrosion attack via the acidic propagation mode would be the lower concentration of refractory metals in the IN 738 compared to B-1900.

Since IN 738 was observed to eventually undergo hot corrosion via alloy-induced acidic degradation, it would be expected that a Ni-16Cr-3.4Al-1.75Mo-2.6W alloy would exhibit similar behavior. Weight change versus time data obtained for Ni-16Cr-3.4Al-1.75Mo-2.6W using conditions that produce hot corrosion attack of IN 738 are presented in Figure 47. No severe attack took place. When about 0.1% carbon was added to Ni-16Cr-3.4Al-1.75Mo-2.6W, substantial hot corrosion attack of this alloy was observed, Figure 47. It appears that carbon causes the effective chromium concentration of the alloy to be lowered via the formation of chromium carbide, since an addition of 0.1% carbon to Ni-16Cr-3.4Al also caused this alloy to become more susceptible to hot corrosion attack. Hence, basic fluxing attack of Ni-16Cr-3.4Al-1.75Mo-2.6W can be initiated more quickly when carbon is present in this alloy and therefore oxides of molybdenum and tungsten become available sooner to initiate the acidic fluxing process. In order to compare the effect of chromium and carbon on the hot corrosion resistance of IN 738 - type of alloys, specimens with a low chromium concentration but no carbon and a high chromium concentration with carbon were tested. It was observed that the alloy with low chromium and no carbon was attacked, whereas the alloy with high chromium and carbon was not, Figure 48. As proposed by Meier et al[34], the attack of carbide phases in IN 738 can also, by itself, be a means of adding molybdenum or tungsten to the salt melt, since the carbide phases contain molybdenum and tungsten. Preferential attack of carbide phases during the hot corrosion of alloys has been observed[7].

A great variety of different fluxing effects can be observed when hot corrosion attack induced by different salts (e.g. Na_2CO_3, $NaNO_3$, etc.) is examined. This paper is concerned with Na_2SO_4 and Na_2SO_4 containing NaCl. Since molybdenum in alloys has been observed to react with Na_2SO_4 to produce Na_2MoO_4, it is of value to compare results obtained by oxidizing alloys coated with deposits of Na_2SO_4 and Na_2MoO_4. Such results obtained with the Ni-8Cr-6Al alloy are presented in Figure 49 which indicates that more severe attack of the alloy took place with Na_2SO_4 than Na_2MoO_4. A substantial difference between the vaporization of these deposits from the specimens was not observed. It is believed that the different amounts of hot corrosion are due to the fact that a substantial amount of oxide ions are produced as a result of sulfide formation in the case of Na_2SO_4 and these oxide ions cause hot corrosion attack. In the Na_2MoO_4 there is not an equivalent means to produce oxide ions (oxide ions can be produced in both Na_2SO_4 and Na_2MoO_4 via evaluation of SO_3, SO_2 or MoO_3) because the Ni-8Cr-6Al alloy does not react with the molybdenum in Na_2MoO_4 as it does with the sulfur in the Na_2SO_4. Hence, the attack induced initially by Na_2MoO_4 probably proceeds by some mechanism such as that described in Figure 44, where the ionic species responsible for the transport of metal away from the alloy surface can be postulated to be MoO_4^{2-} and MoO_4^{5-}.

When experiments to compare the hot corrosion attack induced by Na_2SO_4 and Na_2MoO_4 were performed using Ni-8Cr-6Al-6Mo, alloy-induced acidic fluxing was observed sooner in the case of Na_2SO_4 than Na_2MoO_4, Figure 50. Alloy-induced, acidic fluxing hot corrosion attack of this alloy is caused by the accumulation of MoO_3 in the salt deposit. It may, therefore, seem inconsistent that the attack is observed sooner with Na_2SO_4 than Na_2MoO_4 deposits. Molybdenum

must be supplied by the alloy, however, in the case of both deposits. Sodium sulfate causes more of the alloy to be attacked initially than Na_2MoO_4 and more molybdenum oxide is developed initially in the case of the Na_2SO_4 deposit. After longer times, enough molybdenum is introduced into the Na_2MoO_4 to produce attack via the same propagation mode and the hot corrosion rates are similar, Figure 50.

Summary of Fluxing Processes

The various reactions by which hot corrosion via salt fluxing can occur are summarized in Table IV. In this table, category A covers the basic processes that occur due to the production of oxide ions in the Na_2SO_4, as a result of removal of oxygen and sulfur from the Na_2SO_4 by the alloy. The hot corrosion attack may occur because of the solution of oxide in the Na_2SO_4, A(1), or solution and precipitation A(2). In both cases, the attack is not self-sustaining, but rather is controlled by the amount of Na_2SO_4 unless the gas phase contains SO_3. Category B covers the Rapp-Goto model[24], where hot corrosion attack does not require sulfur removal from the melt, but occurs because of a negative solubility gradient of the corrosion product in Na_2SO_4.

Categories C, D, E and F cover acidic processes. C and D involve solution and precipitation processes where the acidic component comes from the gas phase. Category F is for the same type of processes but the acidic component comes from the alloy. Category E covers the Rapp-Goto concept for acidic melts.

In this table, localized cell activity has not been considered. Coupling between the various charged particles during diffusion is supposed to occur in such a manner that electrical neutrality is maintained. It is possible, however, that the anodic and cathodic reactions may take place at different sites re-

sulting in development of potential differences. This condition possibly results in growth of pits similar to those observed in aqueous corrosion[35]. However, in those cases where hot corrosion attack is localized as pits, the portions of the surface which have not undergone hot corrosion attack are still covered with protective oxide scales. Cathodic reactions closely similar to those of aqueous reactions therefore do not seem possible.

Salt Component-Induced Hot Corrosion

As a result of salt deposition, elements from the salt can be introduced into the corrosion product or the surface regions of alloys and eventually affect their oxidation behavior. A great variety of elements could produce such an effect depending on the deposit composition. In the case of Na_2SO_4 and NaCl deposits, the significant elements are sulfur and chlorine. Another element that can also be important is carbon since the environments that cause hot corrosion attack usually result from the combustion of some type of fuel. Carbon may be formed therefore, on hardware during some phase of the combustion process. In the following, the effects produced by each of the elements will be considered.

Sulfur-Induced Hot Corrosion

The oxygen pressure in Na_2SO_4 deposits at the alloy-Na_2SO_4 or oxide-Na_2SO_4 interfaces can be very low, Figure 24a. For example, the microstructures shown in Figures 26c and 46b show that the oxygen pressure in the Na_2SO_4 at the alloy interface is below that required to oxidize nickel. For such low oxygen pressures in Na_2SO_4 the sulfur pressure is usually high enough to form sulfides of aluminum and chromium, and in some cases even sulfides of cobalt, nickel and iron unless the SO_3 pressure is very low, Figure 25. The accumulation

of these sulfides in the alloy can result in substantial degradation during subsequent oxidation. For example, in Figure 51, weight change versus time data obtained for a Na_2SO_4-coated specimen is compared to that of a presulfidized specimen where the amount of sulfur added to the alloy was controlled to equal the amount of sulfur in each application of the Na_2SO_4. The degradation of the presulfidized specimen is about the same as that for the Na_2SO_4 - coated specimen and both are degraded substantially more than the specimen with no sulfidizing pretreatment nor Na_2SO_4 application. This shows that the primary mode of hot corrosion degradation for Na_2SO_4 - coated specimens of Ni-25Cr-6Al exposed at 1000°C in air is sulfur-induced degradation.

Some alloys are much more susceptible to sulfur-induced hot corrosion degradation than others. For example, the Co-25Cr-6Al alloy is much more resistant to this type of attack than Ni-25Cr-6Al, Figure 52. The greater susceptibility of the nickel-base alloys to sulfur-induced attack is generally observed only when aluminum is present in the alloys, Figure 53. It appears that nickel base alloys with aluminum contents between 6 to 12 weight percent, are relatively resistant to this attack and that degradation takes place after the aluminum has been reduced by oxide spallation in a cyclic test, Figure 3.

Sulfur-induced hot corrosion causes accelerated oxidation as a result of the formation of less protective oxide scales. Such scales are formed due to the presence of sulfides in the alloys. Sulfur-induced accelerated oxidation is also observed during the oxidation of alloys in SO_2-O_2 or H_2S-H_2O-H_2 gas mixtures[25,36], where the sulfide formation occurs, due to sulfur in the gas rather than from the sulfur in the Na_2SO_4. Sulfide formation in alloys, as a result

of sulfur in the gas or in deposits on the surfaces of alloys, can cause the formation of nonprotective oxide barriers on alloys by at least three different mechanisms. In one mechanism the oxidation of aluminum and chromium dissolved in nickel or cobalt sulfide results in the formation of discontinuous particles of Al_2O_3 or Cr_2O_3 rather than continuous, protective layers, Figure 54a and b. Another mechanism involves the formation of nonprotective oxides during the conversion of certain sulfides to oxides, Figure 54c and d. The smaller volume of the oxide compared to the sulfide may cause the oxide to be subjected to tensile stresses. The third mechanism by which nonprotective oxides are formed involves effects produced by internal sulfides on the selective oxidation process. When sulfur diffuses into the surfaces of alloys, it usually reacts with the same elements that are diffusing to the surfaces of alloys to combine with oxygen to form continuous oxide barriers. The formation of such sulfides appears to cause the flux of the elements being selectively oxidized to be decreased. This condition develops even though the sulfide particles usually dissolve and release the metal to react with oxygen. The metal in solution in the alloy is apparently more suitable for selective oxidation than a dispersion of metal sulfides in the alloy. At any rate, the decrease in the flux of such elements to the surfaces of alloys can result in the formation of oxide scales which are less protective than those that would have formed in the absence of the sulfide precipitates.

Chloride-Induced Hot Corrosion

There is a substantial amount of data available[14] which show that extremely small concentrations of NaCl (e.g. ~ 3-5 ppm) in deposits on the surfaces of alloys or in the gas phase cause the oxide scales to spall more

profusely when subjected to growth-induced and thermally-induced stresses. The mechanism by which the scale adhesion is decreased is not understood. It has been found that chloride ions tend to concentrate at the oxide-alloy interface[37].

While the adverse effect produced by NaCl or chloride ion on oxide scale adhesion is a very significant factor in many instances of hot corrosion attack, somewhat larger concentrations of chloride (e.g. ~ 1 weight percent and above) can influence hot corrosion attack by still another process. In Figure 14, the hot corrosion attack of a CoCrAlY-coating at 900°C in air with deposits of Na_2SO_4, Na_2SO_4-5% NaCl and Na_2SO_4-90% NaCl is compared. It is apparent that the severity of the attack increases as the amount of NaCl in the deposit is increased.

It has been observed that rather unique microstructural features are developed when chloride ion is present at concentrations sufficient to influence hot corrosion by a mechanism other than by decreasing oxide scale adhesion. As shown in Figure 55, the corrosion product contains a zone of particulates and voids in advance of the external scale. Microprobe analyses have shown that the zone immediately beneath the external scale appears to be predominantly Al_2O_3 particles, Figure 55b and c. Aluminum but not oxygen was detected in the zone immediately adjacent to the unaffected alloy, Figure 55e and f. Chlorine was also detected in these more interior regions of the zone of internal attack. All of the aluminum had been removed from the alloy in the zone of internal attack and a steep gradient in chromium was detected between the unaffected alloy and the external scale. The inner part of the external scale contained oxides of aluminum and chromium and the outer part

was more rich in cobalt, A detailed examination of the zones of internal attack, Figure 56a, showed that pores extended through these zones, Figure 56b and c. These pores often could be associated with the β-CoAl phase in the CoCrAlY, Figure 56d, but they did not have the exact shape of this phase.

Nickel and cobalt alloys containing chromium but no aluminum are also more severely attacked by Na_2SO_4-NaCl mixtures than pure Na_2SO_4. Data is presented in Figure 57 to show the effect of NaCl in Na_2SO_4 for the cyclic hot corrosion of Ni-25Cr-6Al and Ni-30Cr specimens. The exact degradation microstructure that is developed depends upon the alloy composition and the amount of NaCl in the Na_2SO_4. The end result, however, appears to be generally the same, namely, when chloride is present in the deposit the oxidation of the elements that usually result in continuous and protective oxide barriers occurs in such a manner that these oxides are formed as discontinuous particles, Figure 58.

The mechanism by which chloride causes more rapid consumption of the elements (i.e. Al and Cr) that usually confer oxidation resistance in alloys appears to involve the formation of chloride phases. In view of the greater stability of oxides and sulfides compared to chlorides, the salt must become deficient in oxygen and sulfur before chloride phases may be expected. Hence, the following sequence of reactions can be hypothesized.

$$(1)\quad (Na_2SO_4\text{-}NaCl)_{liq.} \xrightarrow{P_{O_2},\ P_{S_2},\ P_{NaCl}} + (Al,Cr)_{alloy} \rightarrow Al_2O_3 + Cr_2O_3 + CrS + (Na_2SO_4\text{-}NaCl)_{liq.}$$

$$\text{where } P'_{O_2} < P_{O_2},\ P'_{S_2} < P_{S_2},\ P'_{NaCl} > P_{NaCl}$$

(2) $NaCl + 2Al\ (alloy) + O_2 \rightarrow NaAlO_2 + AlCl$

(3) $2AlCl + \frac{3}{2}\ O_2 \rightarrow Al_2O_3 + Cl_2$

(4) $Cl_2 + 2Al(alloy) \rightarrow 2AlCl$

Equation (1) and Figure 59a show that the melt adjacent to the alloy can become enriched in NaCl due to oxide and sulfide formation. In localized areas, the NaCl component of the Na_2SO_4 - NaCl melt may then begin to react with certain components in the alloy as proposed by Equation (2). This reaction takes place first with elements for which the thermodynamic conditions are most favorable. For example, reaction with aluminum is observed before chromium but chromium does react when the aluminum concentration has been reduced. As the metallic chloride moves outward through the melt, oxygen pressures are encountered for which the metallic chloride is converted to a metallic oxide, Equation (3) and Figure 59b, and the chlorine is recycled to react with elements in the alloy, Equation (4). Continuation of this process, results in the development of pores that are coated with discontinuous, nonprotective oxide particles, Figure 59c. The pores have been observed to grow extremely rapid at temperatures as low as 650°C. Strikingly similar structures have been observed at much lower temperatures as a result of aqueous corrosion[38]. In these cases, pore growth via the preferential removal of an element is accounted for by surface diffusion of those elements not reacting with the liquid, or by their solution into the liquid followed by subsequent precipitation on the sides of the pore as indicated in Figure 59d. Such effects would account for the development of pores associated with phases rich in aluminum, or chromium, but not having their exact shapes. As the

process of pore development continues chloride is gradually lost to the gas phase. The time at which the chloride concentration becomes insufficient to react with the alloy depends on temperature, salt composition, gas composition and alloy composition. When such a condition is reached the innermost portions of the pores begin to react with sulfur and the degradation process proceeds via Na_2SO_4 - induced hot corrosion, Figure 59e. The presence of chloride, however, has caused the alloy to become depleted of aluminum and/or chromium, and the surface area of the alloy available for reaction with the Na_2SO_4 has been increased due to the formation of pores.

Carbon-Induced Effects During Hot Corrosion

In processes involving combustion, it is not uncommon to have carbon deposited on materials. Moreover, hardware can become covered with unburned fuel and subsequent combustion will result in very low oxygen pressures over the alloy in the vicinity of the excess fuel. The reduced oxygen pressure due to the presence of carbon or excess fuel causes metals and alloys to become more susceptible to effects produced by other components in the environment (e.g. sulfur, carbon, nitrogen). This condition is especially obvious when salt is also present on the alloy surface. For example, specimens of Ni-16Cr-3.4Al were not substantially degraded after 8 hours exposure at 1000°C in air when coated with Na_2SO_4, Figure 60a, or immersed in an α-Al_2O_3 crucible filled with carbon, Figure 60b. However, the sulfur from the Na_2SO_4 and the carbon did cause a more pronounced transient period of initial oxidation since an extremely thin scale is usually formed on this alloy during exposure to air at 1000°C without Na_2SO_4 or carbon. The attack of this alloy is substantially increased whenever Na_2SO_4 - coated

specimens are immersed in α-Al_2O_3 crucibles containing carbon or liquid fuel, Figure 60c and d. Similar effects will be observed for virtually all alloys but the magnitude of the effect and the dominant microstructural features depend upon the particular alloy's composition, the composition of the salt, temperature and the types of environment developed over the alloy surface by the burning carbon or fuel where this latter parameter changes with time.

The influence of carbon on the Na_2SO_4 - induced hot corrosion of alloys has been studied previously[39]. It is rather apparent that an excess of carbon or unburned fuel causes the oxygen pressure over the alloy to be substantially reduced and elements in the alloy therefore react with the sulfur in the Na_2SO_4. Since sulfur is removed from the Na_2SO_4, oxide ions are produced. Hence, the mechanisms of hot corrosion attack which are influenced by the reducing conditions are the basic fluxing and sulfur-induced propagation modes. An example is presented in Figure 61 to show that reducing conditions resulted in the hot corrosion attack of a CoCrAlY coating alloy via a sulfur-induced propagation mode. This coating is not significantly attacked by Na_2SO_4 in air, Figure 38a, but substantial attack is observed by periodically exposing Na_2SO_4 - coated specimens to excess fuel, Figure 61a.* Examination of such specimens shows that the attack occurs by the formation of sulfides in the coating, Figure 61b, which are subsequently oxidized as the oxygen increases after combustion of the fuel, Figure 61c. Depending upon the combustion cycle, the sequence of sulfidizing-oxidizing conditions can be

---

* The excess fuel test consisted of adding 5 ml of #2 diesel fuel to a platinum or an alumina crucible and suspending the Na_2SO_4 - coated specimen at the top of this crucible. The crucible was then placed in a box furnace at 1300°C for 30 sec. to 1 min. After this exposure the crucible was placed in a box furnace at 700°C for about 10 hrs. This procedure, which constituted one cycle, was repeated until attack of the specimen was evident by visual examination.

rapid enough that little evidence of the oxidized sulfide particles is apparent, Figure 61d. In fact, it is probably best not to assume that such attack, Figure 61d, is indeed caused by sequential sulfidation-oxidation.

While sequential variations in the oxygen pressure of the gas (i.e. reducing - oxidizing cycles) favors hot corrosion attack via basic fluxing and sulfur-induced propagation modes, such conditions can also influence hot corrosion attack via other propagation modes. The IN 738 alloy, when coated with Na_2SO_4 and exposed to air at 1000°C, eventually undergoes very severe attack via the alloy-induced acidic fluxing propagation mode but long exposure times are necessary before this attack occurs, Figure 45. When this alloy is coated with Na_2SO_4 and heated at 1000°C very little attack is evident after 1 hr., Figure 62a. Exposure to an excess of burning fuel at the same temperature but with no Na_2SO_4 also does not cause substantial attack, Figure 62b. When Na_2SO_4 - coated specimens are exposed to excess burning fuel, the features typical of acidic fluxing degradation are observed after exposure times as short as one hour, Figure 61c. The reducing conditions probably cause the attack to be initiated via the basic fluxing and sulfur-induced degradation modes. The attack then causes the molybdenum and tungsten in this alloy to be concentrated in the salt at the alloy-scale interface and attack by alloy-induced acidic fluxing becomes dominating.

Hot corrosion attack induced by chlorides, as described in Figure 59, is especially effective when the oxygen pressure at the salt-alloy interface is low. Such attack is therefore greatly enhanced when in combination with carbon deposits or excess fuel.

Interaction Between the Various Hot Corrosion Propagation Modes

Previously, the interaction between basic fluxing and alloy-induced acidic fluxing was discussed. It was shown that for environments consisting of oxygen and Na_2SO_4, the basic fluxing propagation mode preceeded the alloy-induced acidic fluxing propagation mode. In fact, as a result of basic fluxing, the alloy-induced acidic attack was observed sooner. Interaction between the various propagation modes for Na_2SO_4 induced hot corrosion attack is quite common. One particular degradation mode may be dominant for short exposure periods and another after very long exposures, or the dominant modes may change with temperature. Hence, in attempting to identify the alloys which are degraded via particular propagation modes these interactions must be taken into consideration.

Basic fluxing and sulfur-induced degradation are two propagation modes that are often followed in sequence with the basic fluxing mode preceeding the sulfidation mode. Such a situation arises since the basic fluxing mode requires oxide ions, and sulfur formation in the metal or alloy is a means of producing oxide ions. Eventually, the accumulation of sulfides in the alloy can result in degradation via the oxidation of these sulfides. It must be noted, at this point, that there are some alloys which are degraded much more severely by one particular propagation mode, even though two modes may have been operative sequentially. Nickel- and cobalt-base alloys containing more than 20% chromium and no aluminum are not substantially degraded by basic fluxing and the significant propagation mode for alloys with no refractory metals is sulfidation, Figure 54c and d. On the other hand, the Na_2SO_4-induced hot corrosion of nickel and cobalt via basic fluxing is sign-

ificant in comparison to the oxidation of the sulfides formed in these metals, Figure 29.

Gas induced acidic fluxing and sulfidation degradation are propagation modes whose dominance can change with temperature. For example, SO_3-induced acidic fluxing requires a supply of SO_3 to be furnished from the gas. Consequently, the sulfur pressure in the Na_2SO_4 deposit becomes quite high as oxygen is removed from it by the alloy. At low temperatures (e.g. 600°-750°C), the gas induced acidic fluxing process can be extremely rapid and sulfide formation in the alloy is therefore, often negligibly small, Figure 40. The amount of sulfide formation progressively increases with temperature, however, since the thermodynamic conditions become less favorable for the SO_3-induced fluxing process and sulfur diffusion into the alloy becomes more pronounced. At temperatures of 1000°C excessive amounts of sulfides can be formed and their subsequent oxidation can result in severe degradation, Figure 51.

Alloy-induced acidic fluxing is usually preceded by some other propagation modes since molybdenum or tungsten from the alloy must be oxidized and added as oxides to the salt deposit. The most common propagation modes to precede alloy induced acidic fluxing are basic fluxing and sulfidation. Since these two modes are favored by high temperatures, alloy induced acidic fluxing is often observed at temperatures above 900°C.

Chloride-induced degradation can precede any of the propagation modes described in this paper. Chloride induced attack preceding another propagation mode will normally be observed with alloys that are resistant to degradation, and the chloride-induced attack will produce depletion of elements to levels at which the other propagation modes can become dominant, Figure 58. Carbon-

induced effects are not mechanisms by themselves but do cause conditions to be established (e.g. low oxygen pressures) that can result in the onset of degradation via a propagation mode much sooner than what would have occurred without any carbon.

Even though the hot corrosion propagation modes affect each other and this interaction depends on temperature, it is of value to attempt to describe the alloys which are the most susceptible and most resistant to attack via each of the propagation modes. In Figure 63, alloys which are susceptible or resistant to the various propagation modes are identified, and techniques to inhibit the attack are presented. In this Figure, the influence of environment is indicated by progression from gases with no SO_3, where basic fluxing would be favored, to gases with increasing amounts of SO_3 where gas-induced acidic fluxing could be expected. Sulfur-induced degradation and alloy-induced acidic attack can occur in gases with or without SO_3, and these two propagation modes are therefore, contained in the interior of the diagram. The effects produced by chloride and carbon are included in this diagram by considering their influence on the other propagation modes. This is a reasonable approach for carbon, since it has been found that carbon effects manifest themselves through changes produced in the oxygen and sulfur pressures in Na_2SO_4. A similar condition is not true for the chloride-induced effects because the presence of chlorine can result in hot corrosion attack by a distinct propagation mode, Figure 59. Such effects, however, do cause depletion of certain elements from alloys, and one of the other propagation modes therefore, usually follows the chloride-induced propagation mode.

The metals and alloys which are suceptible to basic fluxing are nickel, cobalt (Figure 29), Ni-Al and Co-Al alloys which are Al_2O_3-formers (Figure 4), and Ni-Cr-Al alloys with chromium and aluminum concentrations below that required to form external scales of Cr_2O_3 or Al_2O_3, (Figures 26 and 27). The most effective procedure to inhibit basic fluxing is to increase the chromium content of the alloys. At low chromium concentrations, chromia reacts with the oxide ions in the Na_2SO_4 rather than NiO or CoO. Hence, protective scales of these latter oxides are formed and grow to thicknesses for which oxide ion production in the Na_2SO_4 is not significant. At higher chromium concentrations, where continuous Cr_2O_3 is formed on alloys, these chromia scales are not as susceptible to solution and reprecipitation from the Na_2SO_4 as Al_2O_3 appears to be in the absence of chromium. Chromia scales are therefore, very effective barriers to basic fluxing. Since basic fluxing requires that an oxygen gradient be developed across the Na_2SO_4, the formation of oxide scales that grow slowly and consume as little oxygen as possible is an effective means to combat basic fluxing. The addition of chromium and aluminum to alloys results in improved resistance to basic fluxing providing, continuous barriers of Al_2O_3 or Cr_2O_3 are formed. When the concentrations of these elements are less than that required to form such scales, it is best not to have any aluminum in the nickel-base alloys, because, under such conditions, large amounts of sulfur are removed from the Na_2SO_4 along with concomitant oxide ion production. Chloride in Na_2SO_4 deposits causes basic fluxing effects to be observed sooner by depleting the alloy of aluminum and chromium. Thin layers of platinum ($\sim 5\mu m$) on the surfaces of alloys have been found to be effective in inhibiting such chloride-induced effects[40]. Carbon causes basic fluxing to be observed sooner

due to the reduced oxygen pressures which develop as a result of its presence.

The oxidation resistance of virtually all alloys deteriorates when sulfur is present to the extent that sulfide phases exist within the alloys. Nickel-base alloys containing between 1 to 6% aluminum are extremely susceptible to this type of hot corrosion attack, Figure 5. Such attack can be inhibited by increasing the aluminum concentration beyond six percent and/or replacing nickel with cobalt. Increased chromium concentrations are a very effective means to inhibit degradation via sulfidation. Chromium combines with sulfur to form sulfides with relatively high melting points. At high (e.g. ~ 20% and greater) alloy chromium concentrations, protective Cr_2O_3 scales are often formed on these sulfides. The chromium concentration should not be so high, however, that the α-Cr phase becomes stable. Even when less protective oxides are formed on the sulfide phases, the degradation rate is still significantly less than that of similar nickel-base alloys containing aluminum, Figure 9. Chloride induced degradation results in accelerated depletion of aluminum and chromium from alloys, and therefore, the presence of chloride in deposits causes sulfidation degradation to be observed after shorter exposure times, Figure 58. The introduction of sulfur into the alloy from the Na_2SO_4 is favored by low oxygen pressures, Figure 24, and hence, carbon in deposits hastens the onset of hot corrosion degradation via the sulfidation propagation mode.

Alloy-induced acidic fluxing results from the accumulation of oxides such as MoO_3, WO_3 or V_2O_5 in salt deposits on alloys. Susceptible alloys are therefore, those with high concentrations of such elements (e.g. NX-188), or

alloys with smaller concentrations of these elements but with compositions that permit severe attack of the alloys by one of the other hot corrosion propagation modes (e.g. B-1900, WI 52). This form of hot corrosion attack can be inhibited by decreasing the concentrations of the refractory elements, molybdenum, tungsten and vanadium. It is not certain whether columbium causes effects similar to these three elements. Tantalum does not, and therefore, appears to be a reasonable replacement for Mo, W and V in alloys. Modifications to inhibit the oxidation of the Mo or W in alloys is an effective means to inhibit alloy-induced acidic attack. Increased chromium concentrations have been used to achieve such a condition, Figure 33 (e.g. IN 738, HA-188). As usual, chloride and carbon in deposits cause alloy-induced effects to be observed sooner, Figure 62.

All alloys can be attacked via gas phase-induced acidic fluxing depending upon the SO_3 pressure and the temperature. Silica and chromia scales on alloys appear to be the most resistant to degradation via this mode but even barriers of these oxides can be destroyed at sufficiently high SO_3 pressures. Nevertheless, increased chromium and silicon concentrations do appear to be a means of inhibiting the attack of alloys by gas phase induced attack. At low temperatures (e.g. $\sim$ 700°C), this attack is only severe when the salt deposit is a liquid. In the case of Na_2SO_4 deposits, a liquid phase usually is developed much sooner on cobalt-base rather than nickel-base systems. A detailed examination is required of the effects of chloride and carbon on gas phase-induced hot corrosion. At present, it appears as though both of these factors will cause the attack to be initiated sooner, but they may not have a substantial effect on the rate of this propagation mode after it has been initiated.

SUMMARY AND CONCLUDING REMARKS

There is no question but that the hot corrosion of multicomponent alloys can be a very complex phenomenon. Nevertheless, progress is being made on understanding hot corrosion. For continued progress, it is necessary to look upon hot corrosion as being composed of an initiation and a propagation stage. During the initiation stage, the alloy is being preconditioned by the salt or ash deposit and the gas environment to degrade via a particular propagation mode. The effects produced by different elements on the hot corrosion process should be qualified as to whether the effect occurs in the initiation stage or the propagation stage, and if in the propagation stage, for which propagation mode. The problems that have resulted due to a lack of unification of the hot corrosion process are presented as follows:

- It has been stated that cobalt base alloys are more resistant to hot corrosion attack than nickel-base alloys. Such a condition is true only for the basic fluxing - sulfidation propagation modes and then only for alloys containing aluminum.
- Some controversy exists as to whether molybdenum and other similar elements, such as W and V, produce beneficial or deleterious effects on the hot corrosion process. This element inhibits basic fluxing effects but causes alloy-induced acidic fluxing. Hence, depending on the propagation mode, it can produce either beneficial or deleterious effects.
- Aluminum has been reported to produce either beneficial or deleterious effects on hot corrosion and this is true. The addition of 1 to 6% aluminum to a nickel chromium alloy greatly

decreases its resistance to attack via the basic fluxing and sulfidation modes. On the other hand the addition of aluminum to Co-Cr or Fe-Cr alloys, or to Ni-Cr alloys at levels above 10%, produces increased resistance to degradation via these propagation modes.

- Hot corrosion attack of materials has been given the misnomer, "sulfidation." One of the propagation modes is indeed sulfidation. Hence, sulfidation is a type of hot corrosion, but all hot corrosion does not necessarily occur via sulfidation.
- A number of explanations have been used to account for the beneficial effects of chromium on the hot corrosion process. However, all of the propagation modes are less effective as the chromium concentration is increased. Hence, indeed, there should be a number of different explanations to account for the effects produced by chromium.

Other elements of significance in hot corrosion attack are: Ta, Ti, Cb, Si, Mn, Zr, B, Cu, P, Zn and Pb. At present, sufficient data on the effects produced by these elements are not available to make any meaningful comments. It is important to emphasize that future investigations directed toward examining the effects of these elements on the hot corrosion process should be mindful that hot corrosion occurs via different propagation modes, and hence the effects attributed to given elements must also be associated with specific propagation modes.

REFERENCES

1. E. L. Simons, G. V. Browning, and H. A. Liebhafsky: Corrosion, 1955, Vol. 11, pp. 505t-14t.
2. A. U. Seybolt: Trans. TMS-AIME, 1968, Vol. 242, pp. 1955-61.
3. N. S. Bornstein and M. A. DeCrescente: Trans. TMS-AIME, 1969, Vol. 245, pp. 1947-52.
4. N. S. Bornstein and M. A. DeCrescente: Met. Trans., 1971, Vol. 2, pp. 2875-83.
5. J. M. Quets and W. H. Dresher: J. Mater., 1969, Vol. 4, pp. 583-99.
6. J. A. Goebel and F. S. Pettit: Met. Trans., 1970, Vol. 1, pp. 1943-54.
7. J. A. Goebel, F. S. Pettit, and G. W. Goward: Met. Trans., 1973, Vol. 4, pp. 261-78.
8. R. F. Reising and D. P. Krause: Corrosion, 1974, Vol. 30, pp. 131-8.
9. J. Balajka and V. Danek: Werkstoffe Korros., 1974, Vol. 7, pp. 513-21.
10. D. M. Johnson, D. P. Whittle, and J. Stringer: Corros. Sci., 1975, Vol. 15, pp. 721-39.
11. J. Stringer: "Role of Sulfur in Hot Corrosion," Proceedings of the 1974 Gas Turbine Materials in the Marine Environment Conference, J. W. Fairbanks and I. Machlin, eds., p. 161, MCIC-75-27, 1975, available from NTIS, U.S. Department of Commerce, Springfield, Virginia.
12. G. C. Fryburg, F. J. Kohl, and C. A. Stearns: "Hot Corrosion Studies of Four Nickel-Base Superalloys: B-1900, NASA-TRW-VIa, IN 713C and IN 738," Proceedings of the Symposium on Properties of High Temperature Alloys, Z. A. Foroulis and F. S. Pettit, eds., pp. 585-94, The Electrochemical Society, Inc., Princeton, N.J., 1976.

13. Y. Bourhis and C. St. John: "On the Role of Refractory Elements in the Hot Corrosion of Nickel-Base Alloys," Proceedings of the Symposium on Properties of High Temperature Alloys, Z. A. Foroulis and F. S. Pettit, eds., pp. 595-606, The Electrochemical Society, Inc., Princeton, N.J., 1976.

14. P. Hancock: "The Role of Halides in High Temperature Gas Corrosion," Proceedings of the Symposium on High Temperature Metal Halide Chemistry, D. L. Hildenbrand and D. D. Cubicciotti, eds., pp. 645-69, The Electrochemical Society, Inc., Princeton, N.J., 1978.

15. M. J. Donachie, Jr., R. A. Sprague, R. N. Russell, K. G. Boll, and E. F. Bradley: Symposium on Hot Corrosion Problems Associated with Gas Turbines, pp. 85-104, ASTM-STP-421, 1967.

16. R. R. Dils and P. S. Follansbee: Corrosion, 1977, Vol. 33, pp. 385-402.

17. P. Kofstad: High Temperature Oxidation of Metals, p. 269, John Wiley & Sons, Inc., New York, 1966.

18. J. Stringer: "Materials for Heat Exchangers in Fluidized Bed Boilers and Related Applications," Third Annual Conference on Materials for Coal Conversion and Utilization, DOE, EPRI, GRI, NBS, pp. K154 to K184, 1978, available from NTIS, U. S. Department of Commerce, Springfield, Virginia.

19. R. H. Barkalow and F. S. Pettit: "Corrosion/Erosion of Materials in Coal Combustion Gas Turbines," Proceedings of the Conference on Corrosion/Erosion of Coal Conversion System Materials, January 24-26, 1979, Berkeley, CA., NACE, Houston, Texas.

20. Metals Handbook, 8th ed., Vol. 2, "Heat Treating, Cleaning and Finishing," pp. 356-63, American Society for Metals, Metals Park, Ohio, 1964.

21. G. Charlot and B. Tremellon: Chemical Reactions in Solvents and Melts, Chapter 15, Pergamon Press, New York, 1969.

22. W. T. Reid: External Corrosion and Deposits, Elsevier Press, New York, 1971.

23. H. Reidick and R. Riefenhauser: VGB Kraftwerkstechnik, 1979, Vol. 12, pp. 915-21.

24. R. A. Rapp and K. S. Goto: "The Hot Corrosion of Metals by Molten Salts," Symposium on Fused Salts, Pittsburgh, PA., 1978, The Electrochemical Society, Princeton, N. J., 1979.

25. C. S. Giggins and F. S. Pettit: Study of Corrosion Mechanisms of Alloys in Multicomponent Gas Mixtures, Final Technical Report (DMR 75-19730) to the National Science Foundation, pp. 1-70, submitted to Oxidation of Metals for publication.

26. G. H. Meier: University of Pittsburgh, Private Communication.

27. W. P. Stroud and R. A. Rapp: "The Solubilities of Cr_2O_3 and α-Al_2O_3 in Fused Na_2SO_4 at 1200°K," Proceedings of the Symposium on High Temperature Metal Halide Chemistry, D. L. Hildenbrand and D. D. Cubicciotti, eds., pp. 574-594, The Electrochemical Society, Inc., Princeton, N. J., 1978.

28. E. M. Levin, C. R. Robbins, and H. F. McMurdie: Phase Diagrams for Ceramists, p. 95, The American Ceramic Society, Columbus, Ohio, 1964.

29. J. A. Goebel, F. S. Pettit, and G. W. Goward: Deposition and Corrosion in Gas Turbines, A. B. Hart and A. J. B. Cutler, eds., pp. 96-114, John Wiley & Sons, New York, 1973.

30. A. W. Coats, D. J. A. Dear, and D. Penfold: J. Inst. of Fuel, 1968, Vol. 41, pp. 129-32.

31. A. J. B. Cutler: J. Appl. Electrochem., 1971, Vol. 1, pp. 19-26.

32. C. H. Liu: J. Physical Chem., 1962, Vol. 66, pp. 164-66.

33. C. Wagner: Corros. Sci., 1965, Vol. 5, pp. 751-64.

34. T. Huang, E. A. Gulbransen, and G. H. Meier: J. of Metals, 1979, Vol. 31, pp. 28-35.

35. M. G. Fontana and N. D. Greene: Corrosion Engineering, pp. 10-16, 2nd Edition, McGraw-Hill Book Co., New York, 1978.

36. R. A. Perkins: "High Temperature Gaseous Corrosion of Incoloy 800 in Sulfidizing Environments," Proceedings of the Petten International Conference, Petten, The Netherlands, March 14-16, 1978, pp. 213-229, North-Holland Publishing Co., New York, 1978.

37. R. C. Hurst, J. R. Johnson, M. Davies, and P. Hancock: Deposition and Corrosion in Gas Turbines, A. B. Hart and A. J. B. Cutler, eds., pp. 143-57, John Wiley and Sons, Inc., New York, 1972.

38. M. G. Fontana and N. D. Greene: Corrosion Engineering, pp. 67-69, 2nd Edition, McGraw-Hill Book Co., New York, 1978.

39. D. W. McKee and G. Romeo: "The Influence of Carbon Particles on Hot Corrosion," Proceedings of the 1974 Gas Turbine Materials in the Marine Environment Conference, J. W. Fairbanks and I. Machlin, eds. pp. 183-194, MCIC 75-27, available from NTIS, U. S. Dept. of Commerce, Springfield, Virginia.

40. R. H. Barkalow and F. S. Pettit: "Degradation of Coating Alloys in Simulated Marine Environments," Prepared for Naval Research Laboratory, Washington, D. C., by Pratt & Whitney Aircraft Group, West Palm Beach, Florida, (Report No. FR-10225), June, 1978.

Table I

Nominal Compositions (Wt.%) of Alloys Used in Investigation

Ni-8Cr
Ni-30Cr
Ni-8Cr-6Al
Ni-16Cr-3.4Al
Ni-15Cr-6Al
Ni-25Cr-6Al
Ni-30Cr-4Al
Ni-30Cr-6Al
Ni-8Cr-6Al-6Mo
Ni-17Cr-11Al-0.5Y (NiCrAlY coating composition)
Ni-25Al-12W
Ni-25Cr-12W
Ni-16Cr-3.4Al-0.1C
Ni-16Cr-3.4Al-1.75Mo-2.6W
Ni-12Cr-3.4Al-1.75Mo-2.6W
Ni-16Cr-3.4Al-1.75Mo-2.6W-0.1C
Ni-25Cr-3.4Al-1.75Mo-2.6W-0.12C
Cobalt
Co-35Cr
Co-25Al
Co-25Al-12W
Co-20Cr-12W
Co-25Cr-12W
Co-25Cr-6Al
Co-17Cr-12Al-0.5Y (CoCrAlY coating composition)
B-1900 (Ni-8Cr-6Al-6Mo-10Co-1Ti-4.3Ta-0.1C-0.15B-0.07Zr)
Mar-M200 (Ni-9Cr-5Al-12.5W-10Co-2Ti-1.0Cb-0.15C-0.015B-0.05Zr)
IN738 (Ni-16Cr-3.4Al-1.75Mo-2.6W-8.5Co-3.4Ti-0.85Cb-1.75Ta-0.1C-0.012B-0.12Zr)
IN792 (Ni-12Cr-3.1Al-1.9Mo-3.8W-9Co-4.5Ti-3.9Ta-0.1C-0.02B-0.1Zr)
X-40 (Co-25.5Cr-10.5Ni-7.5W-0.5C)

Table II

Analyses of Wash Water from
Ni-8Cr-6Al Specimens With
Na_2SO_4 Deposits After Exposure at 1000°C
in Air for Different Times

Time (Min.)	% Remaining Na	% Remaining SO_4^{2-}	Cr (μg)	Al (μg)	Ni (μg)	pH*
1	100	100	<20	40	<5	6.4
2	100	71	50	260	<5	7.9
10	74	29	420	260	<5	8.1
30	72	19	1310	200	<5	8.0

* pH of water prior to use was 5.4.

Table III

Analyses of Wash Water from
Ni-8Cr-6Al-6Mo Specimens
With Na_2SO_4 Deposits After Exposure
at 1000°C in Air for Different Times

Stage (see Figure 35)	Time (Min.)	% Remaining Na	% Remaining SO_4^{2-}	Cr (µg)	Al (µg)	Ni (µg)	Mo (µg)	pH*
1	7	100	97	32	<5	7.5	<6	6.4
2	19	100	100	45	<5	7.5	15	5.8
3	2	93	38	175	143	7.7	900	7.8
3	40	93	27	240	116	7	1100	7.9
4	9	100	67	140	9	7.5	1080	5.9
4	15	100	72	125	<5	92	1150	5.8
5	82	100	72	260	<5	172	2950	5.7
6	336	100	18	102	<5	610	3880	5.3
7	303	99	11	125	<5	900	4250	5.2
8	218	98	24	52	22	1090	4150	5.1

* pH of water prior to use was 5.4.

Table IV

Possible Salt Fluxing Reactions
For Na_2SO_4 Deposits on Alloys

Basic Processes

A. Dissolution of Reaction Product, (i.e. AO) Due to Removal of Sulfur and Oxygen from the Na_2SO_4 by the Metal or Alloy:

$$SO_4^{2-}\ (\text{sulfate deposit}) \rightarrow \tfrac{1}{2}S_2\ (\text{for reaction with alloy}) + \tfrac{3}{2}O_2\ (\text{for reaction with alloy}) + O^{2-}\ (\text{for reaction with AO})$$

Reaction between AO and oxide ions can follow 2 courses;

(1) Continuous dissolution of AO

$$A(\text{alloy}) + \tfrac{1}{2}O_2 + O^{2-} \rightarrow AO_2^{2-}$$

Na_2SO_4 is converted to Na_2AO_2 and attack is dependent on amount of Na_2SO_4 initially present.

(2) Solution and reprecipitation

$$A(\text{alloy}) + \tfrac{1}{2}O_2 + O^{2-} \rightarrow AO_2^{2-}\ (\text{solution}) \rightarrow AO\ (\text{precipitate}) + O^{2-}$$

A supply of SO_3 is required in order for attack to proceed indefinitely, otherwise attack will stop when melt becomes sufficiently basic at precipitation site.

B. Solution and Precipitation of AO as a Result of a Negative Gradient in Solubility of AO in Na_2SO_4[24].

Table IV (Cont'd)

Possible Salt Fluxing Reactions
For Na_2SO_4 Deposits on Alloys

Acidic Processes

Gas Phase Induced

C. Formation of ASO_4 in Na_2SO_4:

$$A(alloy) + SO_3 + \frac{1}{2} O_2 \rightarrow A^{2+} + SO_4^{2-}$$

Continuous solution of ASO_4 in Na_2SO_4 requires continuous supply of SO_3 and O_2 from gas.

D. Solution and Precipitation of AO in Na_2SO_4 Due to Reduction of SO_3:

$$A(alloy) + SO_3 \text{ (from gas)} \rightarrow A^{2+} + SO_3^{2-} \text{ (in melt)}$$

$$A^{2+} + SO_3^{2-} + \frac{1}{2} O_2 \text{ (from gas)} \rightarrow AO \text{ (precipitate)} + SO_3$$

E. Solution and Precipitation of AO as a Result of a Negative Gradient in Solubility of AO in Na_2SO_4 as in $B^{(24)}$.

Alloy Phase Induced

F. Solution of AO in Na_2SO_4 Modified by Second Oxide from Alloy (i.e. BO_3).

- Modification of Na_2SO_4 by BO_3

$$B(alloy) + \frac{3}{2} O_2 + SO_4^{2-} \rightarrow BO_4^{2-} + SO_3$$

Table IV (Cont'd)

Possible Salt Fluxing Reactions
For Na_2SO_4 Deposits on Alloys

- Solution reaction for AC, Na_2SO_4 becomes enriched in ABO_4

$$A(alloy) + B(alloy) + 2O_2 \rightarrow A^{2+} + BO_4^{2-}$$

- Solution - Precipitation

$$A(alloy) + B(alloy) + 2O_2 \rightarrow A^{2+} + BO_4^{2-} \rightarrow AO + BO_3$$

Precipitation of AO in Na_2SO_4 as a result of loss of BO_3 from Na_2SO_4 permits substantial attack with small amounts of Na_2SO_4.

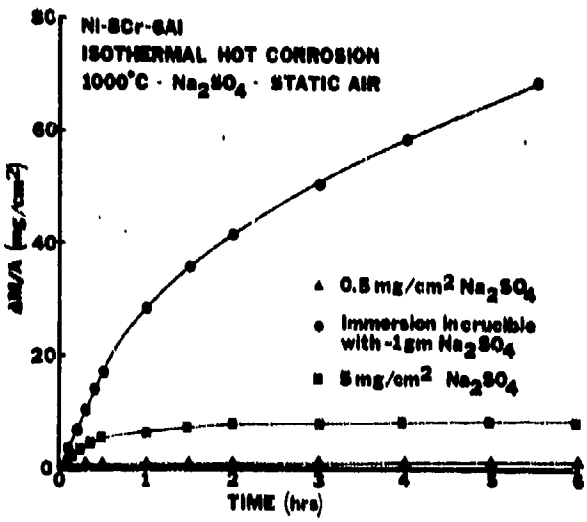

Figure 1. Weight change versus time data for the hot corrosion attack of Ni-8Cr-6Al specimens with different amounts of Na_2SO_4. The amount of degradation increases as the amount of the deposit is increased.

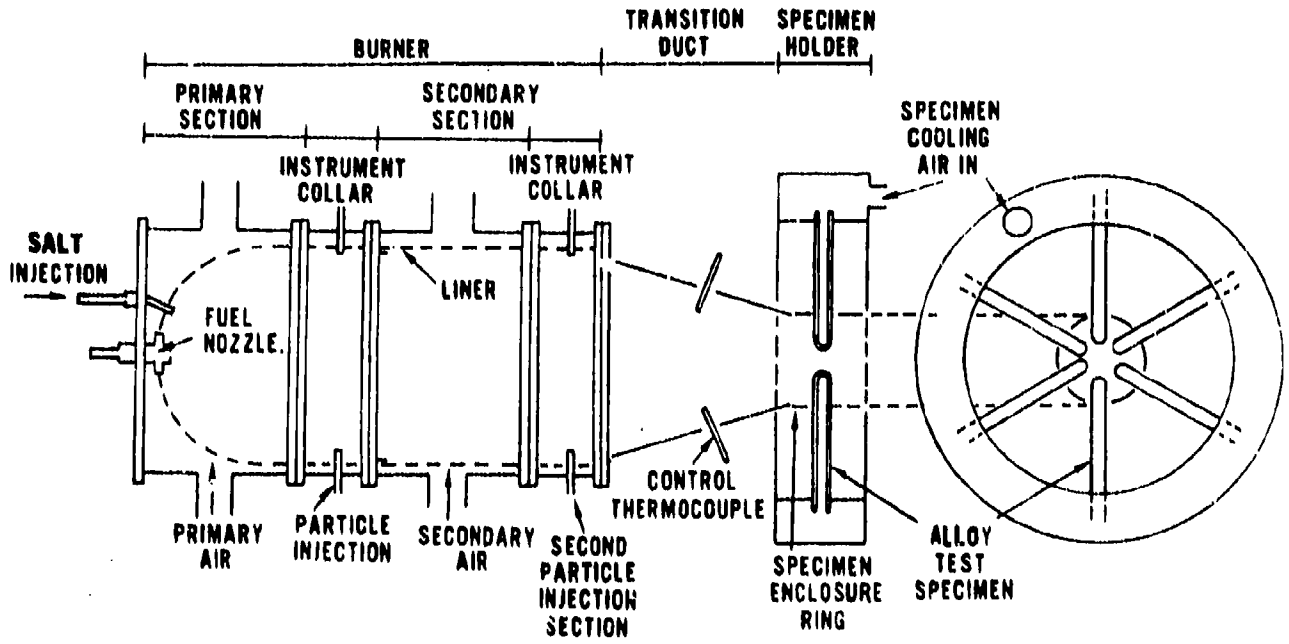

Figure 2. Schematic diagram of dynamic combustor used in the hot corrosion studies. Salts were injected into the rig as an aqueous solution near the fuel nozzle. Particulates could be injected into the burner at the instrument collars to introduce an erosive component into the hot corrosion test.

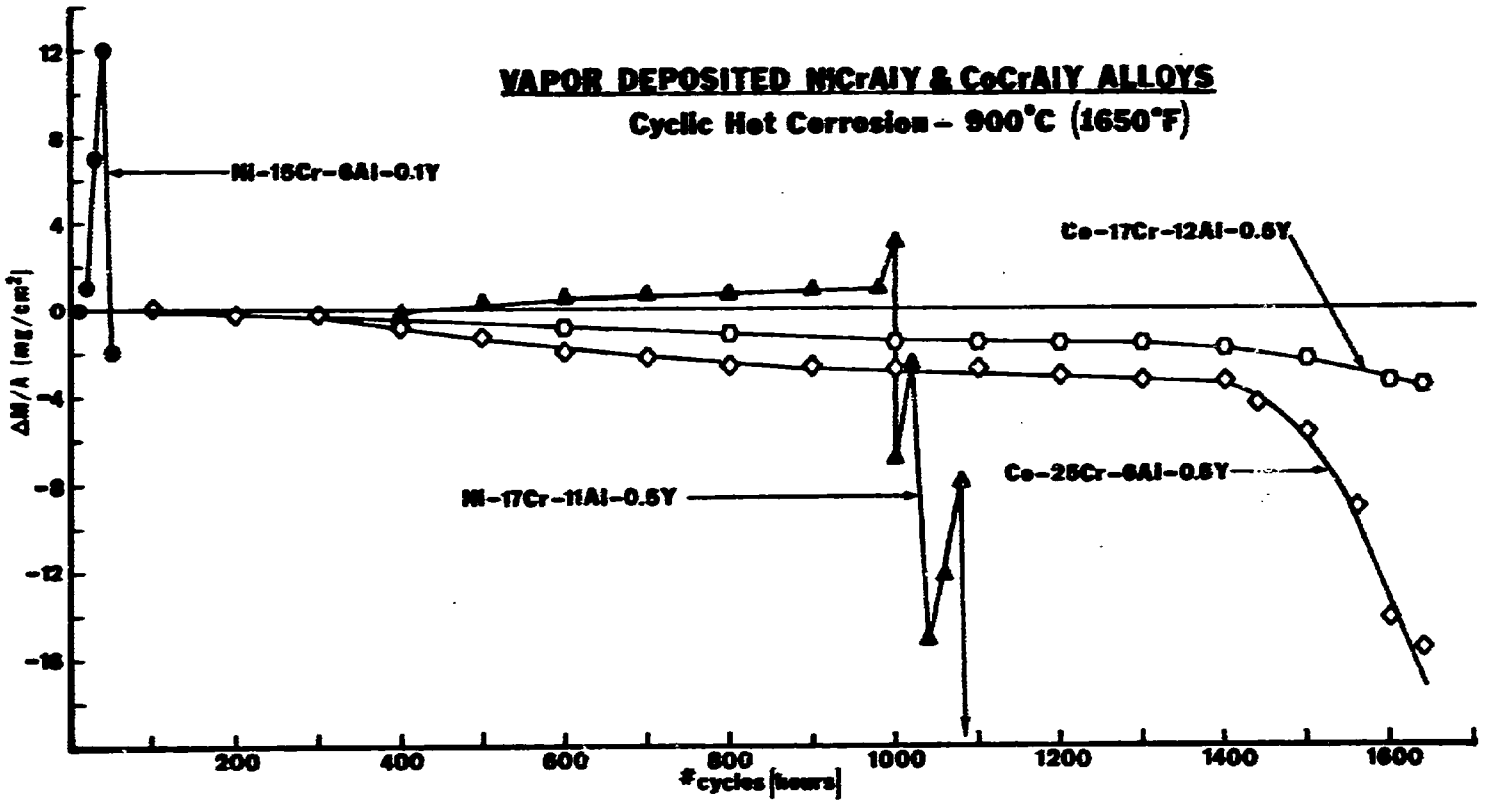

Figure 3. Weight change versus time curves obtained for the cyclic hot corrosion (1 cycle equals 50 minutes in hot zone followed by 10 minutes in cold zone of laboratory furnace) of some NiCrAlY and CoCrAlY alloys in air. These data show that the rate of attack eventually becomes greater providing the exposure time is sufficiently long. (~ 1 mg/cm^2 Na_2SO_4 was deposited on specimens every 20 hrs.)

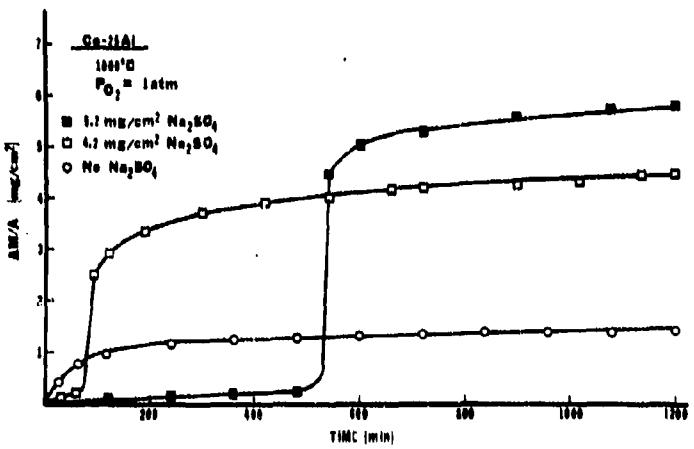

Figure 4. Weight change versus time data for the isothermal hot corrosion of a Co-25Al alloy. The data indicate that the Na_2SO_4-induced corrosion consists of an initial stage over which the attack is not severe and a subsequent stage that involves substantially more attack. In an isothermal test with a fixed amount of salt, the hot corrosion attack can eventually subside.

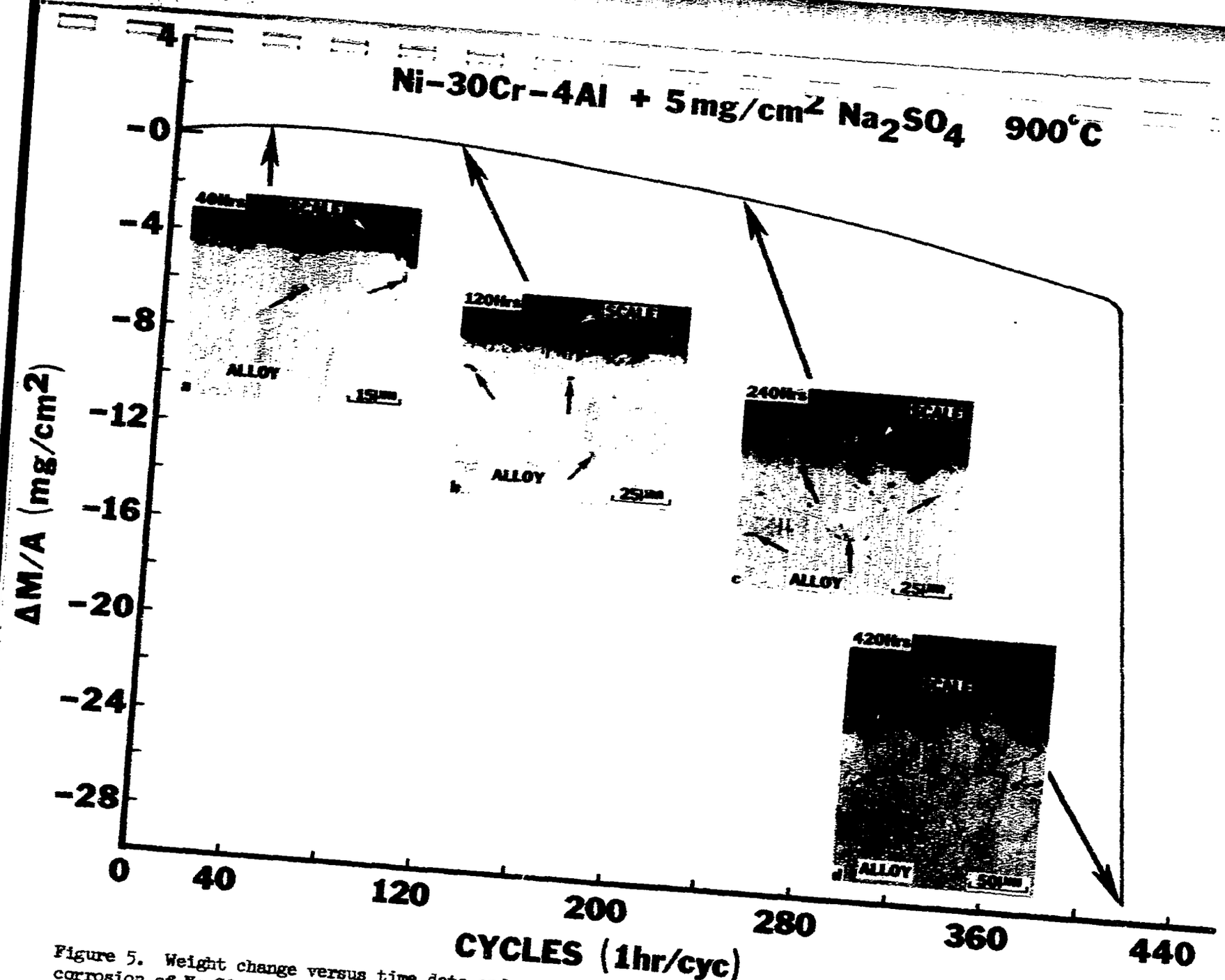

Figure 5. Weight change versus time data and corresponding microstructural features for the cyclic hot corrosion of Na_2SO_4-coated (applied every 20 hrs.) Ni-30Cr-4Al in air. The amount of sulfide particles (small black arrows) increases until the oxidation of the sulfide phases significantly affects the rate of attack.

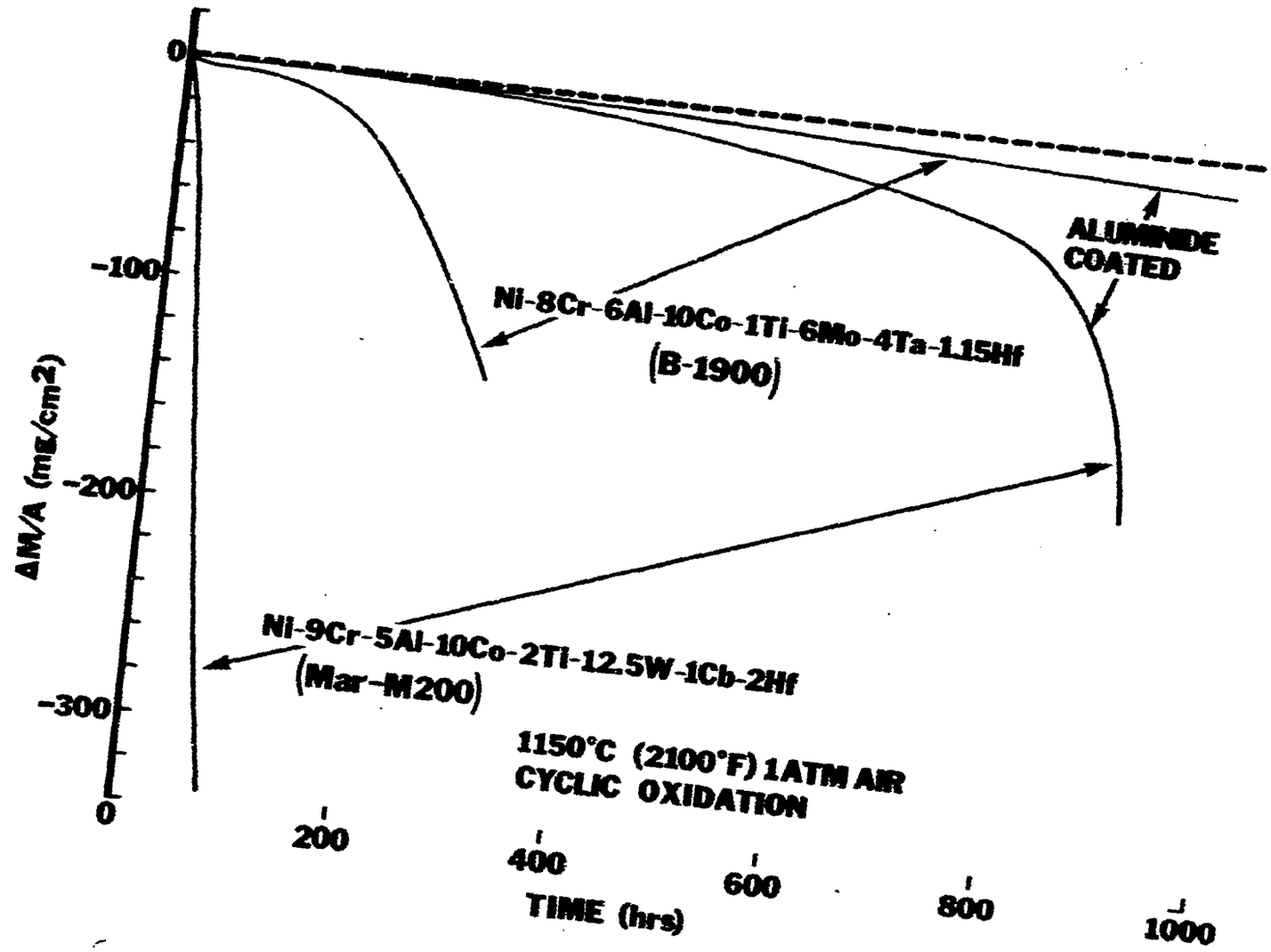

Figure 6. Weight change versus time data for the cyclic oxidation of two nickel-base superalloys and these two alloys coated using a diffusion aluminizing treatment. The degradation of these alloys consists of two stages. An initial stage of less severe attack (not evident on uncoated Mar-M200 for time scale used) and a subsequent stage of more rapid attack.

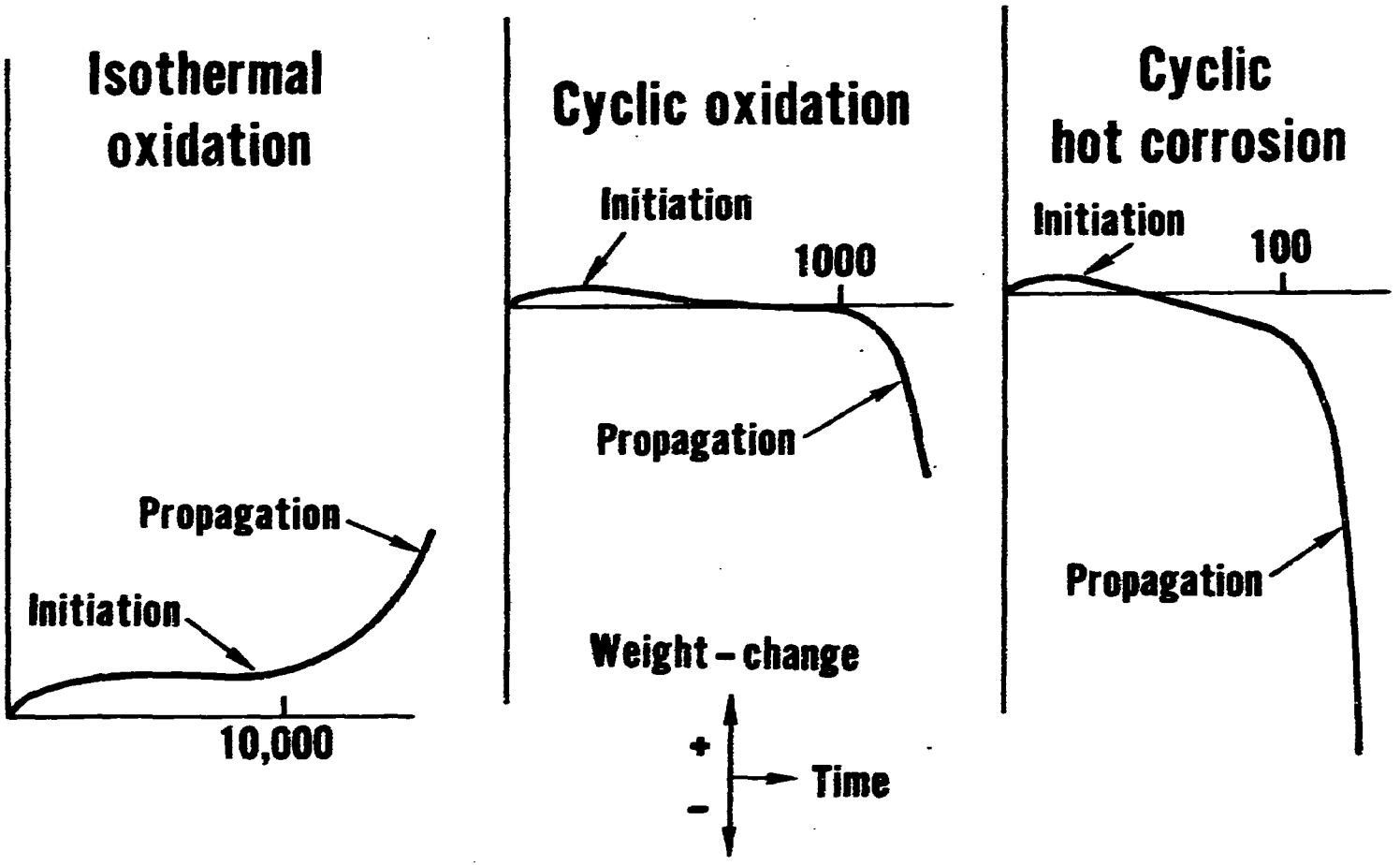

Figure 7. Schematic weight change versus time curves to illustrate that the degradation of corrosion resistant systems consists of an initiation stage and a propagation stage with the more severe attack being associated with the propagation stage. The transition from the initiation to the propagation stage is influenced by factors such as spalling of oxide scales (cyclic oxidation) and salt deposition (hot corrosion).

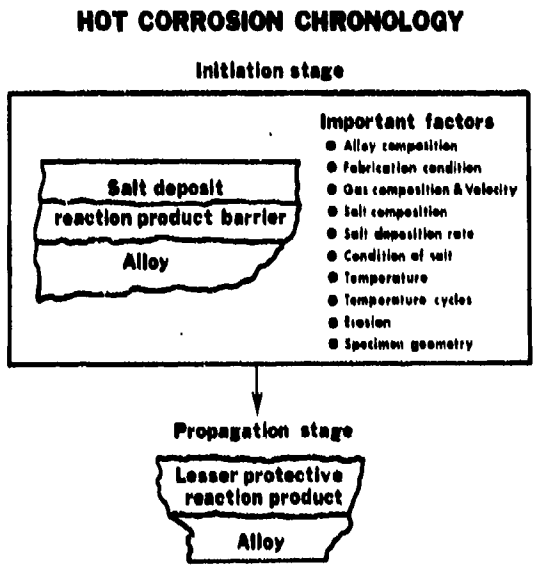

Figure 8. Schematic diagram to illustrate the conditions that develop during the initiation and propagation of hot corrosion attack and to identify the factors that determine the time at which the transition from the initiation stage to the propagation stage occurs.

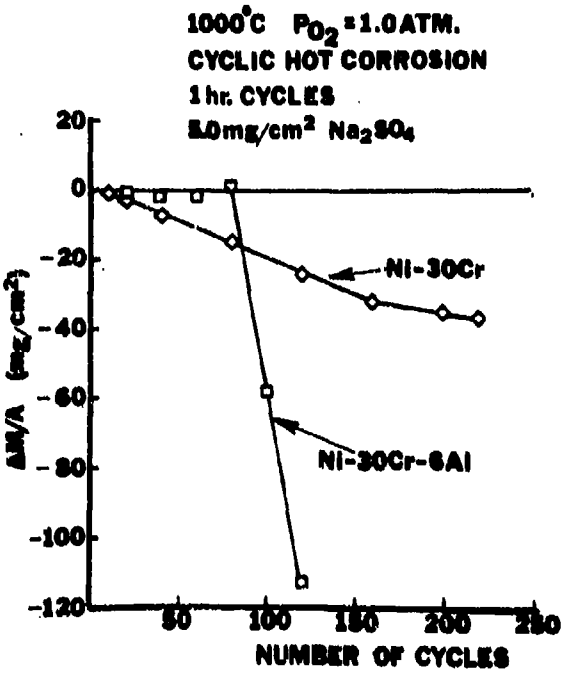

Figure 9. Weight change versus time data for the cyclic hot corrosion of Ni-30Cr and Ni-30Cr-6Al specimens. The aluminum initially causes the Ni-30Cr-6Al to be more resistant than Ni-30Cr, but after longer times it causes more severe attack.

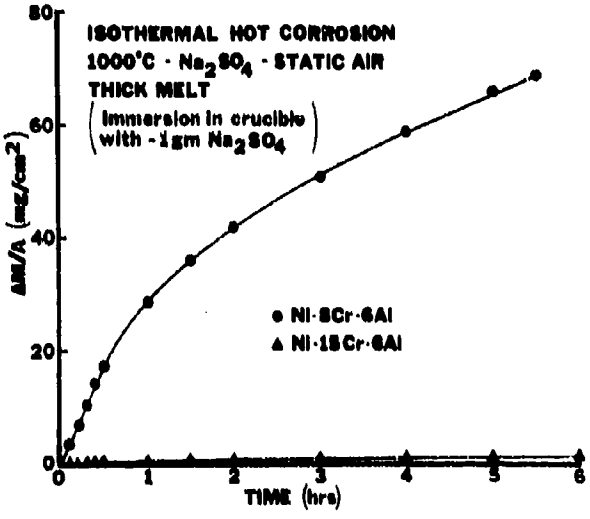

Figure 10. Weight change versus time data showing that increased chromium concentration in Ni-Cr-Al alloys extends the initiation stage for hot corrosion attack induced by large deposits of Na_2SO_4 in air.

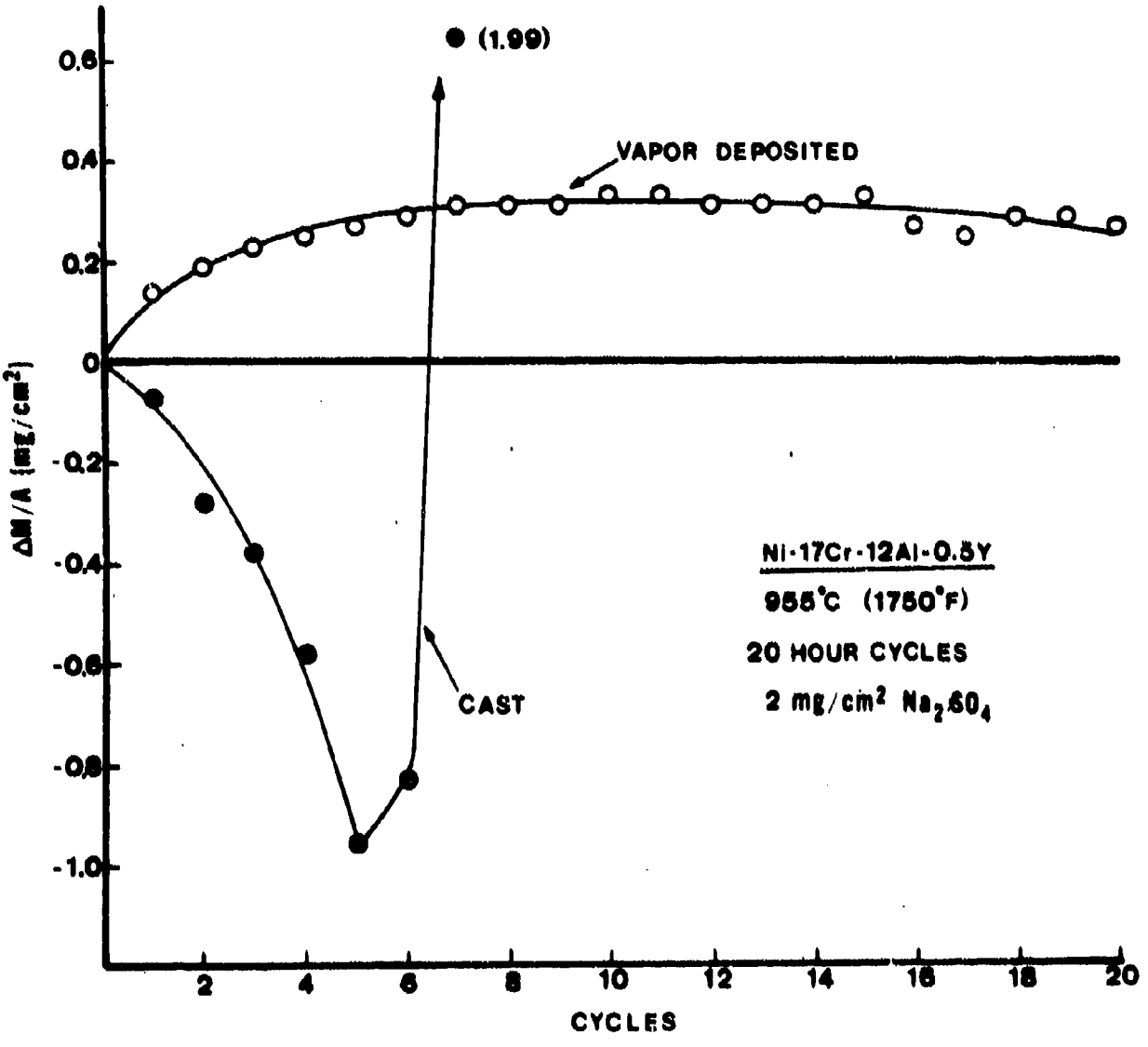

Figure 11. Comparison of weight change versus time data for cyclic hot corrosion of a NiCrAlY alloy in two fabrication conditions. A protective barrier of Al_2O_3 is formed on the vapor deposited alloy but oxides other than Al_2O_3 have been formed on the as cast alloy and it is in the propagation stage of degradation as evidenced by the larger weight changes.

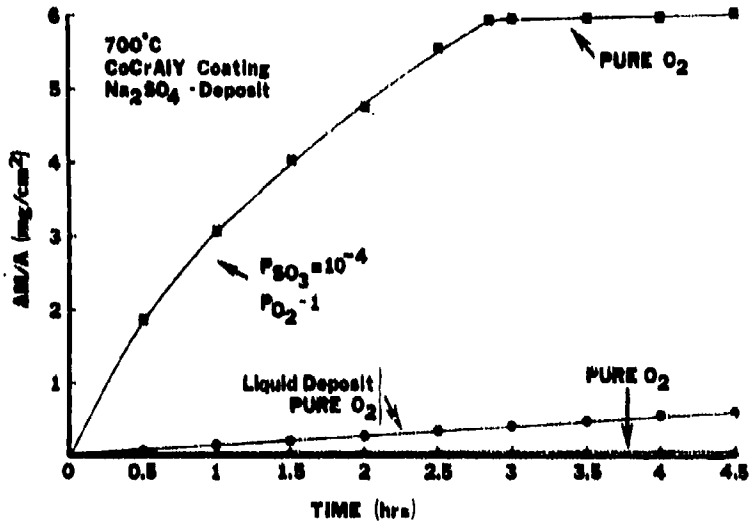

Figure 12. Weight change versus time data obtained for the isothermal hot corrosion of CoCrAlY coated IN 792. Hot corrosion was induced by using Na_2SO_4 deposits (~ 1 mg/cm^2). In one experiment a Na_2SO_4-40 mole percent $MgSO_4$ deposit was used to obtain a liquid deposit at the test temperature. The gas was flowing oxygen except in one experiment where an SO_2-O_2 gas mixture was passed over a platinum catalyst to develop an SO_3 pressure of 10^{-4} atm during the first 2.9 hrs. of the experiment.

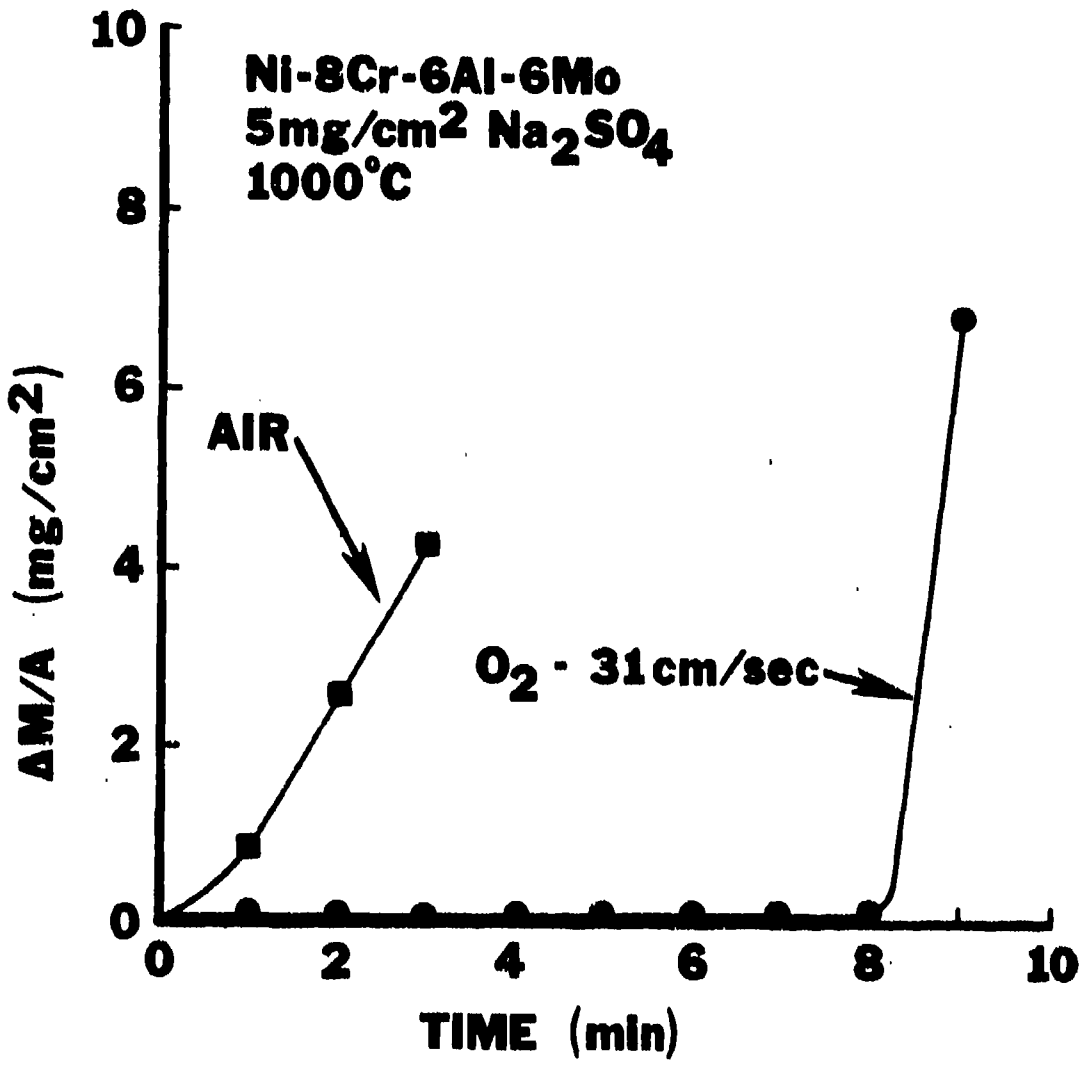

Figure 13. Weight change versus time data obtained for the isothermal hot corrosion of a Ni-8Cr-6Al-6Mo alloy in static air and in oxygen having a linear flow rate of 31 cm per sec.

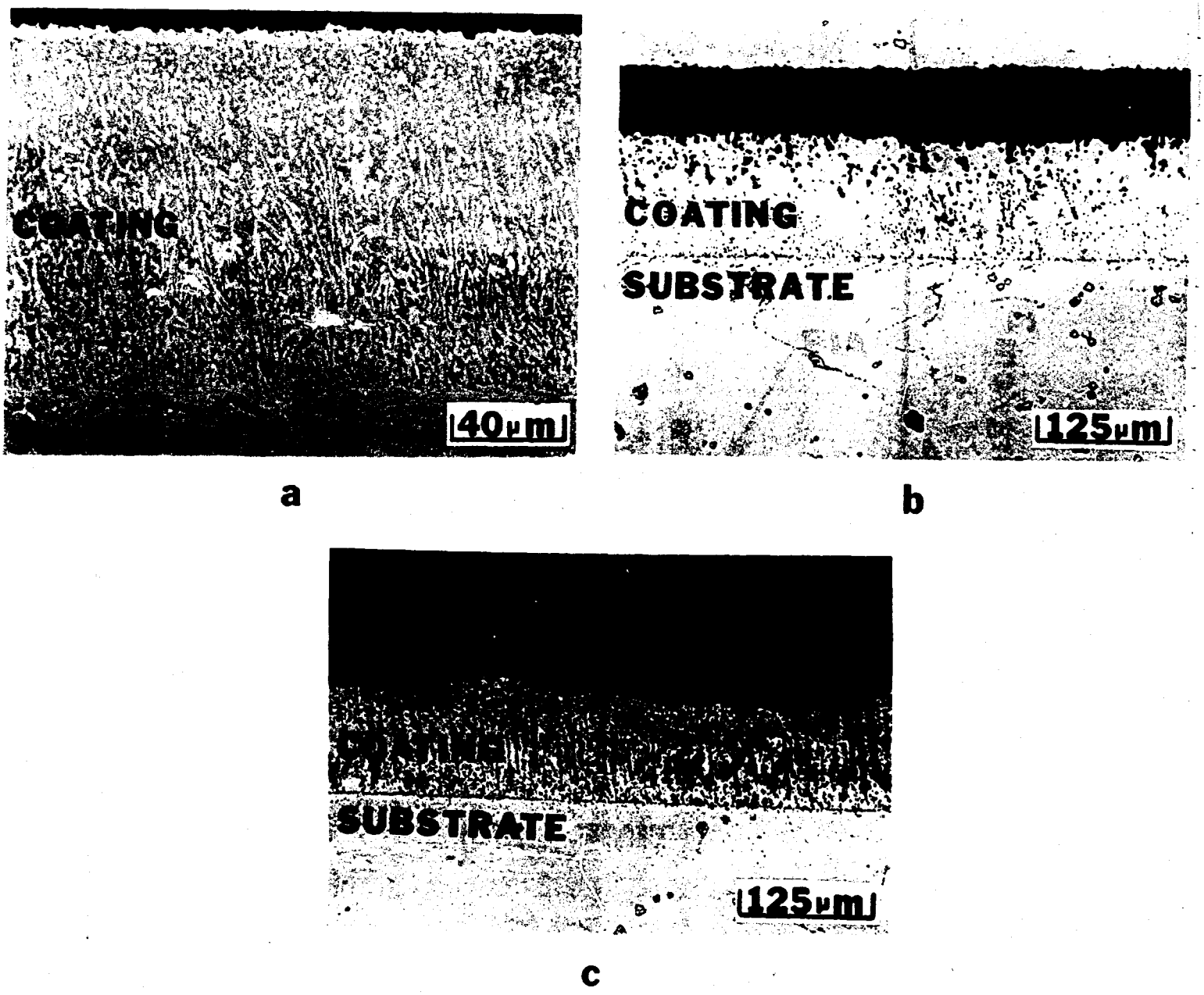

Figure 14. Photomicrographs to compare the degradation of CoCrAlY coatings on IN 738 after exposure at 899°C in air to Na_2SO_4 deposits containing different amounts of NaCl. (a) 500 hrs. with Na_2SO_4, (b) 500 hrs. with Na_2SO_4-5 weight percent NaCl, (c) 40 hrs. with Na_2SO_4-90 weight percent NaCl.

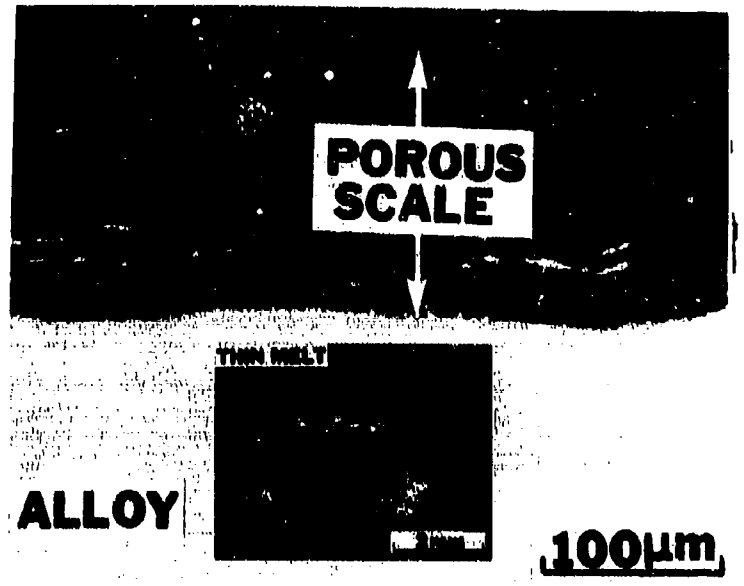

a

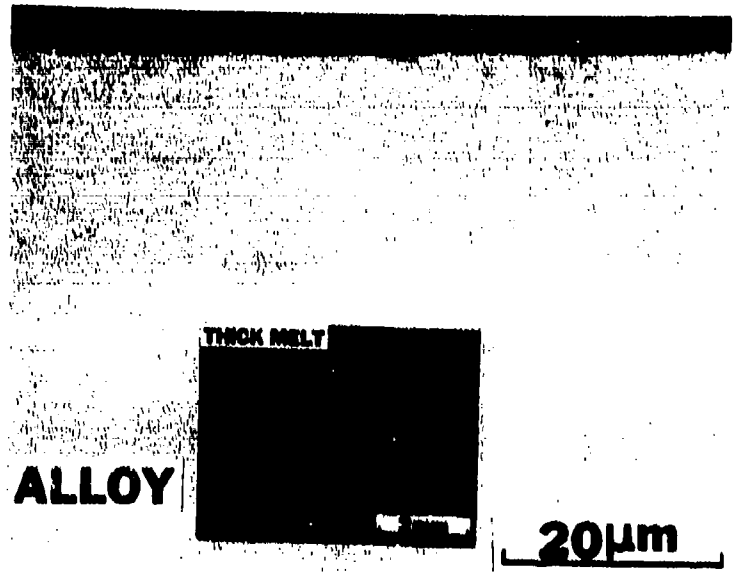

b

Figure 15. Surface and microstructural features developed for Ni-8Cr-6Al-6Mo specimens after exposure at 1000°C in air to thin (a, ~ 5 μm, 7 minutes exposure) and thick melts (b, ~ 1 cm, 4 minutes exposure) of Na_2SO_4. Attack with the thin deposit was evident visually after less than 1 minute and usually spread laterally over the surface from the point of initiation. The specimen in the thick melt showed no attack after 4 minutes.

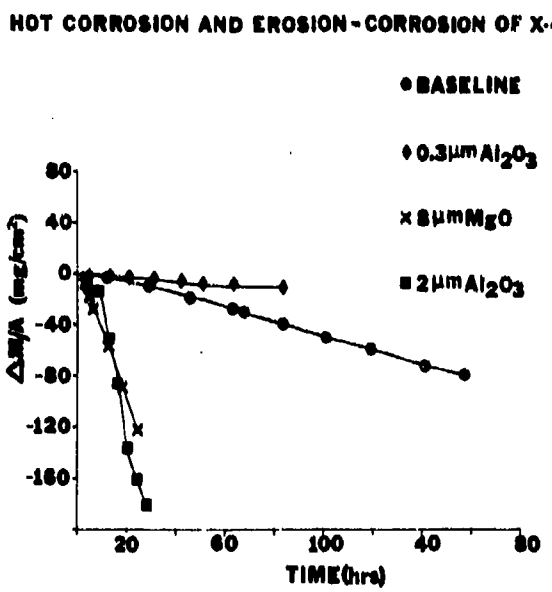

Figure 16. Weight change versus time curves for X-40 specimens (Co-25.3Cr-10.5Ni-7.5W-0.5C) exposed in a high velocity burner rig (gas velocity ~ 180 m/s) at 871°C (1600°F) to hot corrosion conditions (baseline conditions: Na_2SO_4-22 weight percent K_2SO_4 deposited at 0.05 mg/cm^2-hr) and erosion-hot corrosion conditions (baseline conditions plus 300 ppm of oxides having indicated average particle sizes). The 0.03 μm Al_2O_3 particles deposited on the leading edges of specimens.

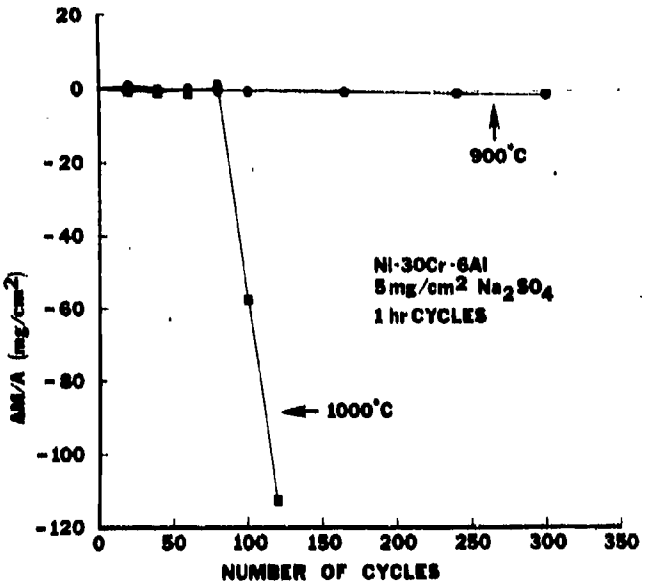

Figure 17. Weight change versus time data for the cyclic hot corrosion in air of Ni-30Cr-6Al specimens using Na_2SO_4 deposits applied every 20 hrs; at 1000°C the initiation stage for hot corrosion is less than 100 hrs, whereas at 900°C it is greater than 300 hrs.

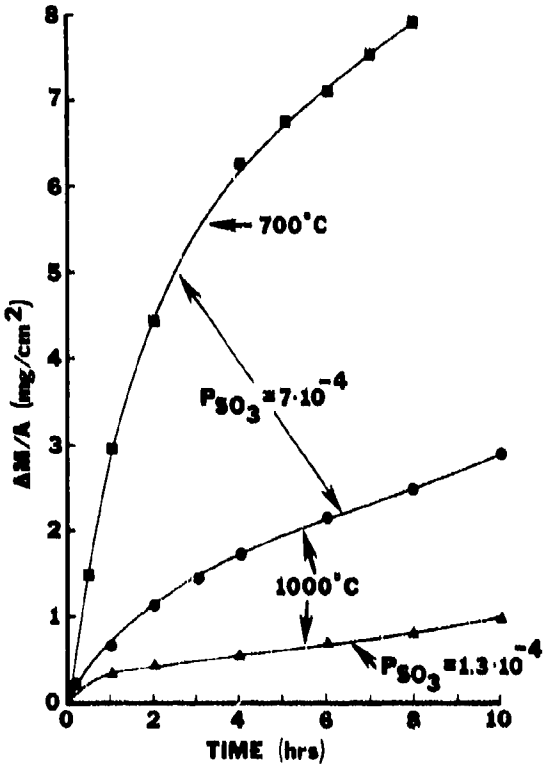

Figure 18. Weight change versus time data for the hot corrosion attack of a CoCrAlY coating on IN 738 using 1 mg/cm^2 Na_2SO_4 deposits and SO_2/O_2 gas mixtures. When the SO_2-O_2 ratios were adjusted to give the same SO_3 pressure, more attack occurred at the lower temperature. When the same ratio was used at both temperatures, a lower SO_3 pressure was developed at the higher temperature.

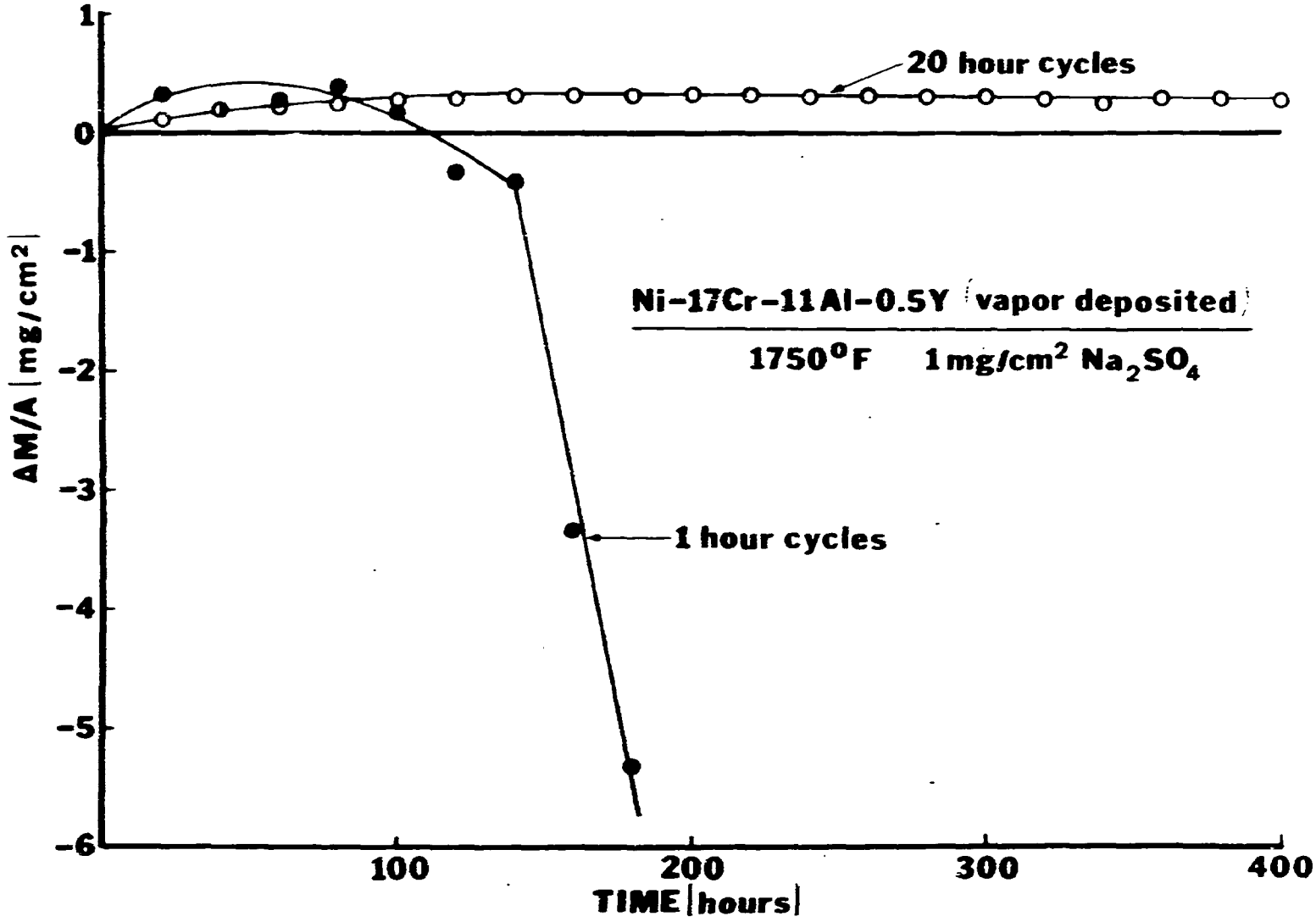

Figure 19. Comparison of weight change versus time data obtained by using two different thermal cyclic frequencies for a cyclic hot corrosion test in air where Na_2SO_4 was reapplied every twenty hours. Hot corrosion attack has been initiated sooner in the specimen subjected to the more frequent number of thermal cycles.

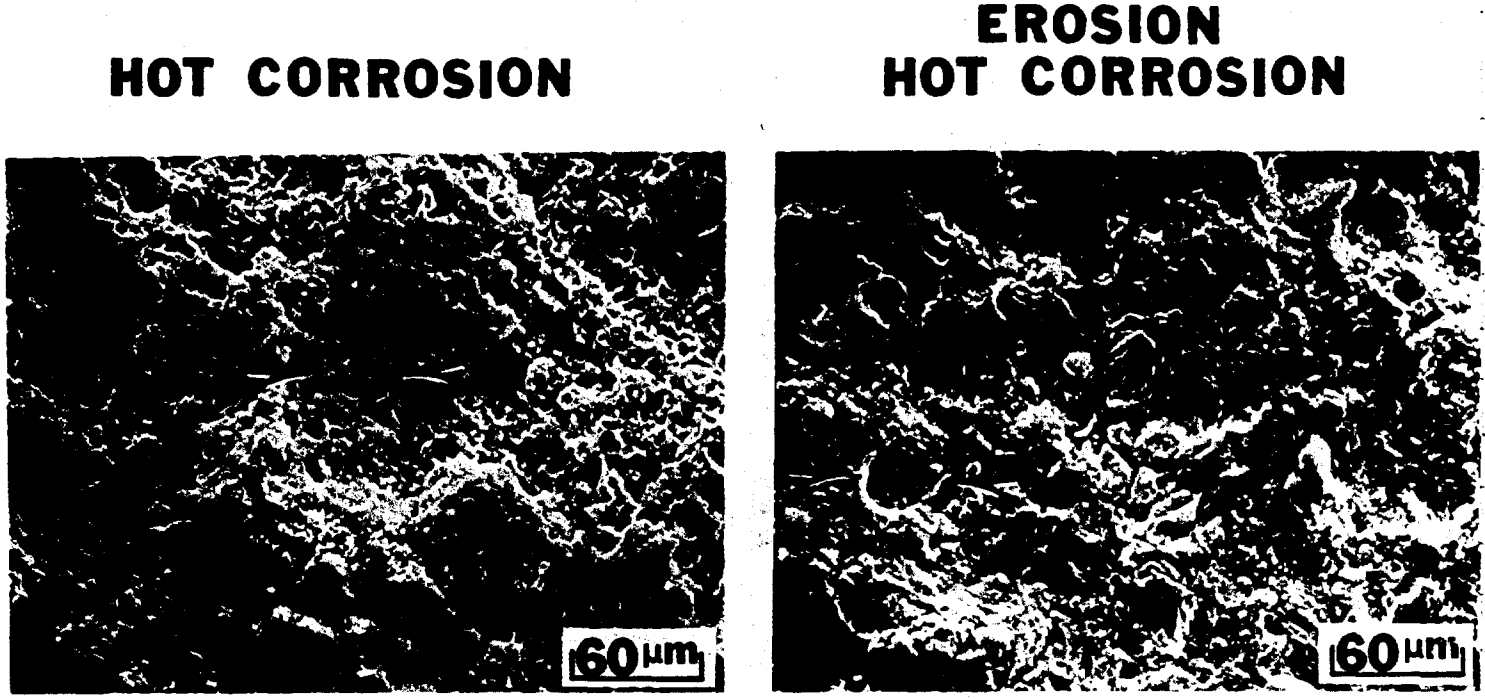

Figure 20. Scanning micrographs comparing features of oxide scales (oxide-gas interface) formed on IN 738 after exposure in a burner rig at 871°C to hot corrosion (0.05 mg/cm^2-hr Na_2SO_4-22 w/o K_2SO_4) and erosion-hot corrosion (0.05 mg/cm^2-hr Na_2SO_4-22 w/o K_2SO_4 and 300 ppm 2.5 µm Al_2O_3 particles at 180 m/s). The erosive component has removed much of the porous oxide that is normally developed on this alloy during hot corrosion attack.

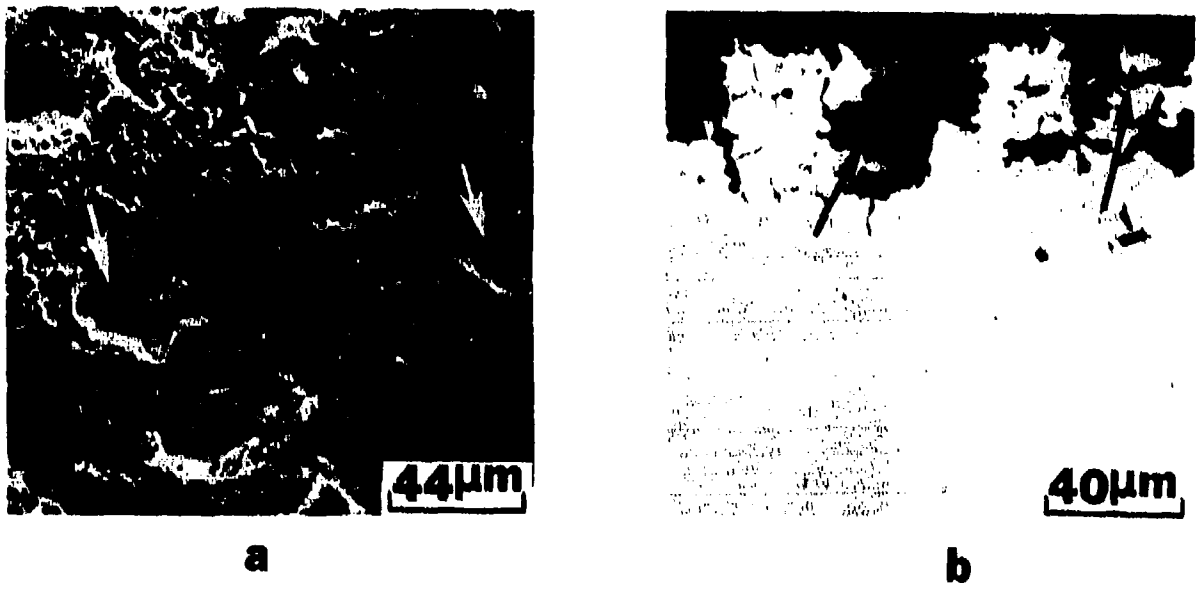

Figure 21. Scanning and microstructural photomicrographs of an IN 738 specimen that was exposed to erosion-corrosion conditions (described in Figure 20); large craters on the specimen surface (white arrows) are believed to be formed because of dislodgement of oxides and alloy (black arrows) by impacting particles.

Figure 22. Photograph of the surface of a Co-25Cr-6Al specimen after 400 cycles at 1000°C in 1 atm of oxygen with 5 mg/cm^2 Na_2SO_4 applied to specimen every 20 hrs; the hot corrosion attack initiated at the edge of this specimen.

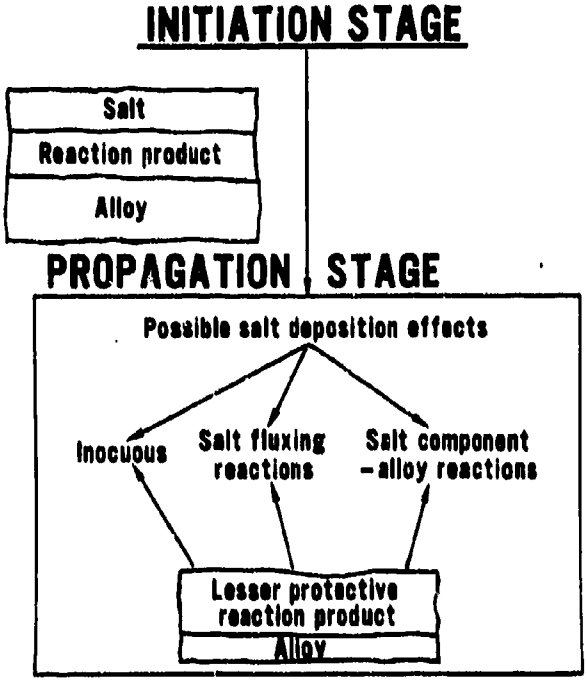

Figure 23. Schematic diagram to illustrate the three general categories of protective scale breakdown to a lesser protective reaction product when a salt deposit is present during the corrosion process.

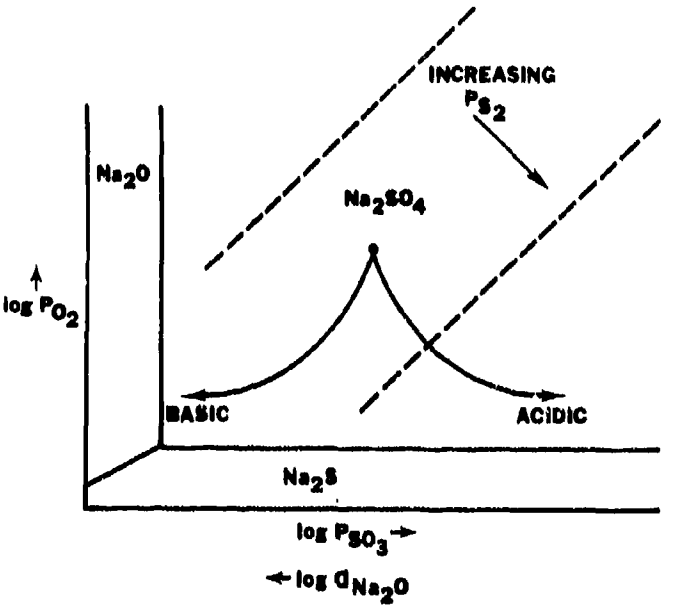

a

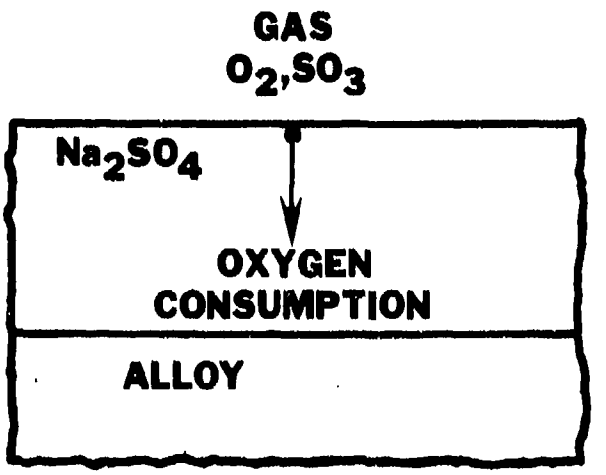

b

Figure 24. Schematic stability diagram for Na-S-O system, (a), depicting the types of compositional variations that can be developed across a layer of Na_2SO_4 on an alloy (b).

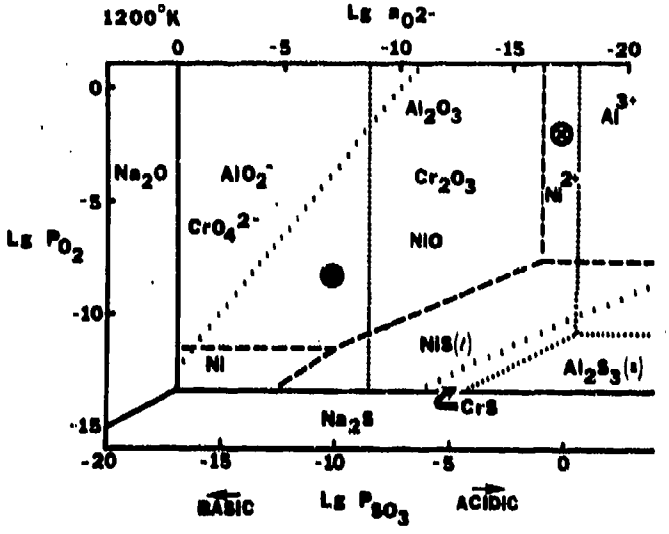

Figure 25. Stability diagram to illustrate the phases of nickel (---), aluminum (....) and chromium (xxx) which can exist in a Na_2SO_4 layer on a Ni-Cr-Al alloy. The Na_2SO_4 region is bounded by Na_2O and Na_2S and indicated by solid straight lines. In Na_2SO_4 of the composition ⊗, NiO will dissolve making the Na_2SO_4 more basic whereas Al_2O_3 will not react with the melt. In Na_2SO_4 of the composition ●, Al_2O_3 will dissolve making the melt more acidic while Cr_2O_3 will not react.

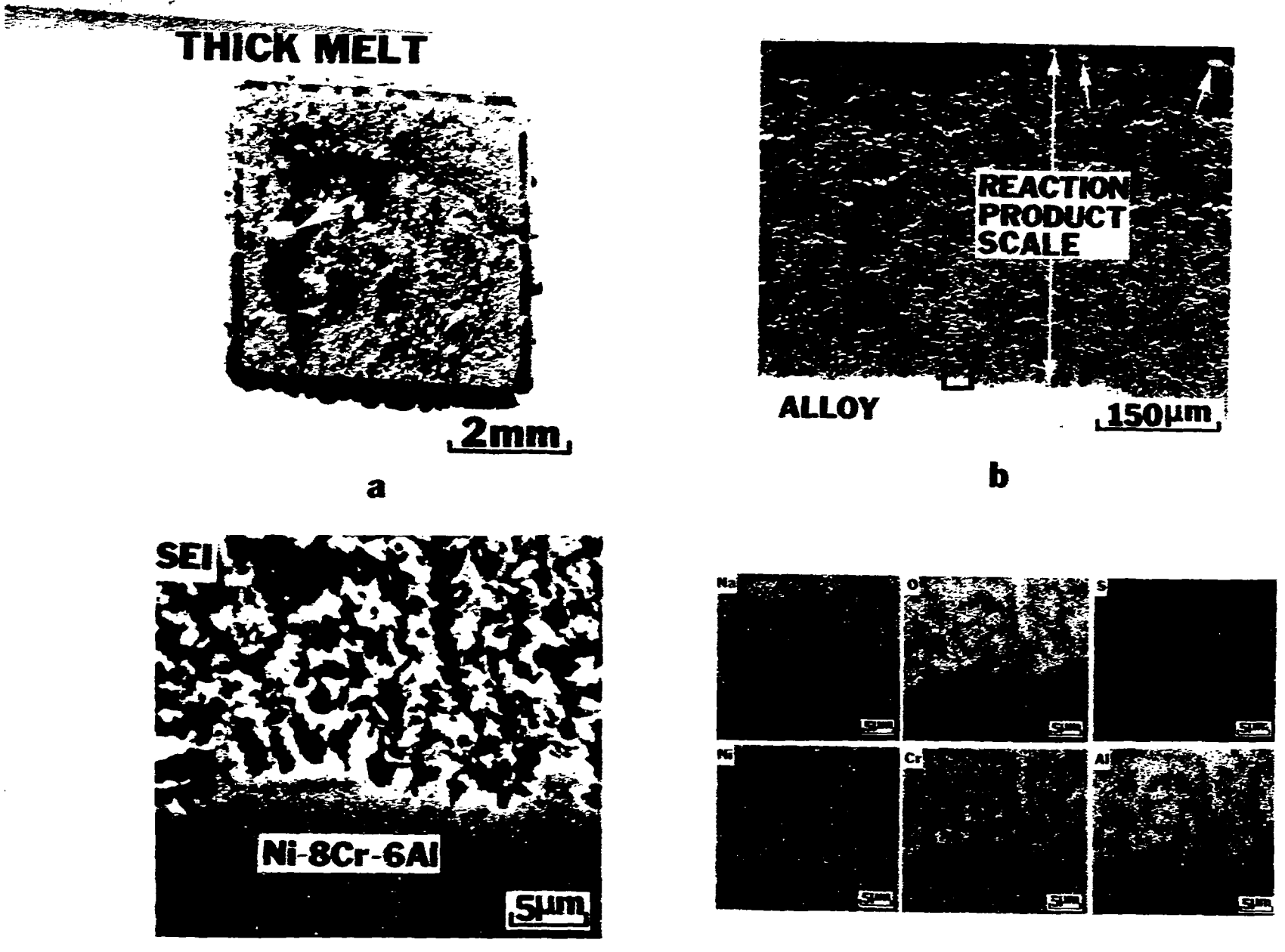

Figure 26. Surface, (a), and microstructural features, (b) and (c), developed in Ni-8Cr-6Al specimen after exposure at 1000°C in air to thick melts (1 gm Na_2SO_4) for 10 minutes. These features are typical of hot corrosion via the basic fluxing propagation mode. Nickel sulfide is evident in the outer part of the reaction product (arrows, a and b) and the X-ray images show that the reaction product scale adjacent to the alloy, (c), consists of nickel ~~particles,~~ stringers and Na_2SO_4 containing aluminum and chromium.

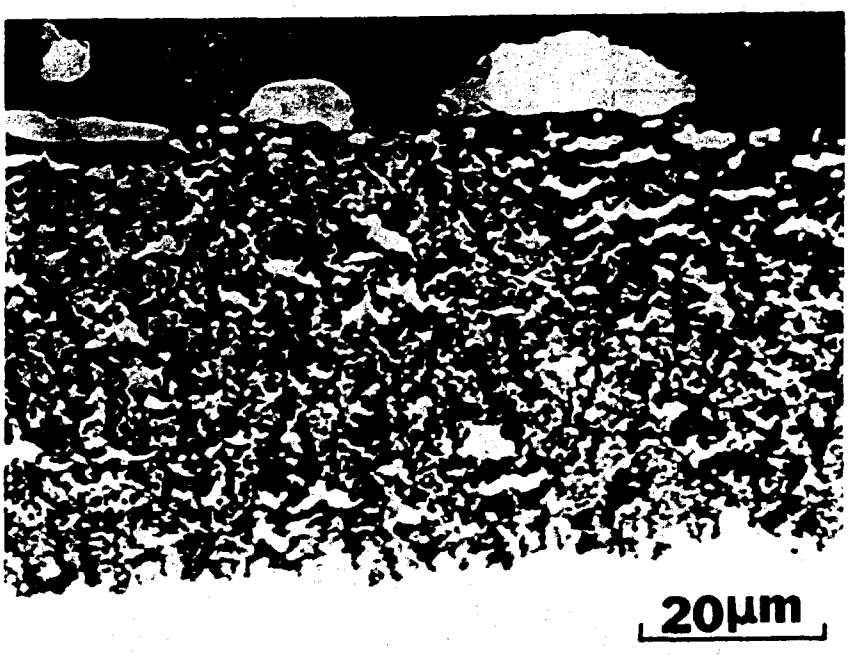

a

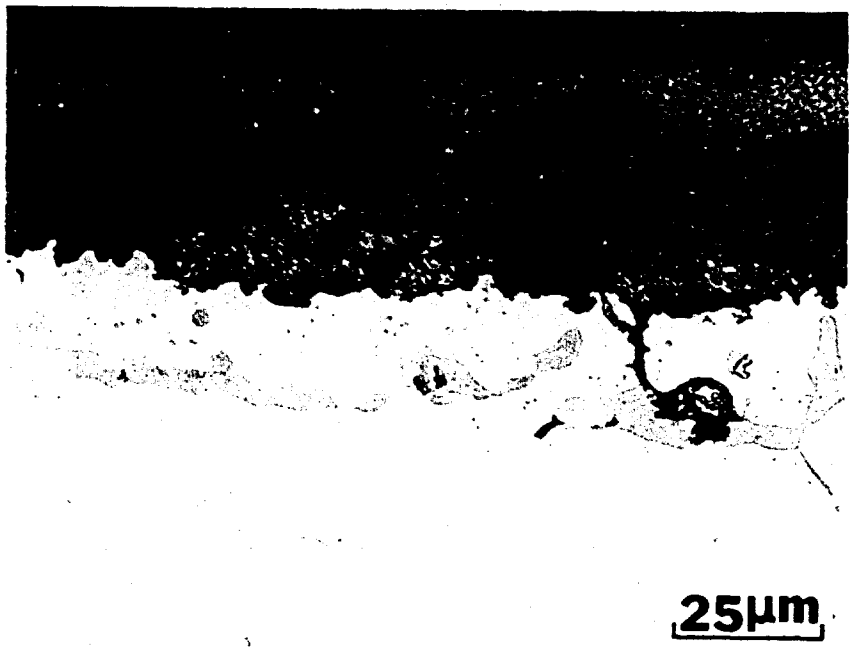

b

Figure 27. Microstructural photomicrographs showing features of Ni-8Cr-6Al specimens after exposure at 1000°C in air to 5 mg/cm^2 Na_2SO_4 for 2 minutes, (a), and 1 hr, (b). Degradation via basic fluxing is evident after two minutes, (a), but the Na_2SO_4 becomes consumed after 1 hr, hence the rapid attack ceases and the microstructure no longer exhibits the basic fluxing features, (b).

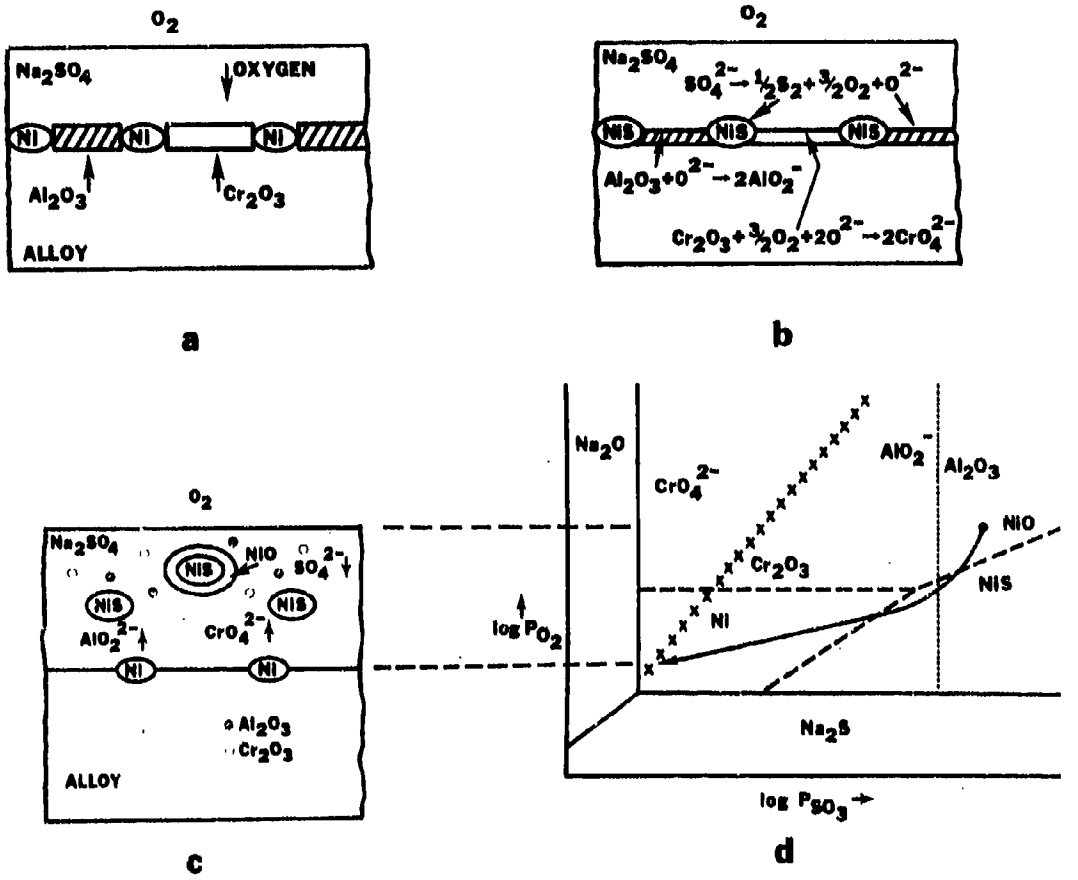

Figure 28. Schematic diagrams to illustrate the Na_2SO_4-induced hot corrosion of a Ni-8Cr-6Al alloy in air. Oxygen depletion occurs, (a), and sulfide formation results in the production of oxide ions which react with Al_2O_3 and Cr_2O_3, (b). At higher oxygen pressures the Cr_2O_3 and Al_2O_3 precipitate from the melt, (c). A phase stability diagram, (d), is used to account for the stability of phases in (c).

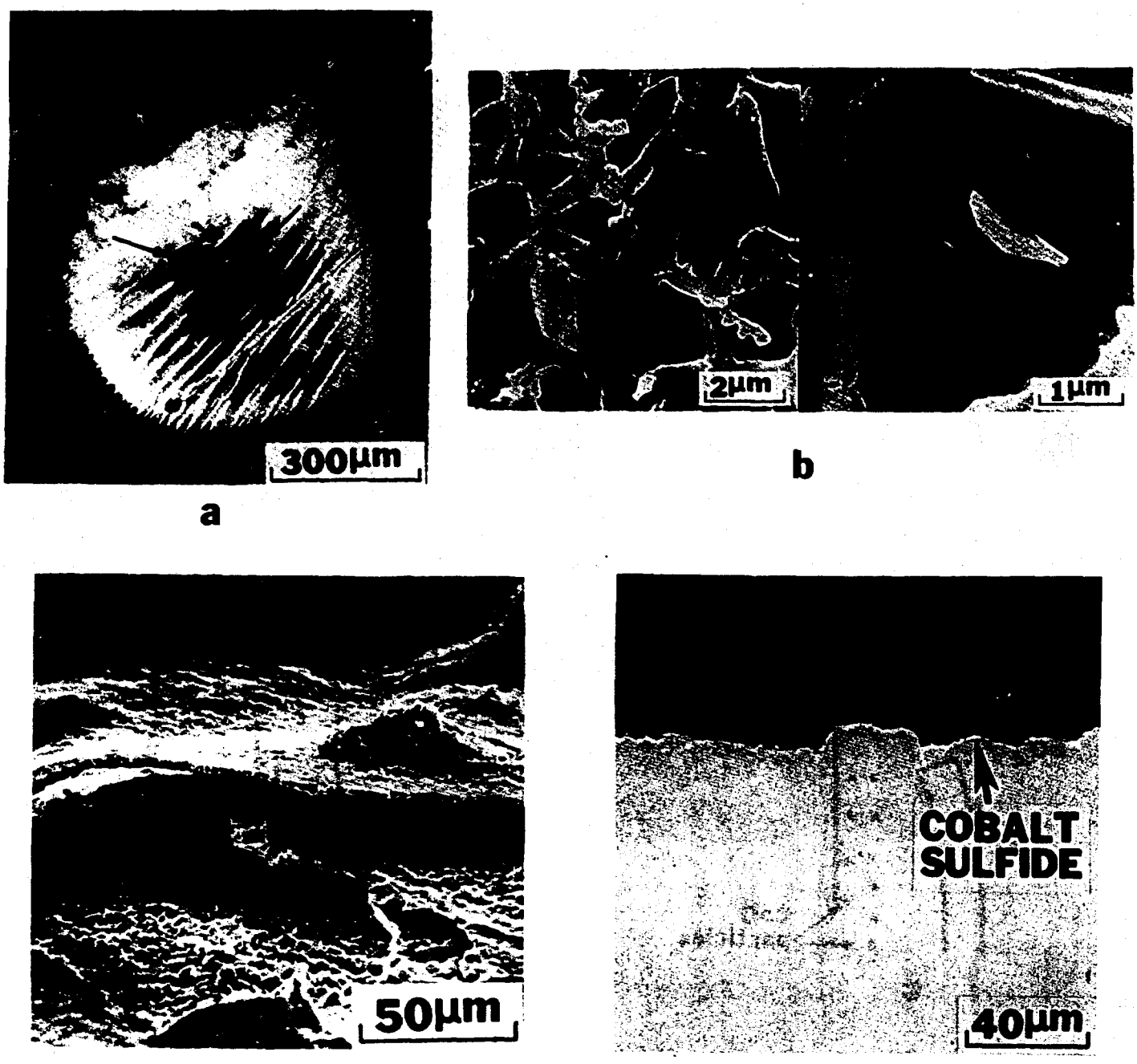

Figure 29. During the oxidation of Na_2SO_4-coated cobalt specimens at 1000°C in air, puddles of Na_2SO_4 (white arrows) are formed in which particles of oxide (black arrows) were suspended (a, 30 sec). The oxide beneath these puddles of Na_2SO_4 contained deep depressions and small holes at oxide grain boundaries (b, 30 sec). The oxide scale was composed of layers and sulfide could be detected in the metal adjacent to the scale, (c and d, 3 min).

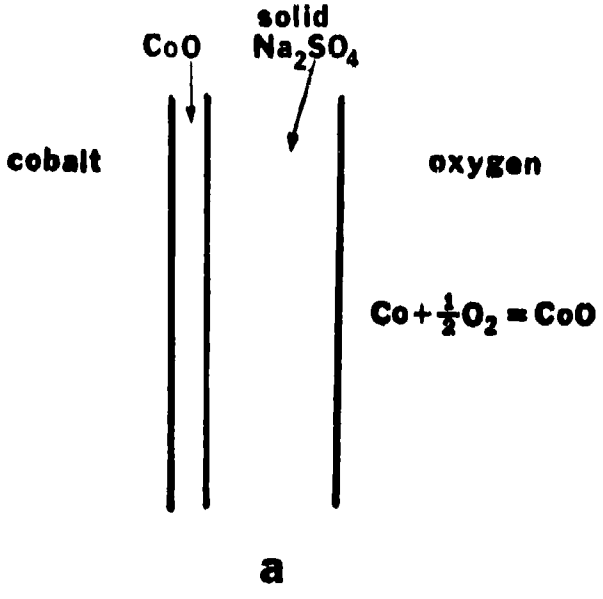

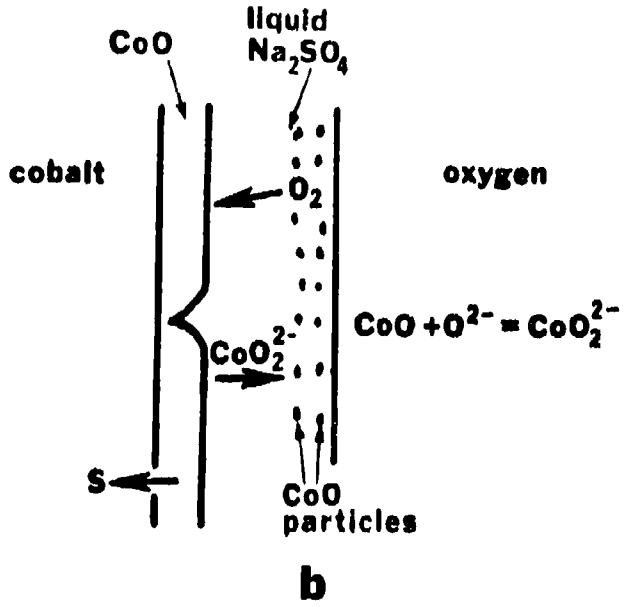

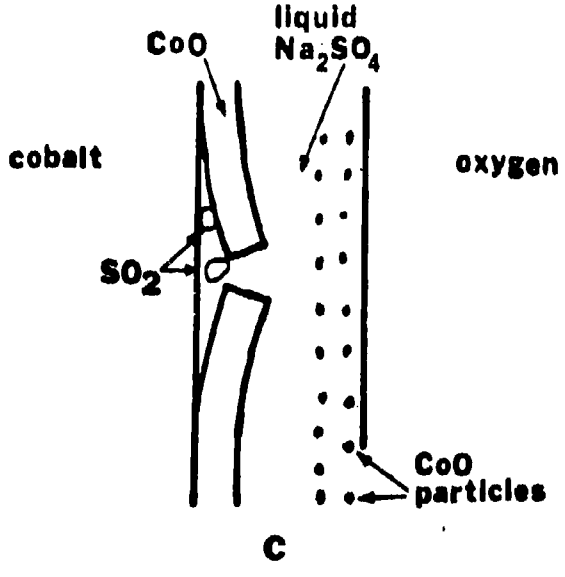

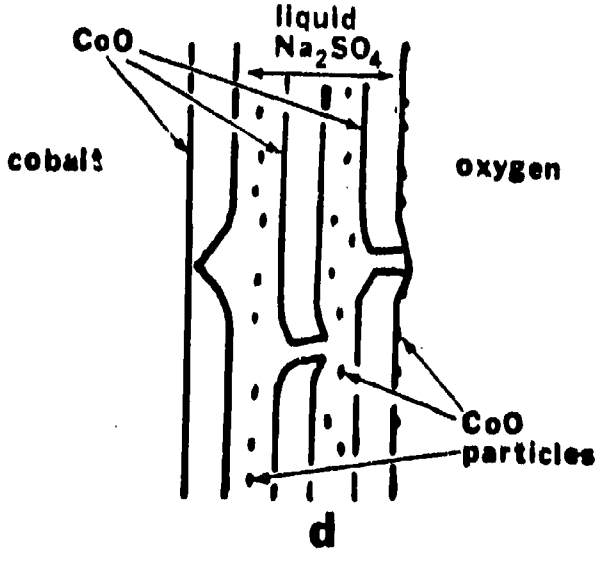

Figure 30. Schematic model illustrating the sequential steps in the Na_2SO_4-induced hot corrosion of cobalt in oxygen.

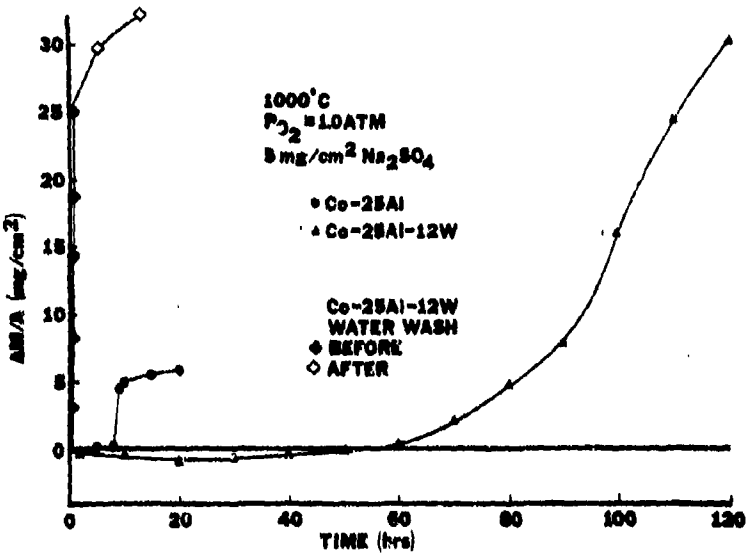

Figure 31. Weight change versus time data to compare the hot corrosion attack of Co-25Al and Co-25Al-12W alloys. Preannealing of the Na_2SO_4-coated specimens of Co-25Al-12W for 1 hour at 1000°C in dry argon (◇ data points) greatly reduced the time required to initiate hot corrosion attack. Data for oxidation without Na_2SO_4 was about the same for both alloys, Figure 4.

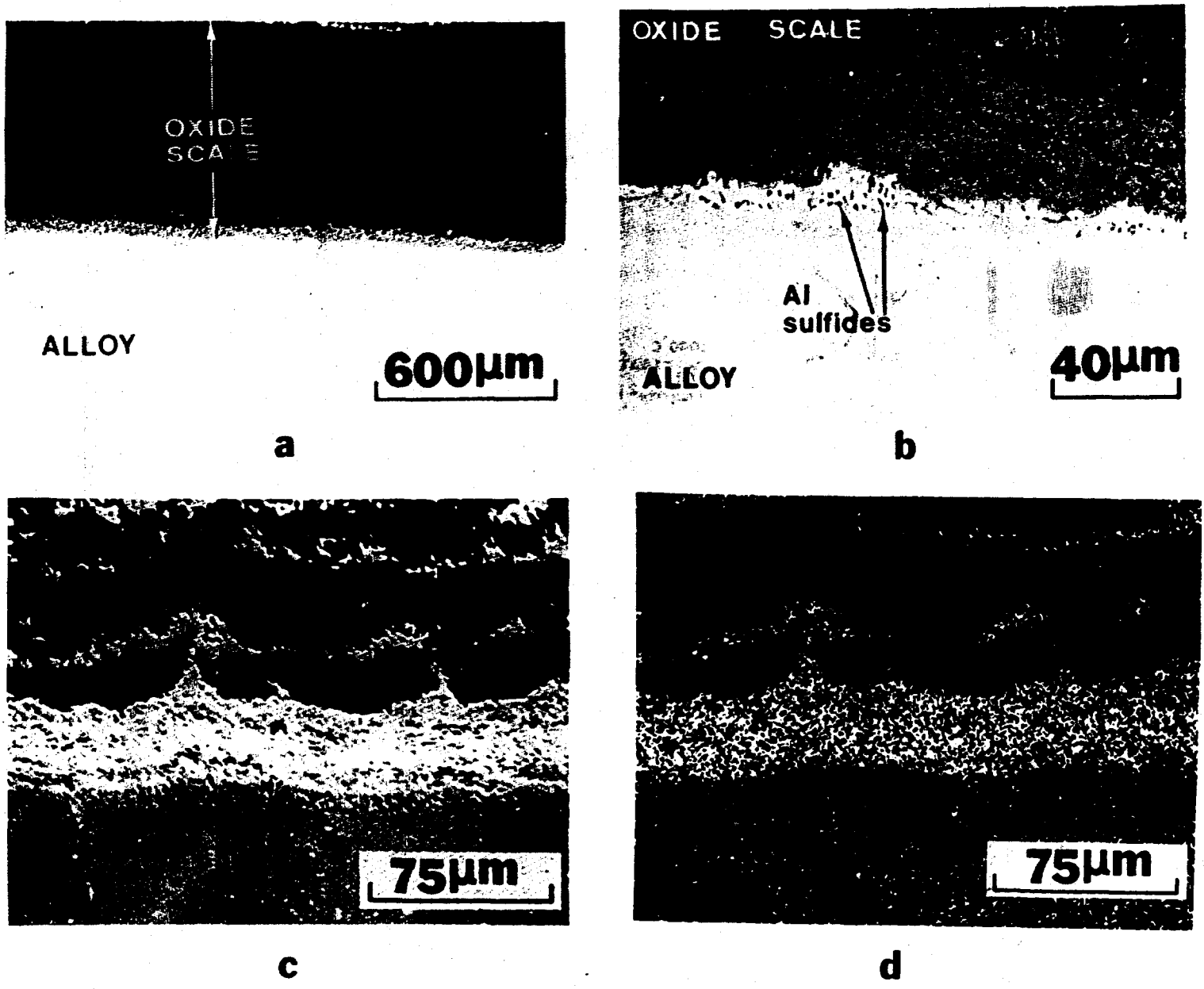

Figure 32. Microstructural photomicrographs and microprobe images of a Co-25Al-12W alloy specimen after 20 hrs. of oxidation in 1 atm of oxygen at 1000°C. Prior to oxidation the specimen was coated with 5 mg/cm^2 Na_2SO_4 and annealed for 1 hr. in argon at 1000°C. Weight change data for this specimen are presented in Figure 31. (a) Optical micrograph showing overall scale thickness. (b) and (c) Optical micrograph and electron backscatter image, respectively, of scale-alloy interface. (d) Tungsten X-ray image showing that tungsten is enriched in the oxide scale at the alloy-scale interface.

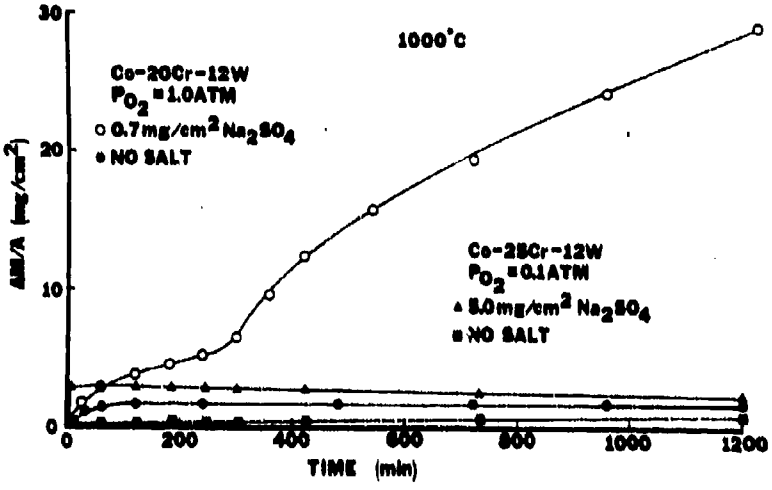

Figure 33. Comparison of isothermal oxidation for Co-20Cr-12W and Co-25Cr-12W alloys with and without Na_2SO_4 deposits. Hot corrosion attack was initiated only in the Co-20Cr-12W alloy coated with Na_2SO_4.

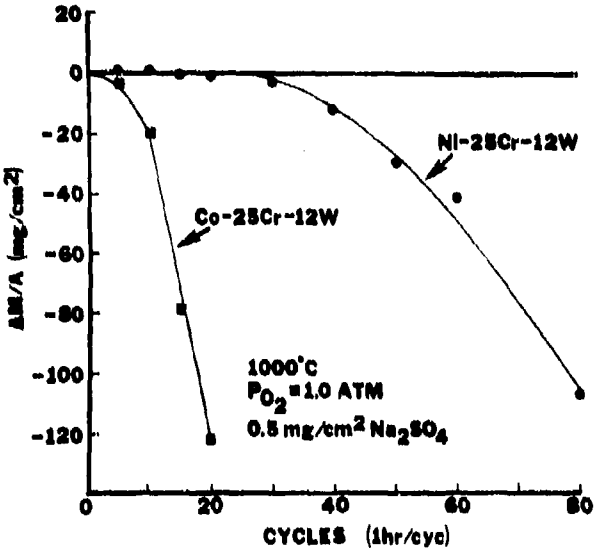

Figure 34. Comparison of cyclic hot corrosion data for specimens of Co-25Cr-12W and Ni-25Cr-12W. Both alloys were severely degraded via hot corrosion.

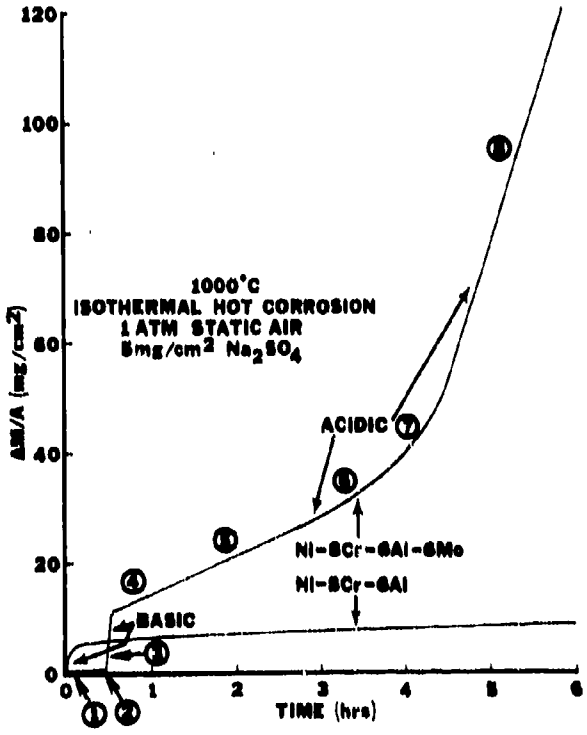

Figure 35. Comparison of the isothermal hot corrosion of Na_2SO_4-coated Ni-8Cr-6Al and Ni-8Cr-6Al-6Mo alloys; both alloys have undergone hot corrosion attack. Degradation microstructures for Ni-8Cr-6Al are presented in Figure 27. The circled numbers in the Figure identify various stages during the hot corrosion of the Ni-8Cr-6Al-6Mo and typical degradation microstructures for this alloy are presented in Figures 36 and 46.

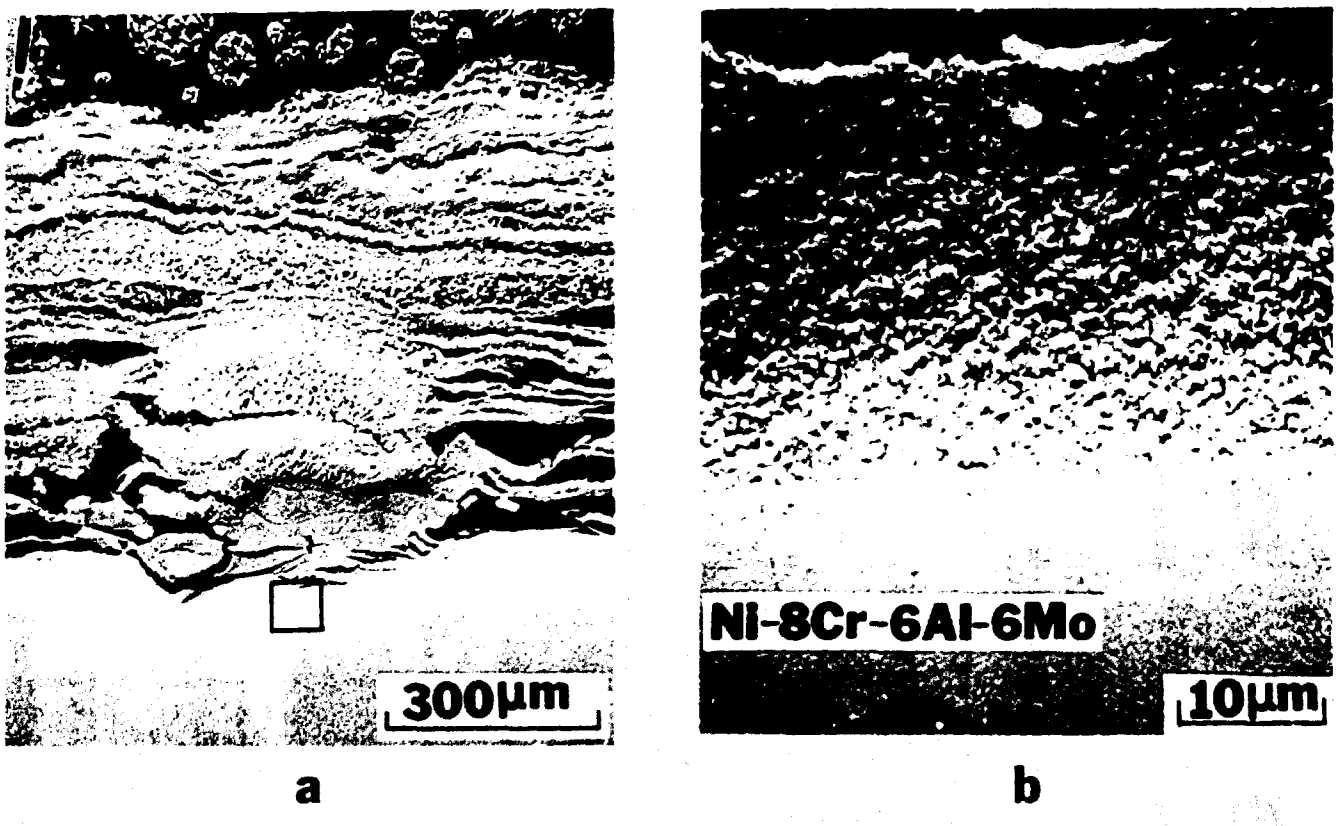

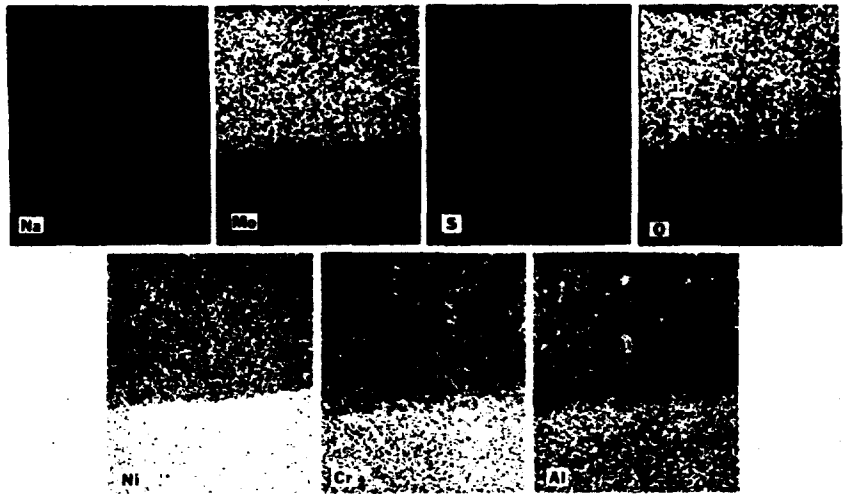

Figure 36. Photograph showing structure of corrosion product formed on Na_2SO_4-coated Ni-8Cr-6Al-6Mo after exposure at 1000°C in flowing oxygen (a). This structure corresponds to stage 8 of Figure 35. Higher magnification of area indicated in (a) showing scale-alloy interface (b). (c) X-ray images of area shown in (b).

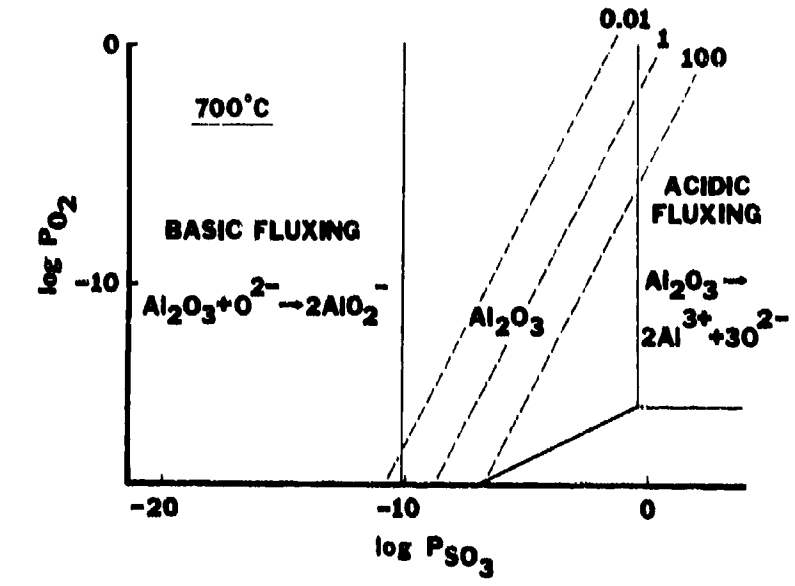

a

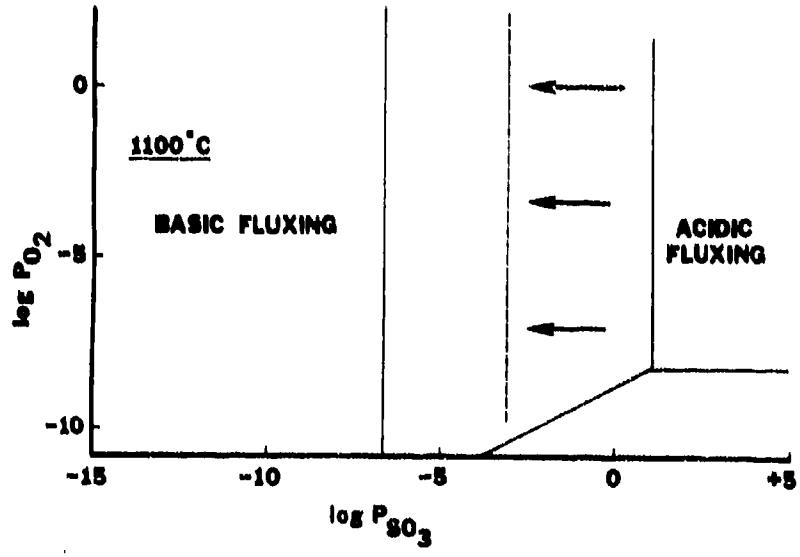

b

Figure 37. Stability diagrams showing the phases of aluminum that can be stable in Na_2SO_4 at 700°C, (a), and 1100°C, (b), and defining regions where basic or acidic fluxing of Al_2O_3 appear possible. Very high SO_3 pressures are required for acidic fluxing at temperatures of 1000° and 1100°C and refractory metal oxides are believed to make acidic fluxing reactions favorable at lower SO_3 pressures as indicated by the displaced boundary in (b) (arrows). Dashed lines in (a) are SO_2 isobars (atms).

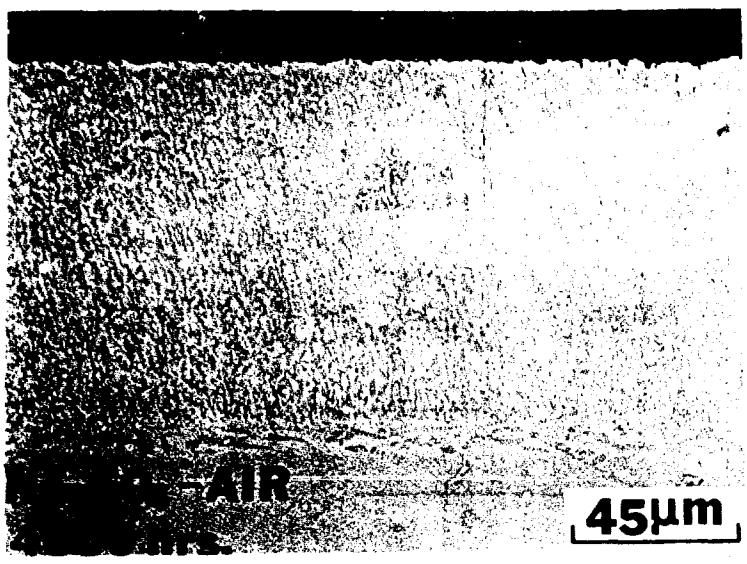

a

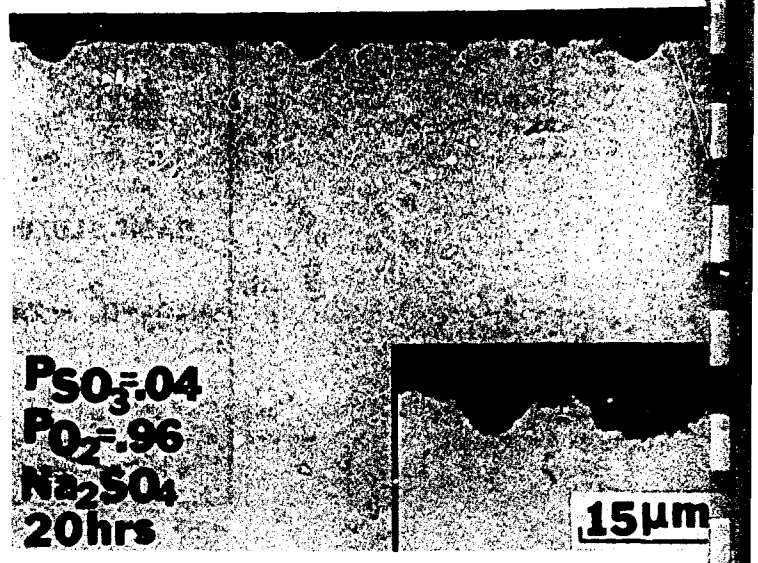

b

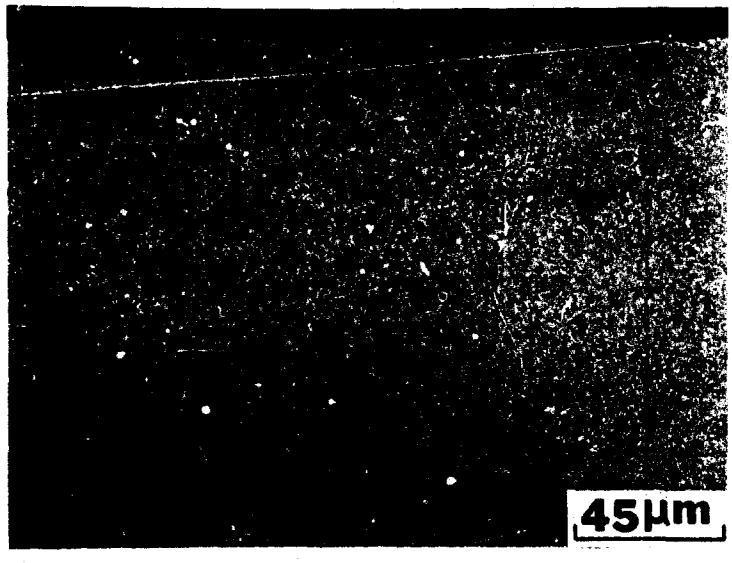

c

Figure 38. Microstructural photomicrographs to compare the attack of CoCrAlY coatings on IN 738 after exposure at 649°C. The combination of Na_2SO_4 and SO_3 is very effective in producing attack whereas a significant amount of attack at 649°C is not observed for Na_2SO_4 or SO_3 acting independently.

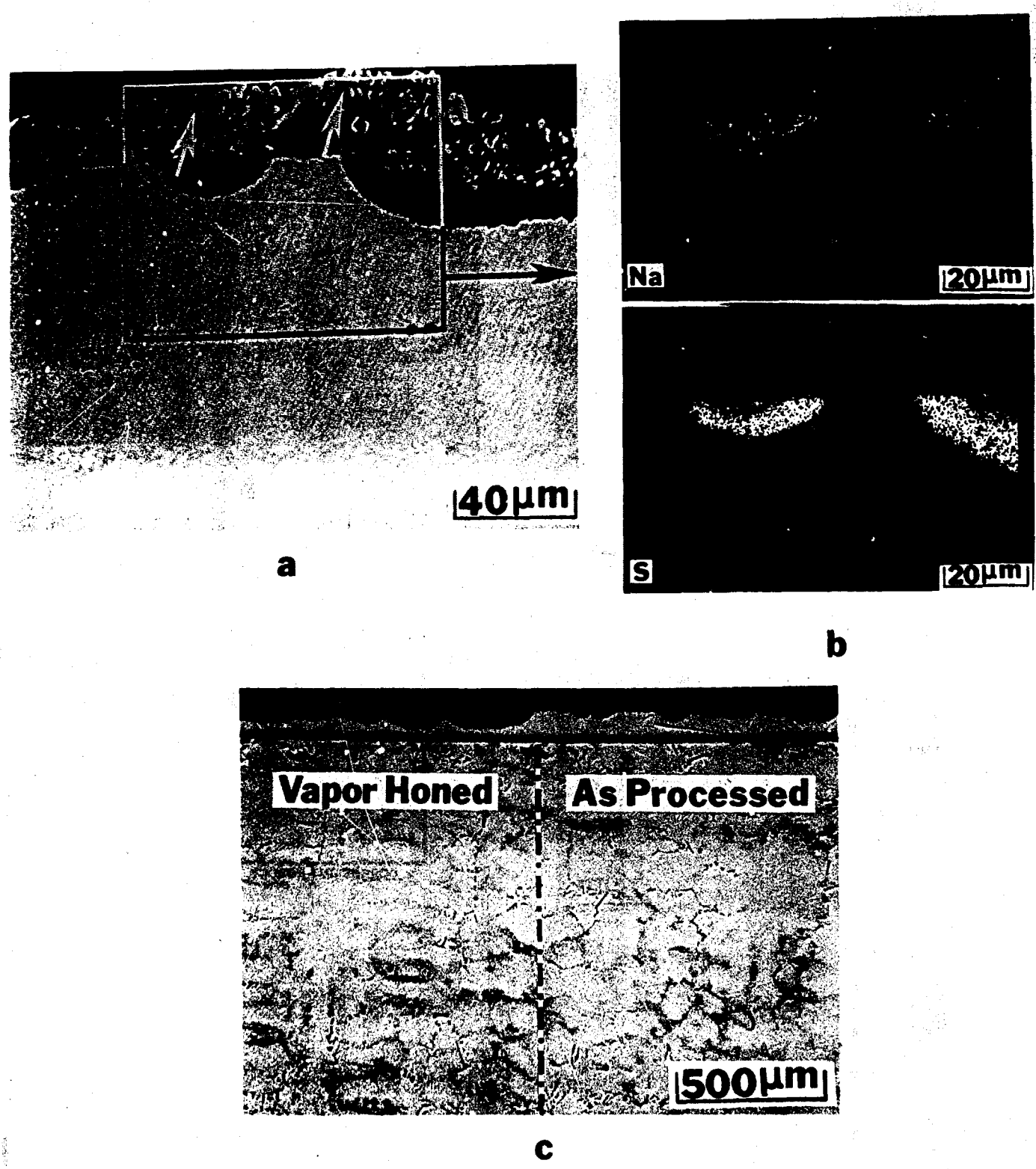

Figure 39. Degradational features developed during the hot corrosion of CoCrAlY coatings as a result of exposure at 704°C to Na_2SO_4 deposit (~ 1 mg/cm^2) and oxygen containing SO_3 at $7 \cdot 10^{-4}$ atm; (a) localized attack is evident and the outer zone of the corrosion product (arrows) is rich in cobalt, (b) X-ray images show that sodium and sulfur are present in the corrosion product, (c) the localized nature of the attack is less evident on vapor honed specimens.

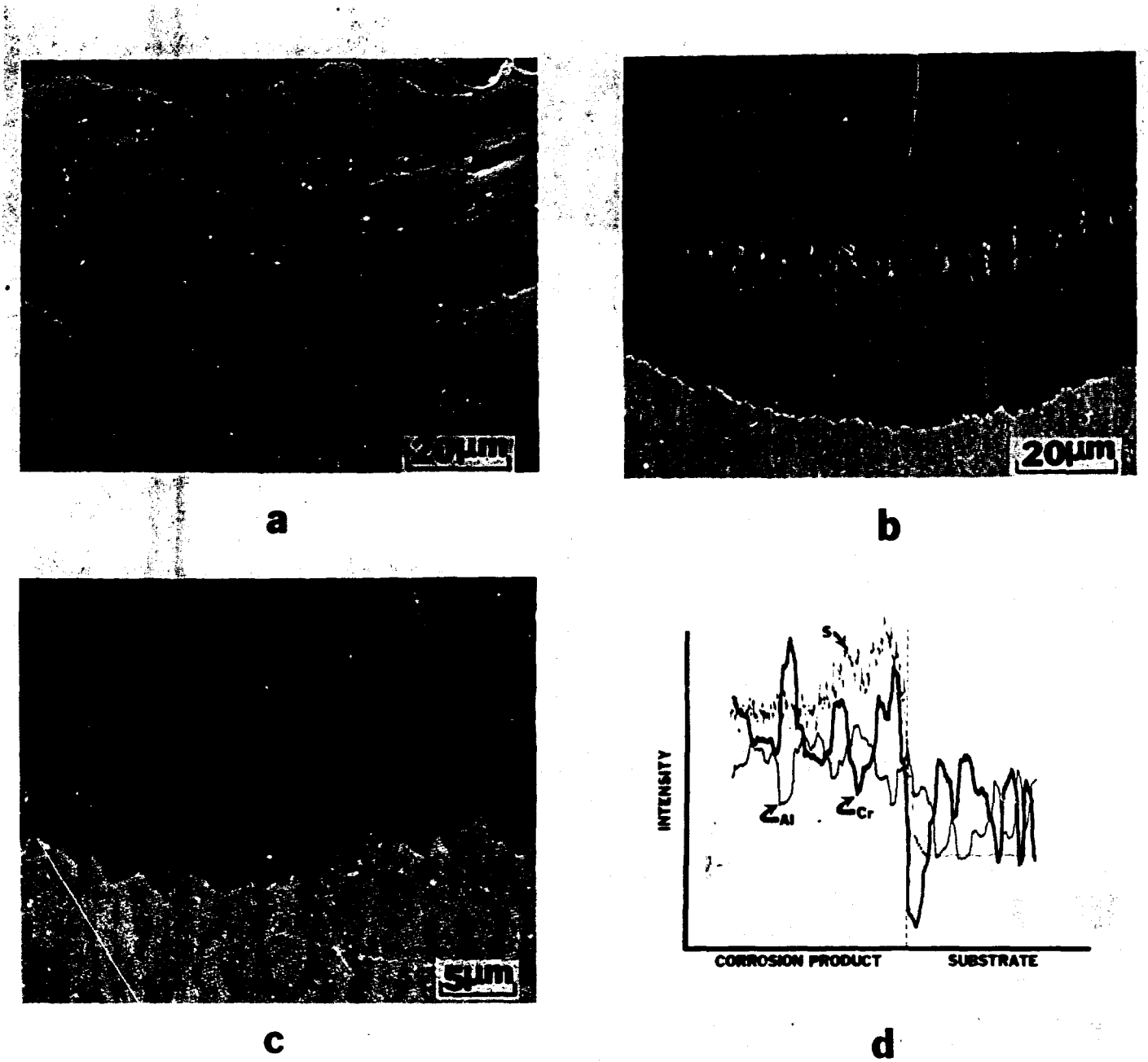

Figure 40. Microstructural features developed in a CoCrAlY alloy during 17.3 hrs. of exposure to a Na_2SO_4 deposit (2.5 mg/cm^2) and oxygen containing SO_3 ($7 \cdot 10^{-4}$ atm) at 704°C. Ghost images of the corrosion front, (a), and the α-cobalt phase in the alloy, (b) and (c), are evident. Results obtained from microprobe analyses of the corrosion product are presented in (d).

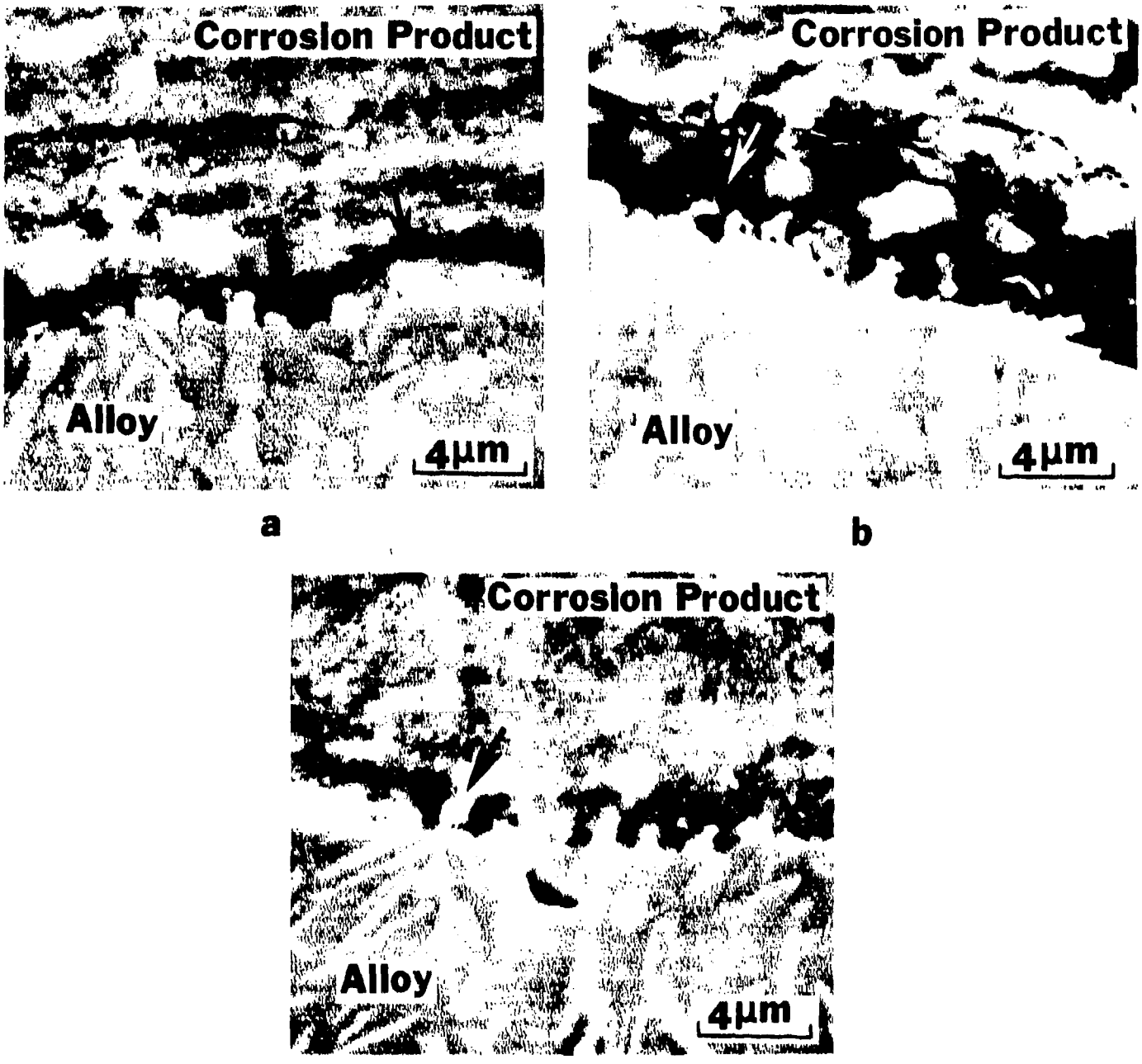

Figure 41. Microstructural features that are developed at the corrosion product-CoCrAlY interface during hot corrosion attack. (704°C, 17.3 hrs., 2.5 mg/cm^2 Na_2SO_4, SO_3 ($7 \cdot 10^{-4}$ atm) in flowing oxygen). The light and dark phases in the corrosion product are chromium and aluminum enriched, respectively, and arrows indicate particles of the α-cobalt phase being converted to the chromium enriched oxide phase.

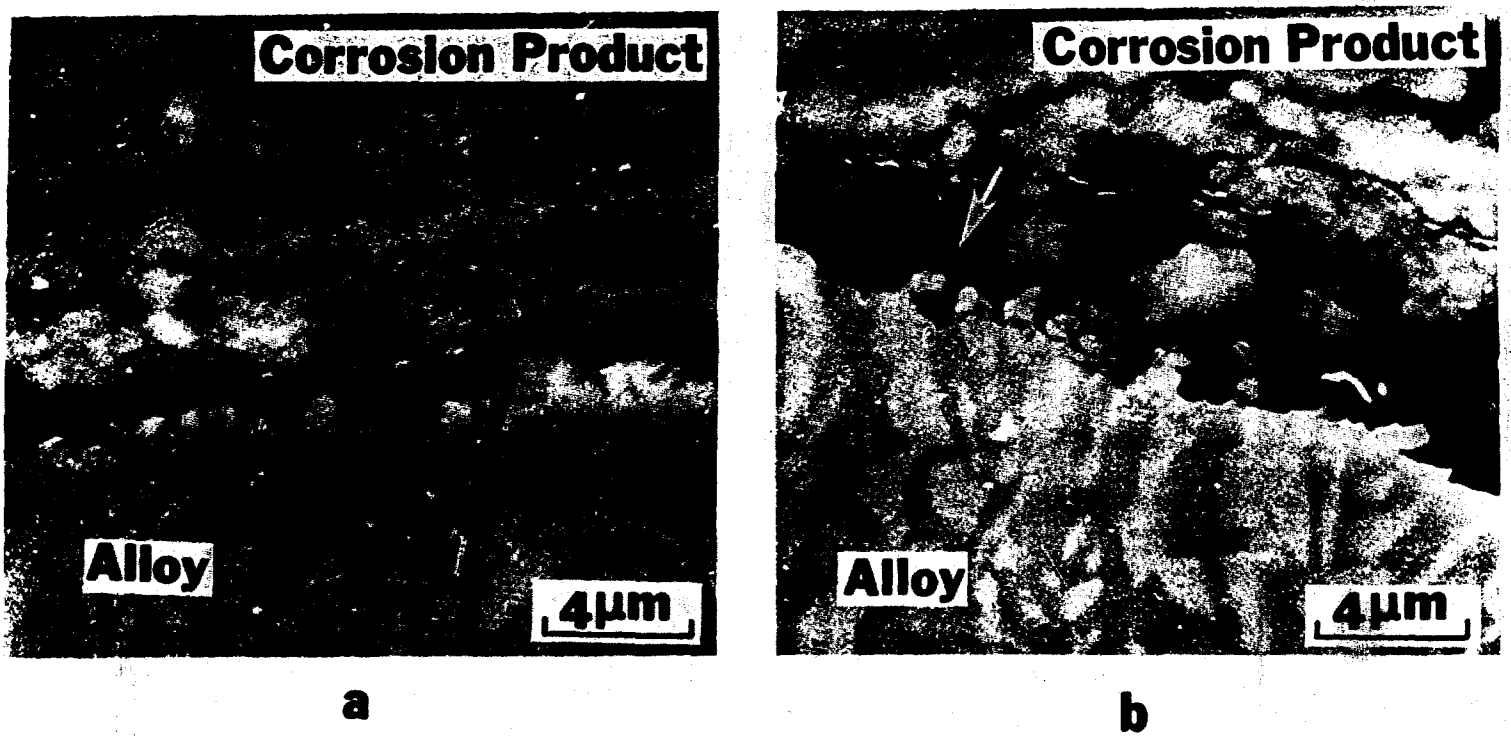

Figure 41. Microstructural features that are developed at the corrosion product-CoCrAlY interface during hot corrosion attack. (704°C, 17.3 hrs., 2.5 mg/cm^2 Na_2SO_4, SO_3 ($7 \cdot 10^{-4}$ atm) in flowing oxygen). The light and dark phases in the corrosion product are chromium and aluminum enriched, respectively, and arrows indicate particles of the α-cobalt phase being converted to the chromium enriched oxide phase.

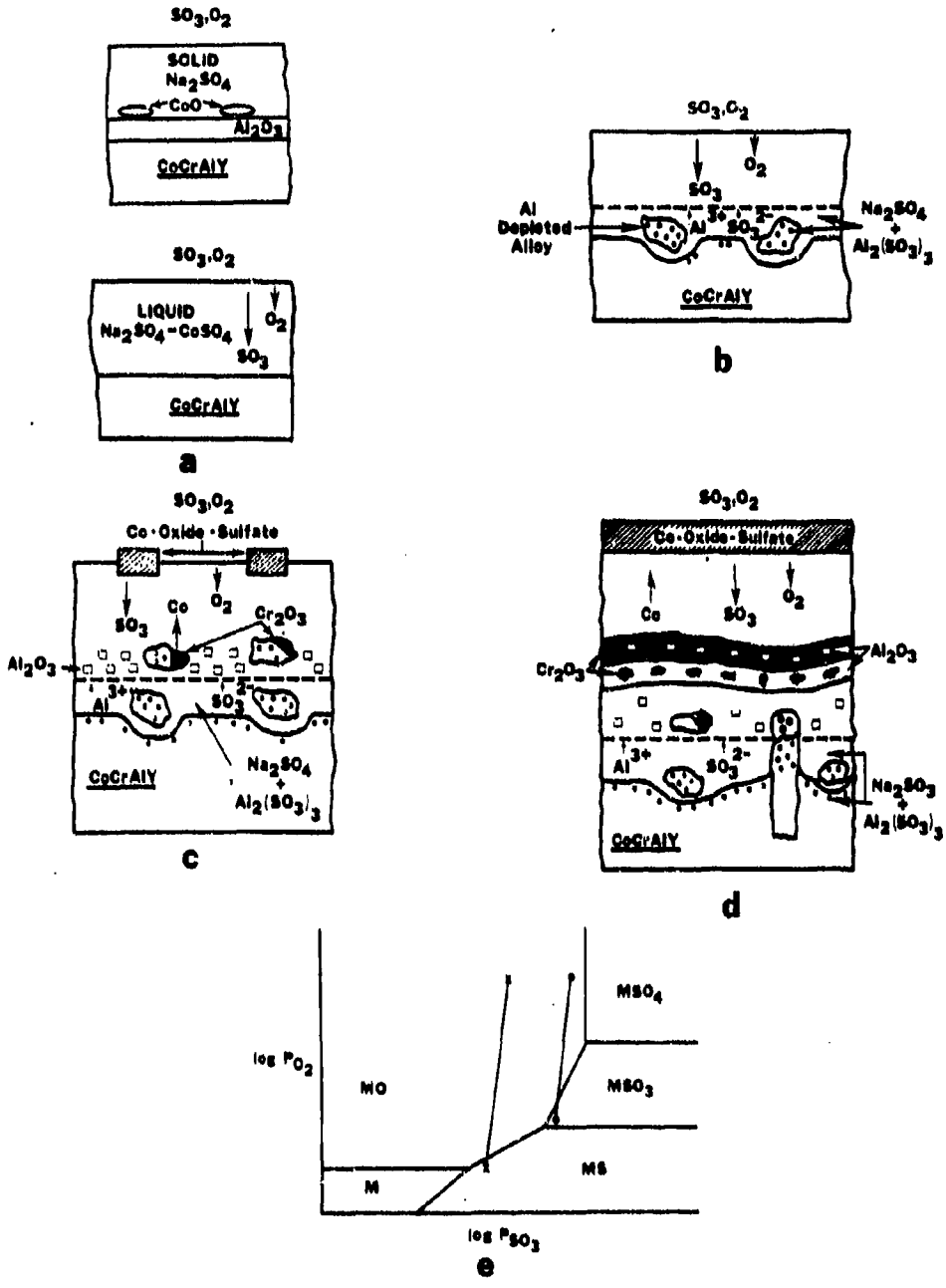

Figure 43. Schematic diagrams to illustrate the hot corrosion attack of a CoCrAlY alloy when SO_3 is present in the gas. At low temperatures solid Na_2SO_4 can be converted to a liquid Na_2SO_4-$CoSO_4$ solution due to the formation of small amounts of cobalt oxide, (a). This liquid can penetrate the Al_2O_3 at cracks and produce attack of the alloy as indicated schematically in (b), (c), and (d). The proposed solution and precipitation of oxide can be rationalized by using a stability diagram, (e), that assumes a region of sulfite as well as regions of metal, sulfide, oxide and sulfate in Na_2SO_4. The two lines terminated by dots and x's indicate possible gradients across a Na_2SO_4 layer on CoCrAlY. The gradient identified by dots is conducive to solution and precipitation of an oxide, a condition that can be expected at lower temperatures. The gradient identified by x's is more common for higher temperatures and is not suitable for acidic fluxing.

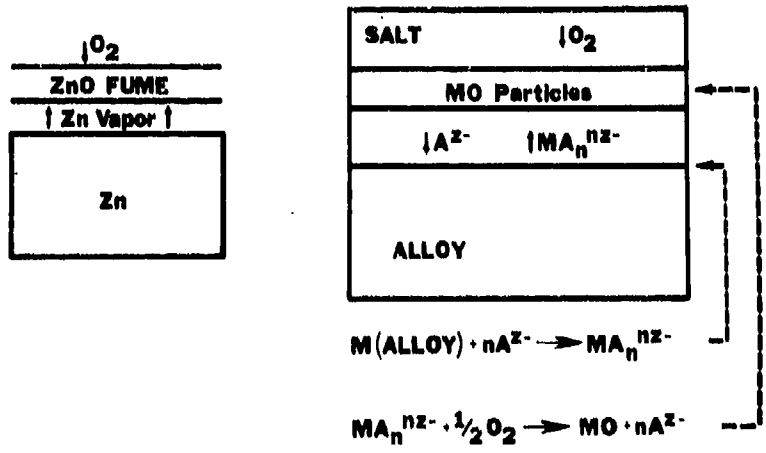

Figure 44. Schematic diagrams to illustrate the similarity between the oxidation of zinc where a nonprotective oxide fume is formed, above the metal and the hot corrosion of alloys via fluxing processes involving solution and subsequent precipitation of nonprotective oxide in the melt away from the surfaces of alloys.

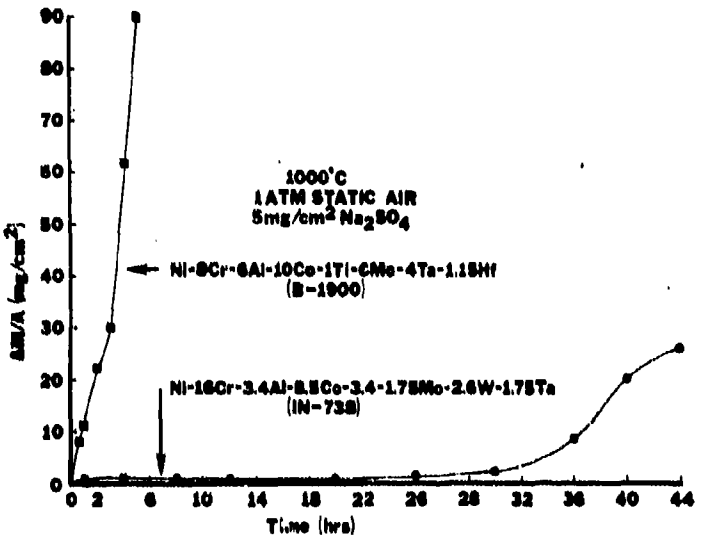

Figure 45. Comparison of weight change versus time data for the Na_2SO_4-induced hot corrosion in air of B-1900 and IN 738.

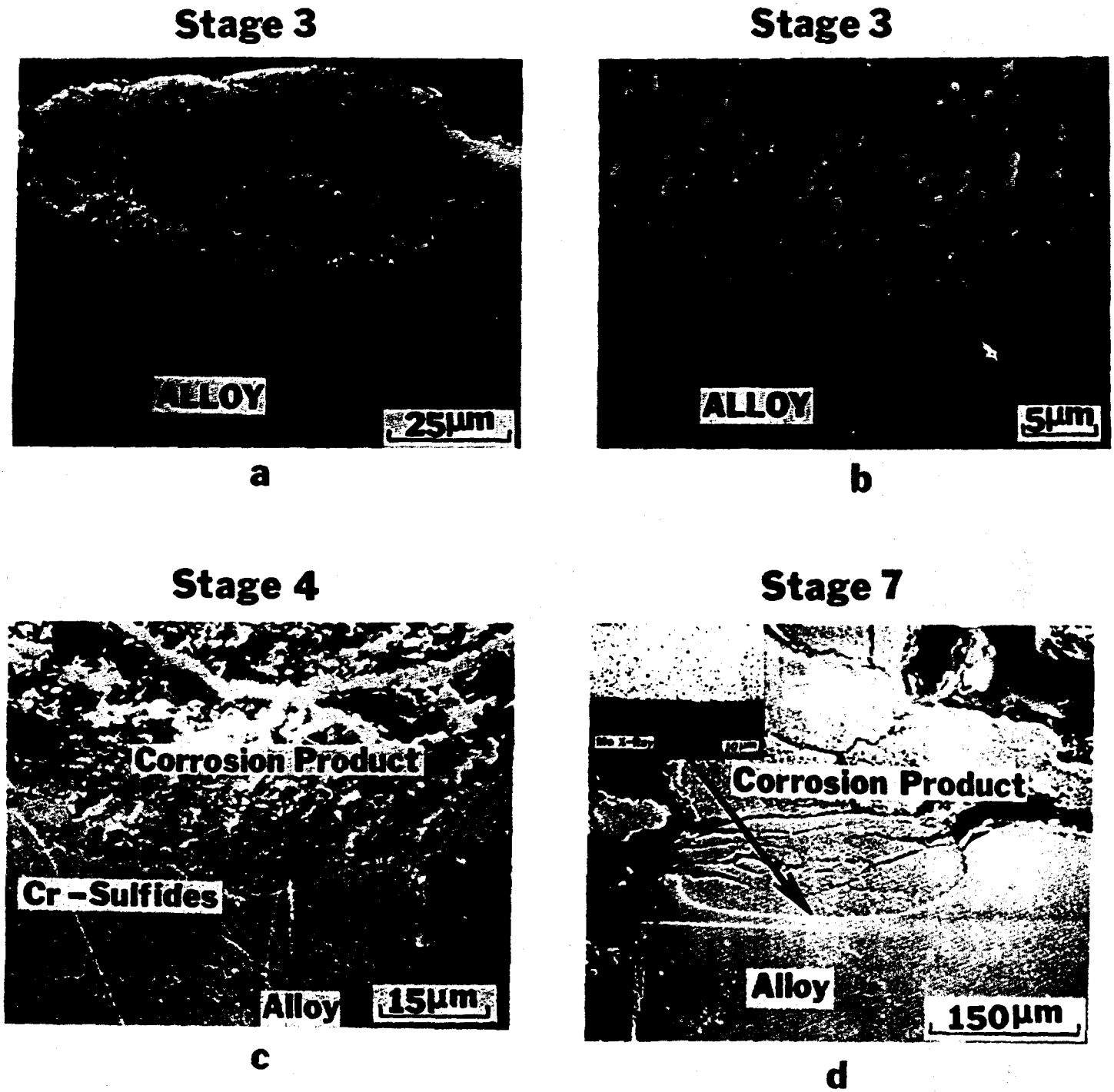

Figure 46. Photomicrographs showing the microstructural features that developed during Na_2SO_4-induced hot corrosion of Ni-8Cr-6Al-6Mo alloys at 1000°C; (a) and (b) 2 min. in static air, (c) 14.5 min. in flowing oxygen, (d) 1.5 hrs. in static air.

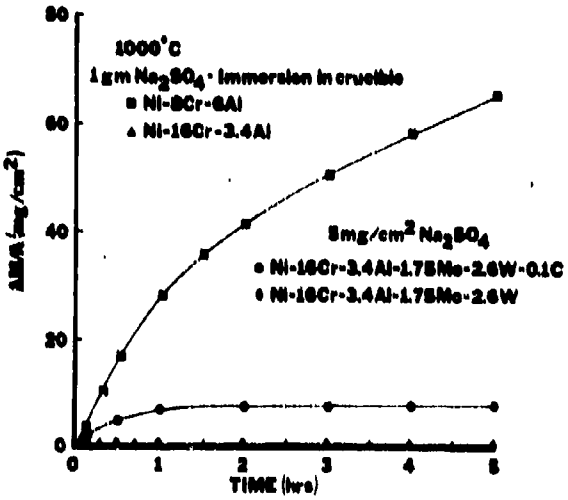

Figure 47. Weight change versus time data to compare the hot corrosion attack of Ni-8Cr-6Al and Ni-16Cr-3.4Al in Na_2SO_4 - immersion tests, and the hot corrosion attack of two IN 738-type of alloys.

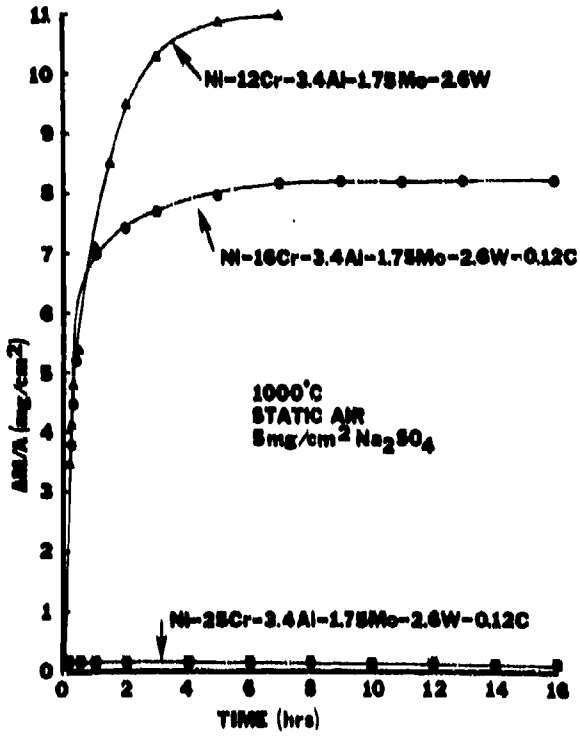

Figure 48. Weight change versus time data to compare the hot corrosion attack of alloys with compositions related to IN 738 but having different chromium and carbon concentrations.

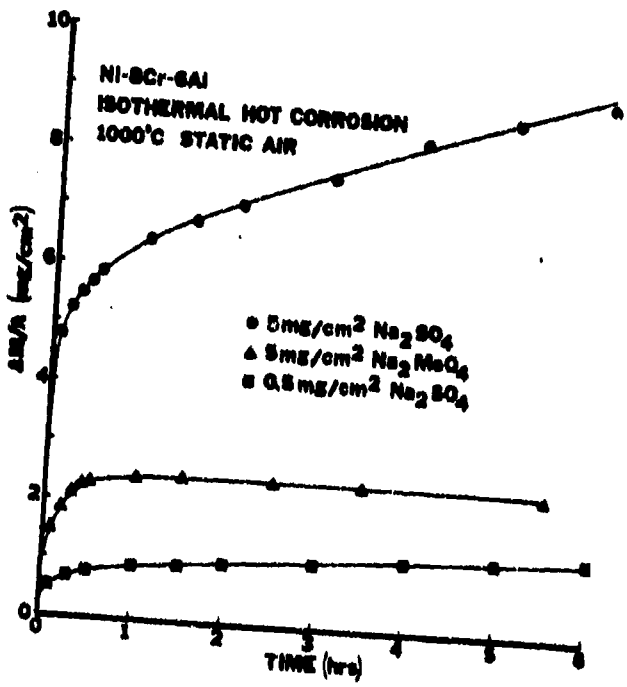

Figure 49. Weight change versus time data to compare the hot corrosion attack of a Ni-8Cr-6Al alloy initiated by deposits of Na_2SO_4 and Na_2MoO_4.

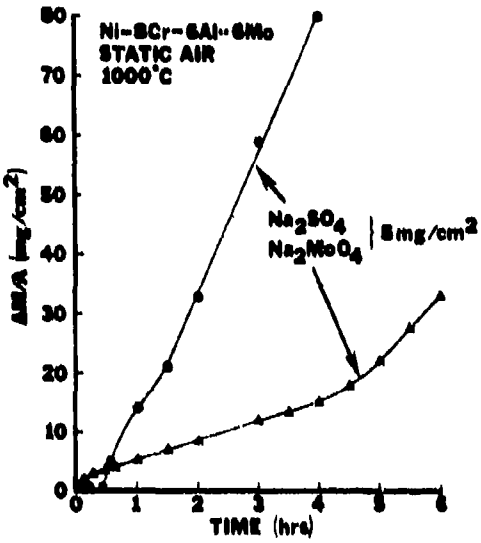

Figure 50. Weight change versus time data to compare the hot corrosion attack of a Ni-8Cr-6Al-6Mo alloy by deposits of Na_2SO_4 and Na_2MoO_4.

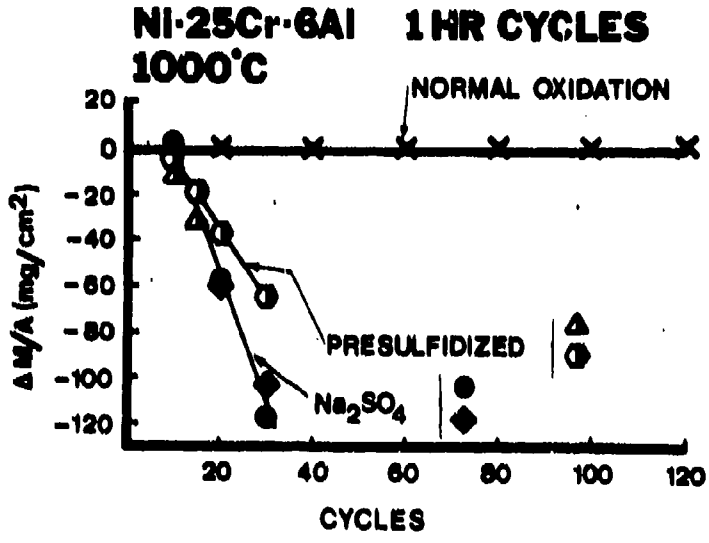

Figure 51. Comparison of the cyclic oxidation data obtained for Ni-25Cr-6Al specimens that were coated with Na_2SO_4 to those presulfidized in an H_2S-H_2 gas mixture. Approximately 5 mg/cm^2 of Na_2SO_4 was added to one specimen after every 5 hrs. of exposure up to 20 hrs. and then after every 10 hr. interval beyond 20 hrs. The presulfidation was performed at the same time intervals that the Na_2SO_4 was applied and the sulfur picked up was equivalent to the sulfur in a 5 mg/cm^2 Na_2SO_4 deposit.

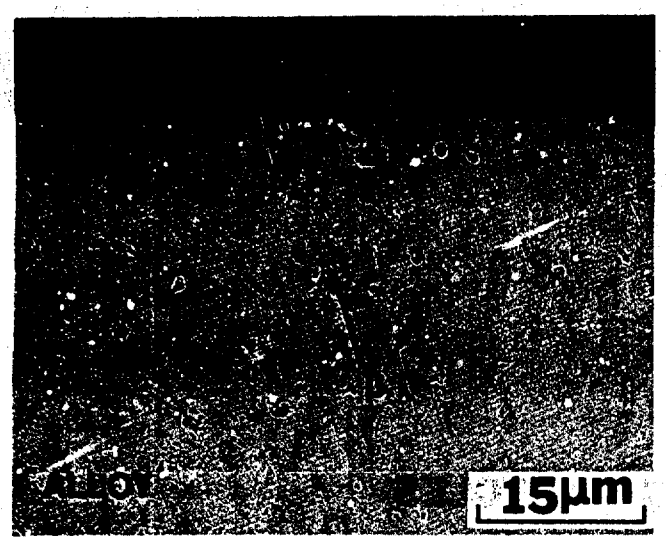

a

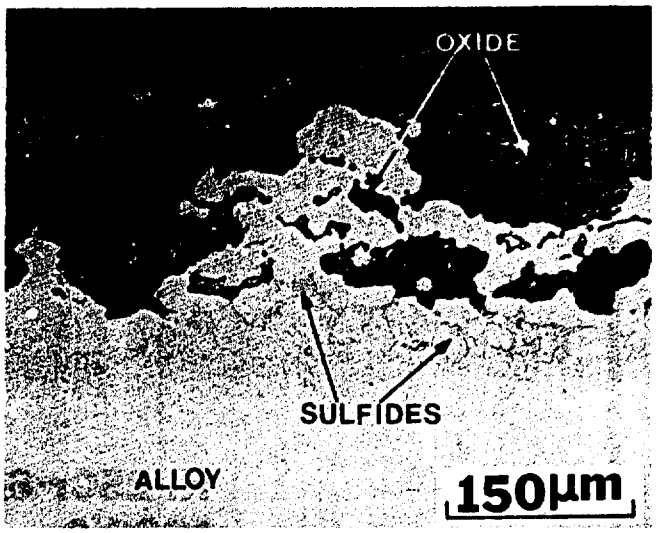

b

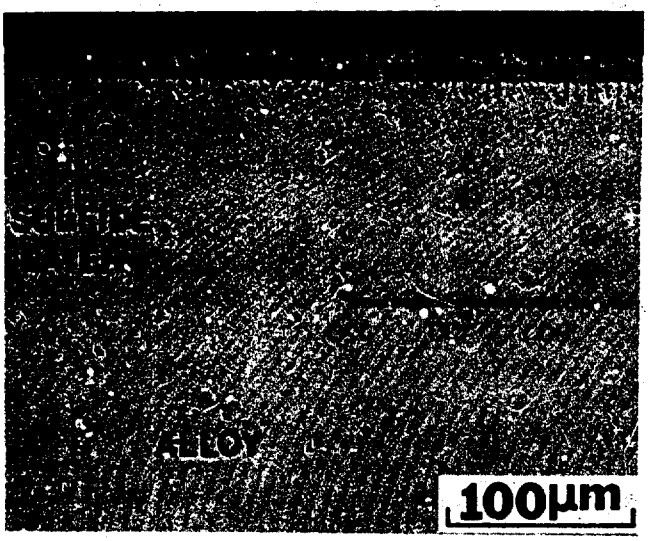

c

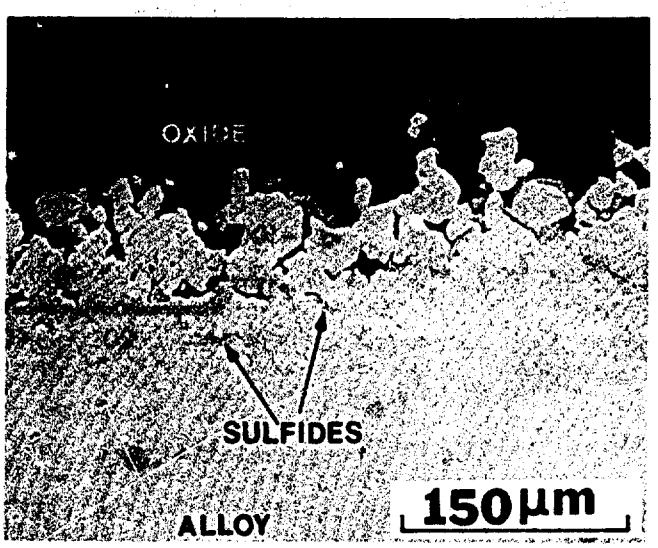

d

Figure 52. Comparison of the microstructures developed in Co-25Cr-6Al, (a), (c), and Ni-25Cr-6Al, (b), (d), specimens after isothermal oxidation at 1000°C in 1 atm of oxygen where the specimens were; coated with 5 mg/cm^2 Na_2SO_4, (a), (b), or presulfidized for 20 sec. in an H_2S-H_2 gas mixture with H_2S/H_2 = 0.2, prior to oxidation, (c), (d).

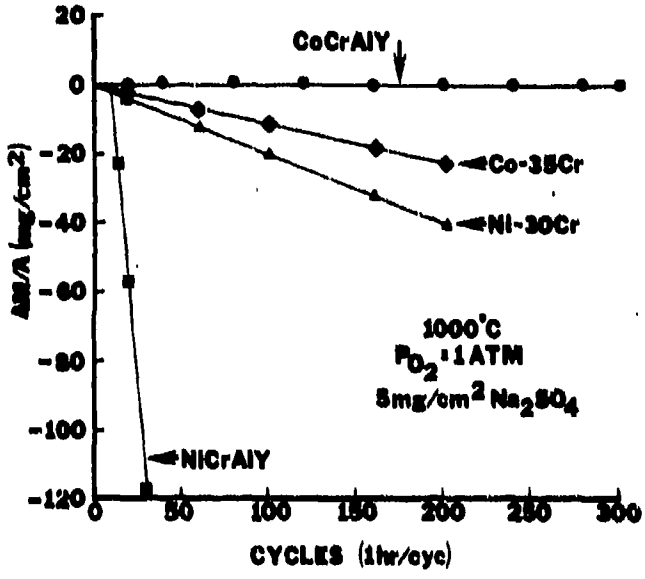

Figure 53. Comparison of the cyclic hot corrosion data obtained for Ni-25Cr-6Al-.2Y, Co-25Cr-6Al-.5Y, Ni-30Cr and Co-35Cr specimens; the Na_2SO_4 was applied every 20 hrs. The attack of NiCrAlY was much more severe than CoCrAlY whereas such a difference was not evident between Co-35Cr and Ni-30Cr.

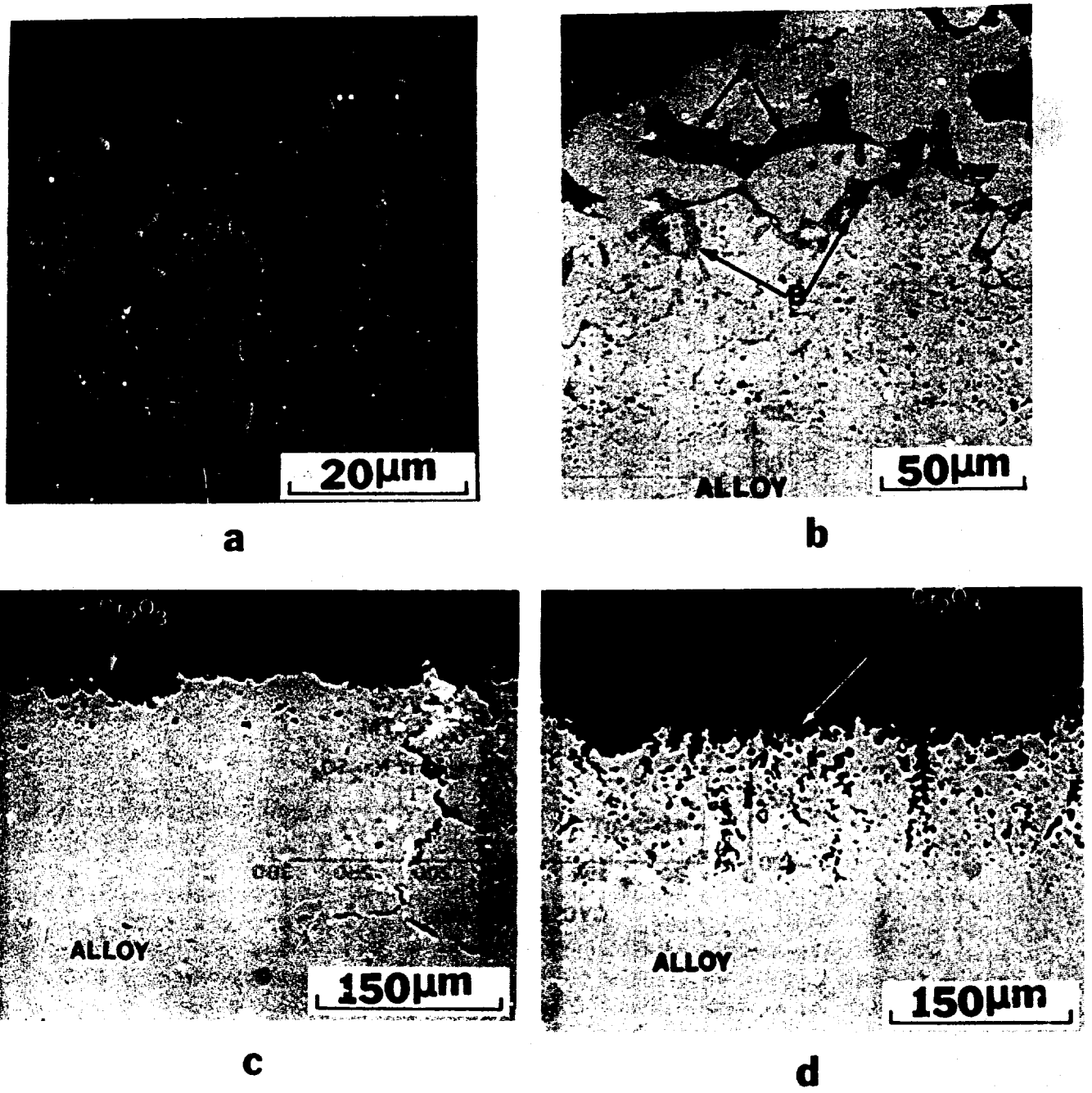

Figure 54. Photomicrographs to illustrate two mechanisms by which sulfide phases in alloys can result in the formation of nonprotective oxide scales during oxidation. Sulfide phases, (a), (electron backscatter image showing sulfide stringers: liquid nickel sulfide, A, and chromium sulfide, B) in a Na_2SO_4-coated (5 mg/cm^2)NiCrAlY specimen after 47 hrs. of oxidation at 1000°C in 1 atm of oxygen are preferentially oxidized, (b), (nonprotective Cr_2O_3 and Al_2O_3 scales, A, and unoxidized nickel-chromium sulfide stringers, B). Nonprotective Cr_2O_3 is formed on Ni-30Cr, (c), and Co-35Cr, (d), specimens due to the oxidation of chromium sulfide particles during 240 hrs. of cyclic hot corrosion exposure (0.5 mg/cm^2 Na_2SO_4 applied every 20 hrs.) at 1000°C in air.

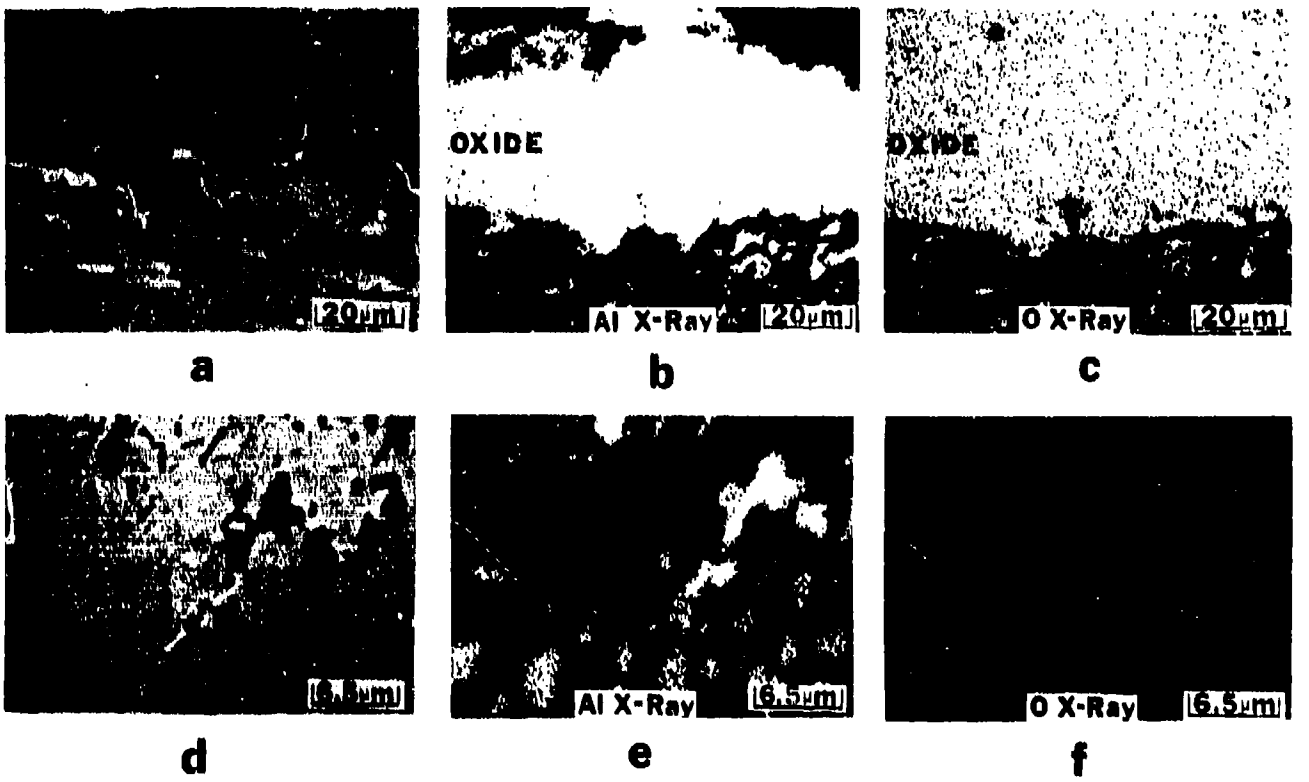

Figure 55. Microstructural photomicrographs and X-ray images of a Co-25Cr-6Al-.5Y specimen after 100 hrs. of cyclic hot corrosion testing at 900°C where 1 mg/cm^2 Na_2SO_4-90% NaCl was applied after every 20 hrs. The structural features at the external scale - alloy porous zone interface and at the alloy porous zone - unaffected alloy interface are shown in (a) and (d), respectively. (b) and (c) are X-ray images of the area shown in (a), and (e) and (f) are X-ray images of the area defined in (d).

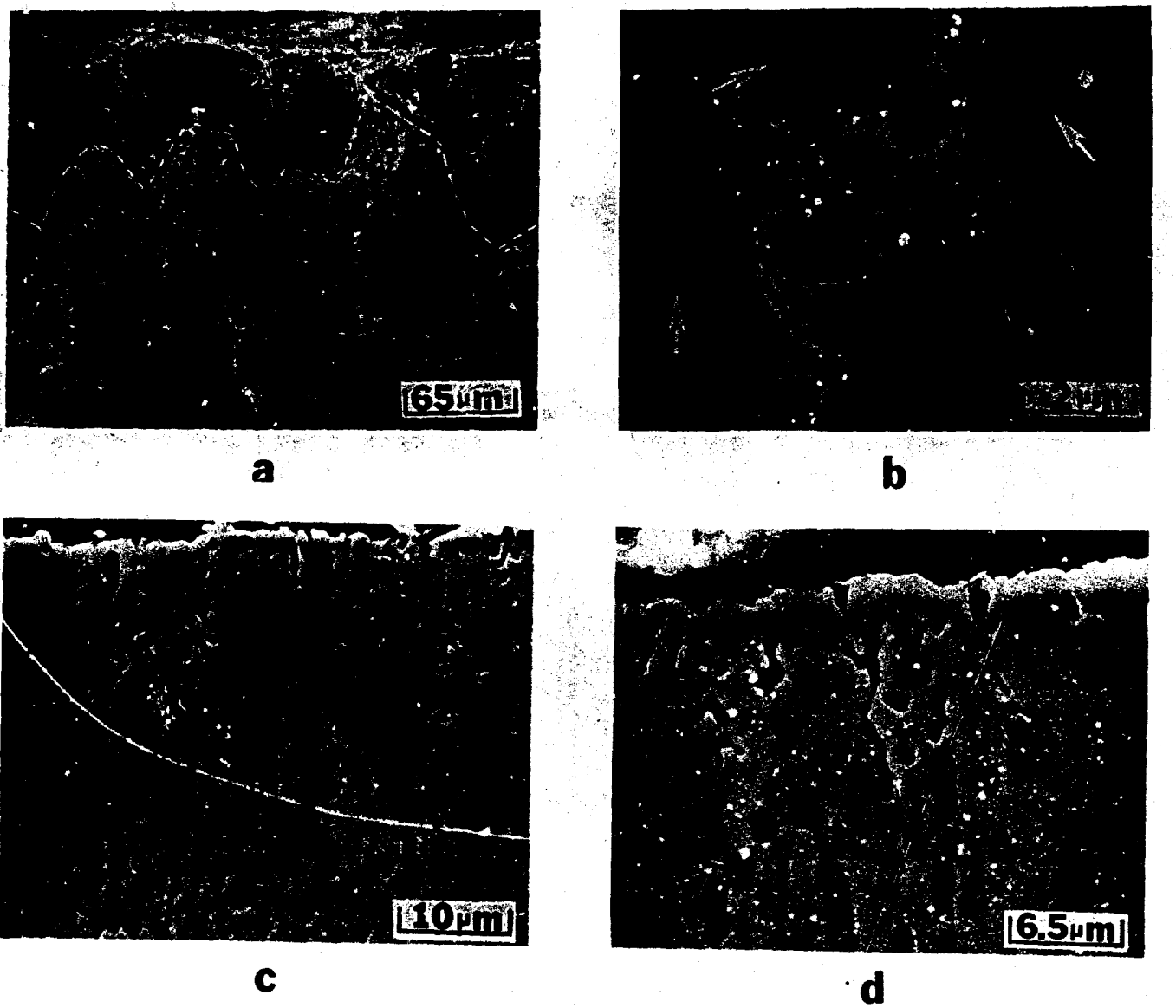

Figure 56. Scanning electron micrographs of Co-25Cr-6Al-.5Y specimens after exposure to a Na_2SO_4-90% NaCl deposit at 900°C in air. The dashed lines in (a) define the zone of internal attack which is composed of a network of coarse (white arrows) and small (black arrows) pores, (b). This porous network appears to coincide with the β-CoAl phase of the alloy, (c), but the pores do not have the exact shape of the β-phase, (d).

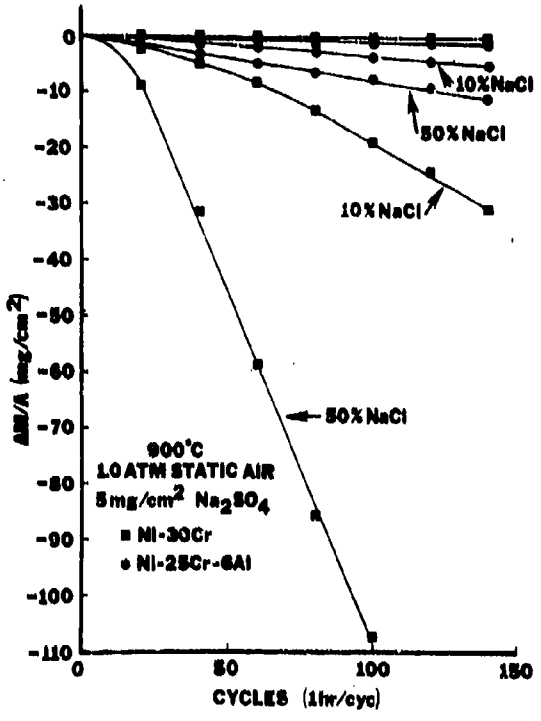

Figure 57. Weight change versus time data to compare the hot corrosion attack of two alloys induced by Na_2SO_4 - NaCl mixtures.

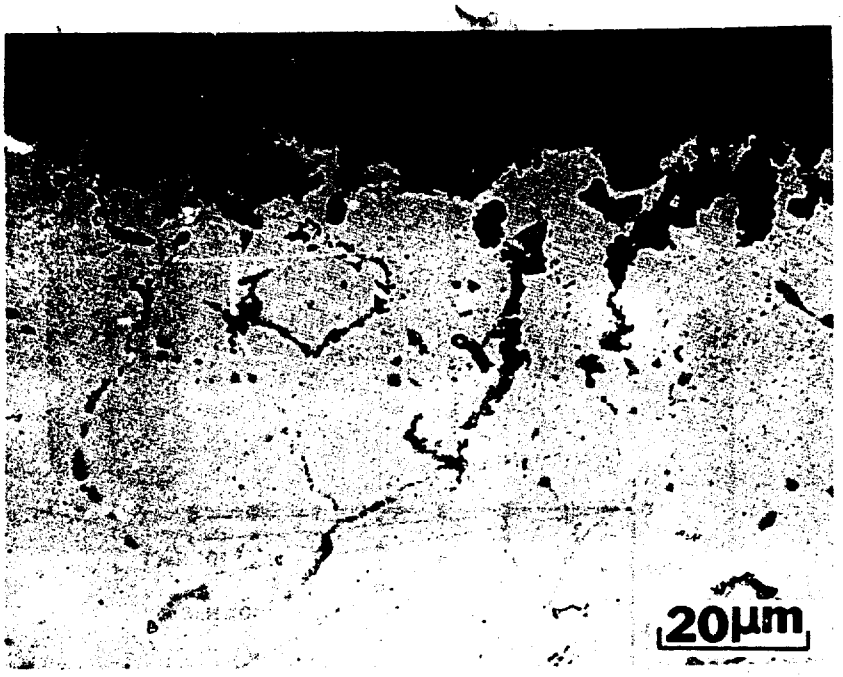

a

b

Figure 58. Photomicrographs to compare the attack of Ni-30Cr specimens after exposure at 900°C in air for 1190 cycles (1 cycle ~ 1 hr.) with 1 mg/cm^2 Na_2SO_4 applied every 20 hrs., (a), and for 275 cycles with 1 mg/cm^2 Na_2SO_4 - 10% NaCl applied every 20 hrs., (b).

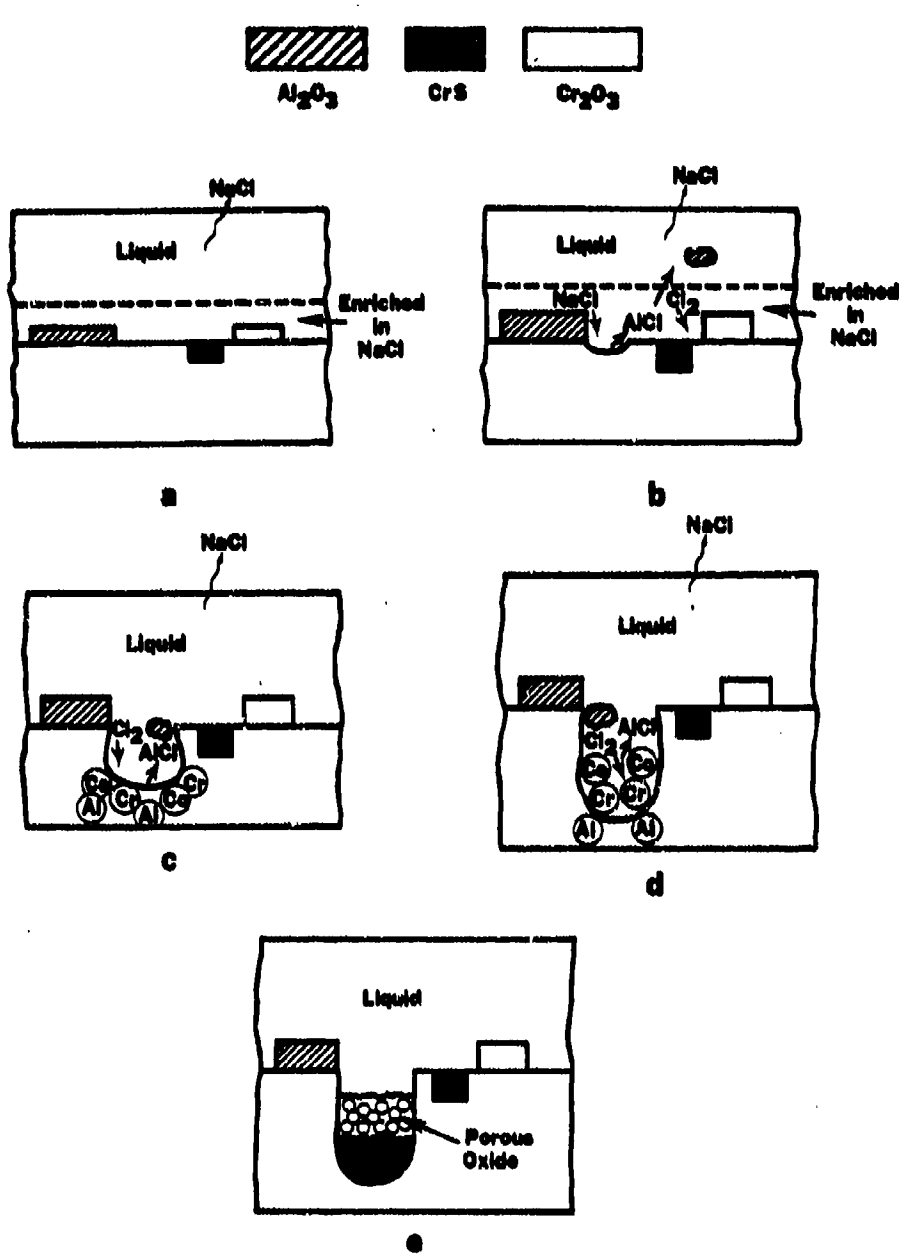

Figure 59. Schematic diagrams to illustrate the hot corrosion attack of alloys induced by mixtures of Na_2SO_4 - NaCl.

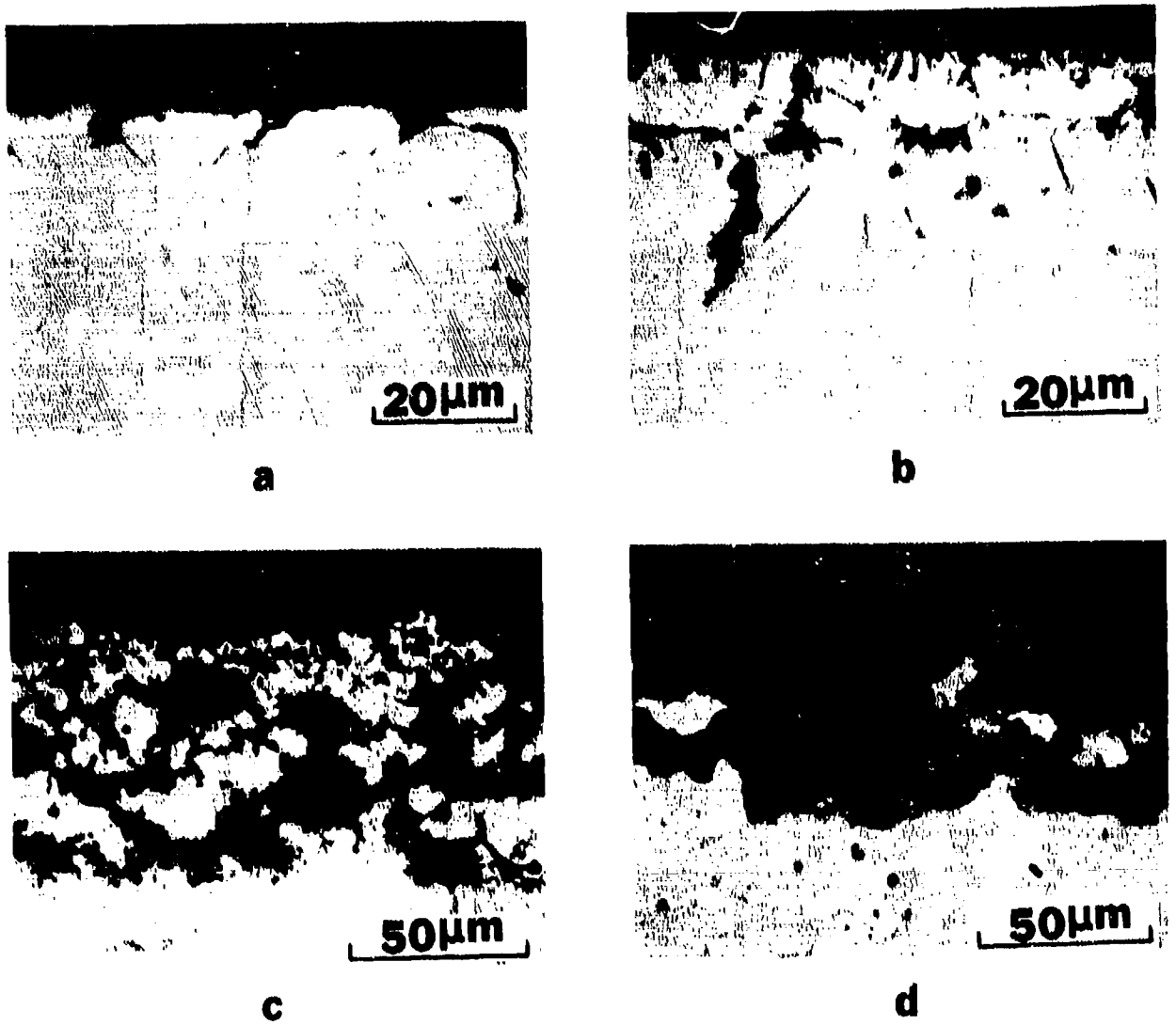

Figure 60. Photomicrographs of Ni-16Cr-3.4Al specimens after exposure at 1000°C in air to: (a) a 5 mg/cm^2 deposit of Na_2SO_4 for 8 hrs., (b) a thick carbon deposit for 8 hrs., (c) a 5 mg/cm^2 deposit of Na_2SO_4 and a thick carbon deposit for 1 hr., (d) a 5 mg/cm^2 deposit of Na_2SO_4 and an excess of liquid fuel (Jet A) for 1 hr.

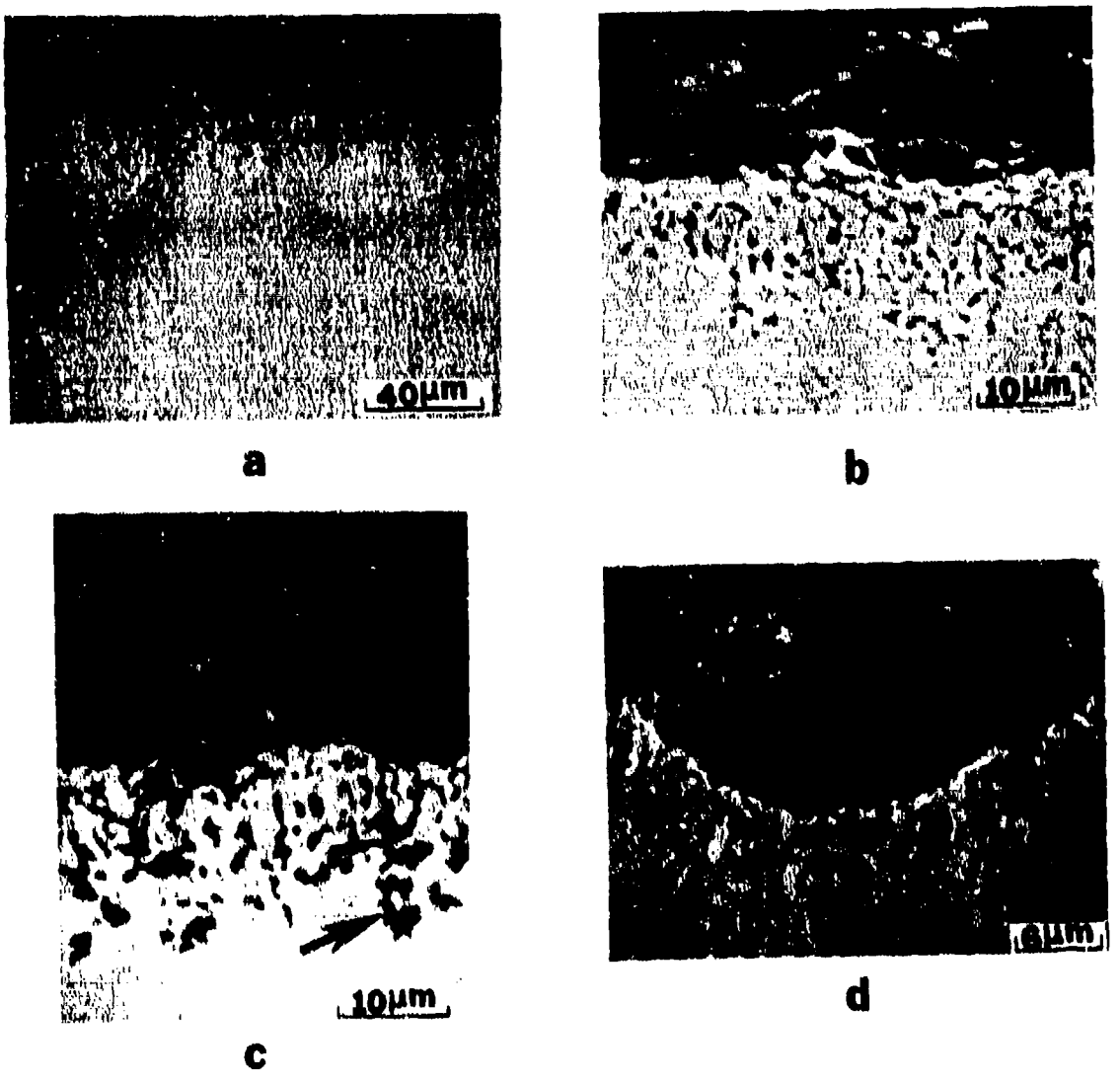

Figure 61. Microstructural photomicrographs of CoCrAlY coatings after exposure of specimens with 1 mg/cm^2 Na_2SO_4 to an excess fuel test. When specimens were exposed for 1 minute in the furnace at 1300°C, large areas of their surfaces exhibited sulfide particles, (a) and (b), and close inspection showed that these sulfides had been preferentially oxidized, (c). In specimens exposed for only 30 sec. at 1300°C, sulfides were not as readily apparent but substantial attack was evident, (d).

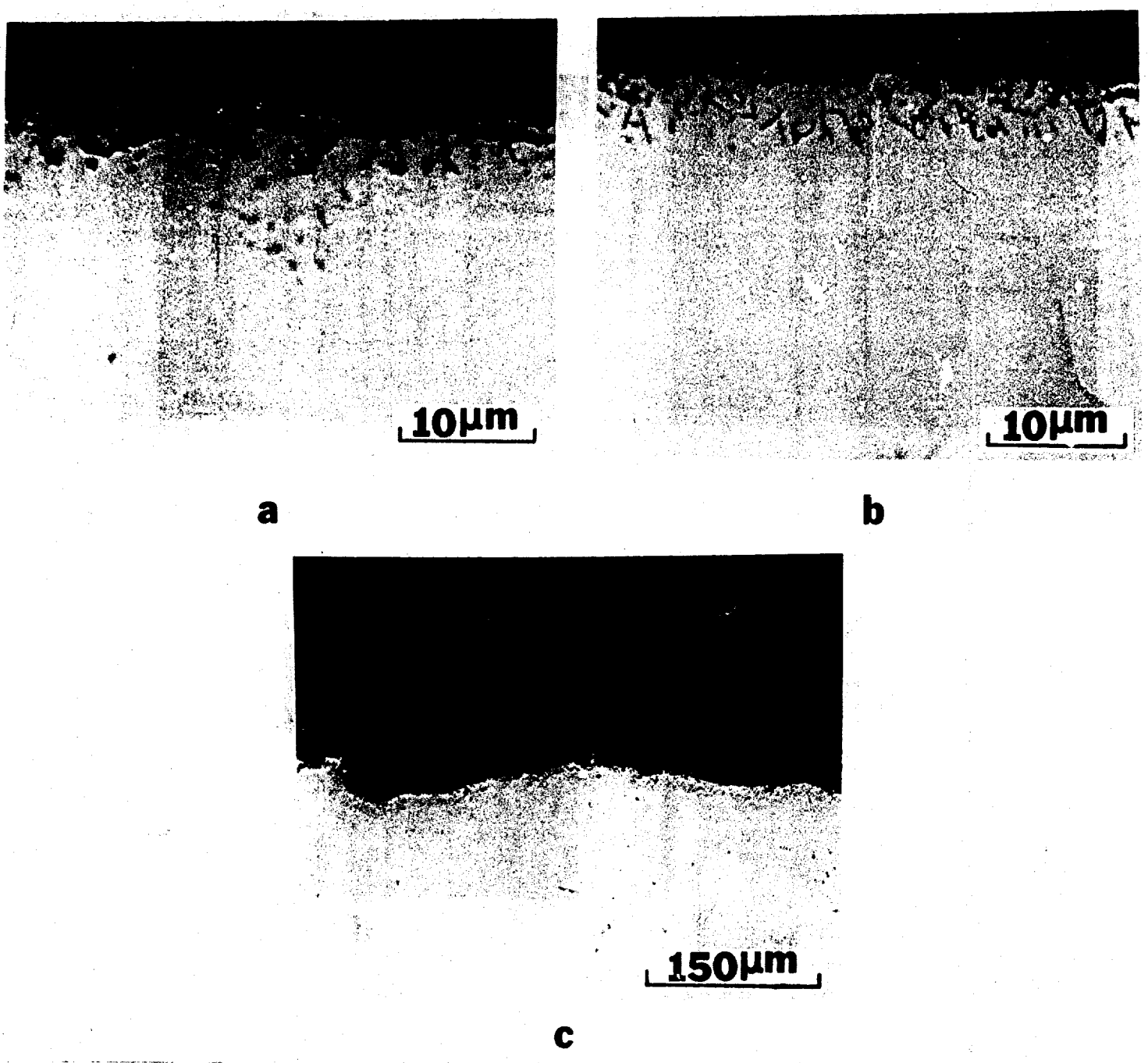

Figure 62. Photomicrographs to compare IN 738 specimens after a 1 hr. exposure at 1000°C in air to: (a) a Na_2SO_4 deposit (1 mg/cm^2), (b) immersion in crucible containing 5 ml of Jet A fuel, (c) a Na_2SO_4 deposit (1 mg/cm^2) and immersion in crucible with 5 ml of Jet A fuel.

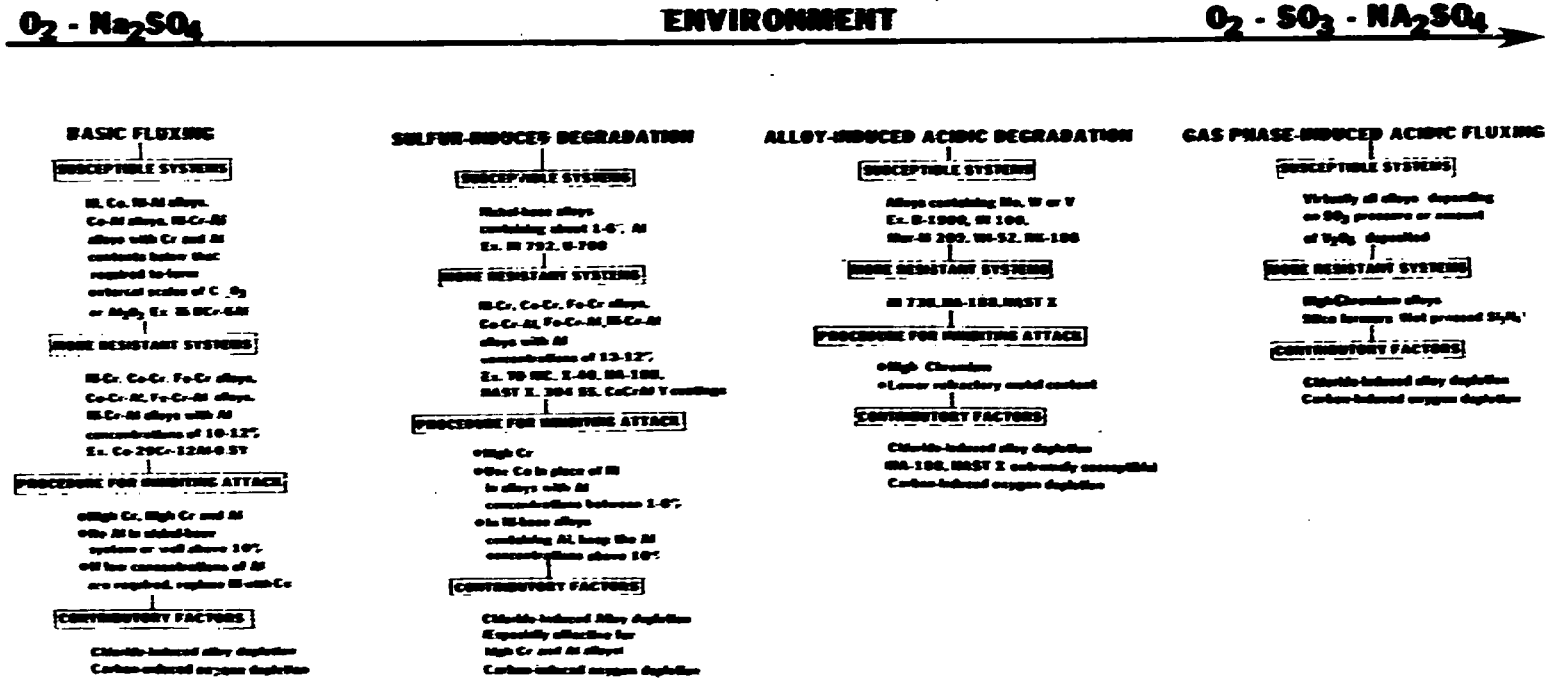

Figure 63. Diagram to identify the alloy systems which are susceptible to attack via the principal hot corrosion propagation modes and to describe procedures to inhibit such degradation.

LIST OF PUBLICATIONS PLANNED FOR PUBLICATION

1. Hot Corrosion Degradation of Metals and Alloys
   - A Unified Theory -
   Part I

   To be submitted to Metallurgical Transactions (AIME, ASM) for publication.

2. Hot Corrosion Degradation of Metals and Alloys
   - A Unified Theory -
   Part II

   To be submitted to the Metallurgical Transactions (AIME, ASM) for publication.

   (The preceding report will be divided into two parts and submitted for publication).